FACTORS CONTROLLING PORE PRESSURE GENERATION DURING K_o CONSOLIDATION OF LABORATORY TESTS

by

Erin A. Force

Bachelor of Science in Civil and Environmental Engineering
Tufts University, Medford, Massachusetts
(1996)

Submitted to the
Department of Civil and Environmental Engineering
in partial fulfillment of the requirements for the degree of

Master of Science in Civil and Environmental Engineering

at the

MASSACHUSETTS INSTITUTE OF TECHNOLOGY

August 1998
[September 1998]

© Massachusetts Institute of Technology, 1998
All rights reserved.

Signature of Author _____
Department of Civil and Environmental Engineering, August 31, 1998

Certified by _____
Dr. John T. Germaine, Thesis Supervisor

Accepted by _____
Prof. Joseph M. Sussman
Chairman, Departmental Committee on Graduate Studies

MASSACHUSETTS INSTITUTE OF TECHNOLOGY
OCT 26 1998
LIBRARIES

ARCHIVES

FACTORS CONTROLLING PORE PRESSURE GENERATION DURING K_O CONSOLIDATION OF LABORATORY TESTS

By

Erin A. Force

Submitted to the Department of Civil and Environmental Engineering on August 31, 1998
in partial fulfillment of the requirements for the degree of
Master of Science in Civil and Environmental Engineering

ABSTRACT

During triaxial testing of cohesive soils, the specimen is consolidated to the desired stress state prior to either drained or undrained shear. Advances in technology have allowed more realistic simulation of field conditions, including continuous K_o consolidation rather than incremental hydrostatic consolidation. However it is necessary to select a conservatively slow consolidation strain rate to ensure negligible excess pore pressure which results in exceedingly long test durations. This experimental study of the factors controlling excess pore pressure generation provides insight for selecting more acceptable rates.

An extensive experimental program was conducted on Resedimented Boston Blue Clay to study the behavior during constant rate of strain consolidation. Strain rate sensitivity was measured using the Wissa constant rate of strain device with tests ranging from 0.07 %/hr to 12.7 %/hr. The influence of specimen height and boundary drainage conditions was measured using a modified version of the MIT automated stress path triaxial apparatus. A special base with a removable needle probe was used to measure excess pore pressure in the middle of the test specimen.

The results from tests without radial drainage firmly establish the relationship between excess pore pressure, hydraulic conductivity of the soil, strain rate, and height. Further, they support the use of equations based on a linear soil model developed for the CRS test to predict excess pore pressure. A second method of analysis for continuous loading based on equations for drained shear was also examined since it considers the presence of filter drains and the effectiveness of the drains. The results do not support the use of this theory in constant rate of strain tests and indicate a need for a more general model to account for radial drains.

The research also provides several practical recommendations for testing. Regarding the CRS test, the current findings strongly support the use of the linear theory over the nonlinear theory in test interpretation. The results at higher strain rates indicate that the current ASTM guidelines for limits on the pore pressure need to be reduced and redefined in terms of hydraulic gradient in order to obtain correct hydraulic conductivities. Finally, the current consolidation strain rate of 0.1 %/hr for RBBC in the triaxial apparatus results in negligible pore pressures and may be increased by almost an order of magnitude.

Thesis Supervisor: Dr. John T. Germaine
Title: Principal Research Associate in Civil and Environmental Engineering

Acknowledgements

My appreciation goes to the following:

Fugro for the funds to support this research and the MIT Department of Civil and Environmental Engineering for providing the Schoettler Fellowship to support me during my first year.

Dr. John T. Germaine for his enthusiasm and optimism through many painstaking experiences. This project would not have been possible without his insight and abundant suggestions.

Professors Charles C. Ladd, Andrew J. Whittle, Herbert H. Einstein, and Patricia J. Culligan for their geotechnical courses that kept my interest in the subject alive.

The geotechnical laboratory group for both their social and technical input: Amy Varney for introducing me to the lab. Catalina Marulanda for her cheerful support through coursework and the associated emotional spells. Kurt Sjoblom, Laurent Levy, and Lana Aref for always providing a social break from technical difficulties. Marika Santagata for being a helpful and encouraging triaxial neighbor. Joe Sinfield and Greg DaRe for their good-natured sharing of knowledge. Guoping Zhang and Anne Chen for being generous officemates.

My parents and family, both old and new, for their unconditional support. Their encouragement through the years has allowed me to achieve all that I have.

Finally, my husband for his complete understanding during this demanding period, his confidence in my ability, and his constant love and patience.

Table of Contents

List of Tables

List of Figures

Chapter 1 Introduction

The triaxial test is one of the principal methods of measuring the stress-strain-strength properties of cohesive soils in geotechnical engineering practice because it allows testing under a range of stress and boundary drainage conditions. The tests also have a range of time and cost requirements depending on the level of sophistication. The following are the four types of tests performed: unconfined compression, unconsolidated-undrained, consolidated-undrained, and consolidated-drained. The shear phases of the last three tests may be performed in extension or compression by either loading or unloading.

Significant disturbance frequently occurs in sampling cohesive soils, leading to highly variable strengths measured in unconsolidated testing. This necessitates the use of consolidation prior to shear to minimize the effects of disturbance. C.C. Ladd (1991) presents two techniques for determining shear strengths after K_o consolidation: Recompression and SHANSEP. The Recompression technique consolidates the specimen to the in situ vertical effective stress prior to shear. The SHANSEP technique performs shear tests on specimens consolidated past the in situ preconsolidation pressure and also on specimens rebounded to various overconsolidation ratios. Each method applies only to certain soil conditions, but they both require K_o consolidation.

Until recently, triaxial testing was performed manually, and therefore incremental hydrostatic consolidation was the easiest and most common method to follow. Advances in understanding of soil behavior, however, illustrated the importance of K_o consolidation in soil characterization. Finally, the improvement of computer controlled testing has made continuous K_o consolidation the standard procedure.

Incremental consolidation had the advantage that properties measured during the last increment could be used to compute shear rates. The consolidation occurred at an optimal rate depending on the drainage conditions, and the shear rate was therefore adjusted to the particular specimen conditions. With continuous K_o consolidation, estimates of the soil properties must be made to calculate rates for both consolidation and shear. Because the test does not yield data regarding the specific test conditions, conservatively slow rates must be chosen to ensure minimal excess

pore pressure, resulting in unreasonably long testing times. Existing methods of relating the specimen pore pressure with soil properties and drainage boundaries are based on approximate conditions and have not been verified with detailed experimental investigation.

1.1 Objectives and Scope of Research

The goal of this research is to determine the fastest rates possible for the K_o consolidation phase of triaxial testing. The rate must be chosen to ensure negligible excess pore pressures, therefore the focus of the research is on defining and quantifying the factors controlling pore pressure generation.

The experimental program conducted tests on Resedimented Boston Blue Clay to determine the behavior of the soil during constant rate of strain consolidation. Strain rate effect was studied through tests in the Wissa CRS apparatus performed under a range of consolidation rates. The height and radial drainage effects were investigated through tests performed in a modified version of the MIT automated stress path triaxial apparatus. A new base with a removable pedestal allowed a needle probe to be inserted into the center of the specimen to measure excess pore pressure.

The test results were used to analyze several models relevant to pore pressure generation during continuous loading. The first model developed for the CRS test relates the excess pore pressure to the strain rate, height, and hydraulic conductivity of the soil. The second model was developed for drained shear and relates the excess pore pressure to the coefficient of consolidation and loading rate. A modification to the second theory accounts for the presence of filter drains and the effectiveness of the drains. Finally, some practical recommendations for testing are considered.

1.2 Organization of Thesis

This thesis presents the background, results, and interpretation of the experimental study of factors controlling excess pore pressure generation.

Chapter 2 provides a background on consolidation testing in the triaxial apparatus. The chapter explains the evolution from incremental hydrostatic consolidation to the current standard of continuous K_o consolidation. The previous methods of choosing strain rate from the incremental data are explained, and two theories are presented to consider for modeling the new method of consolidation. Finally, information on the use of side filter drains to decrease testing time is presented.

Chapter 3 describes the test material, equipment, and procedures used to characterize pore pressure generation. Both the batching process and the index properties of Resedimented Boston Blue Clay are presented. The standard apparatus and procedures used for the constant rate of strain consolidation test are described. Finally the modifications to the MIT automated stress path triaxial apparatus are explained. One modification allowed constant flow tests on the filter paper while the second modification allowed a needle probe to measure the excess pore pressure in the center of a triaxial specimen.

Chapter 4 summarizes the results of the testing program. The measured hydraulic conductivity of both Whatman 1 and Whatman 54 filter paper is compared to values reported in the literature. Complete results from both CRS tests and triaxial tests in the modified equipment are summarized to determine trends and repeatability.

Chapter 5 interprets the excess pore pressure data with changes in rate, height, and coverage of filter drains. The CRS model, the drained shear model, and the equations of effectiveness are applied to the data to determine which theories best characterize the behavior. An initial estimate of both the hydraulic conductivity and the compressive resistance of the filter drains is included.

Chapter 6 summarizes the results and conclusions of the research and makes recommendations for future research.

In addition to the six chapters, an appendix is included to provide detailed procedures for the filter paper hydraulic conductivity measurement, CRS test, and K_o consolidation test with probe measurement of the excess pore pressure.

Chapter 2 Background

2.1 Overview of Triaxial Testing of Cohesive Soils

During triaxial testing, the two factors that may be controlled are the boundary drainage conditions and the stress path. The drainage condition determines if the test is consolidated or unconsolidated prior to shear and if it is drained or undrained during shear. A variety of stress paths may be followed, but the two of most interest to this research are the hydrostatic stress path and the K_o stress path during consolidation. Until recently, consolidation was typically performed using hydrostatic increases in stress with a load increment ratio of one. This was the easiest method to follow when manually controlling the test. It also provided the benefit that properties measured during the last increment of consolidation could then be used to estimate the correct strain rate during the shear phase of the test.

Advancement in testing techniques, however, allowed consolidation of triaxial specimens along anisotropic stress paths, in addition to the previous hydrostatic consolidation. Results of shear tests performed on specimens consolidated by the two different methods made it clear that the stress system induced anisotropy has a large effect on the strain to failure and the modulus of the material. There may also be an impact on strength depending on soil type. Figure 2.1 shows the stress strain behavior of Resedimented Boston Blue Clay after hydrostatic consolidation compared to behavior after K_o consolidation. This illustrates the importance of K_o consolidation in properly estimating field properties.

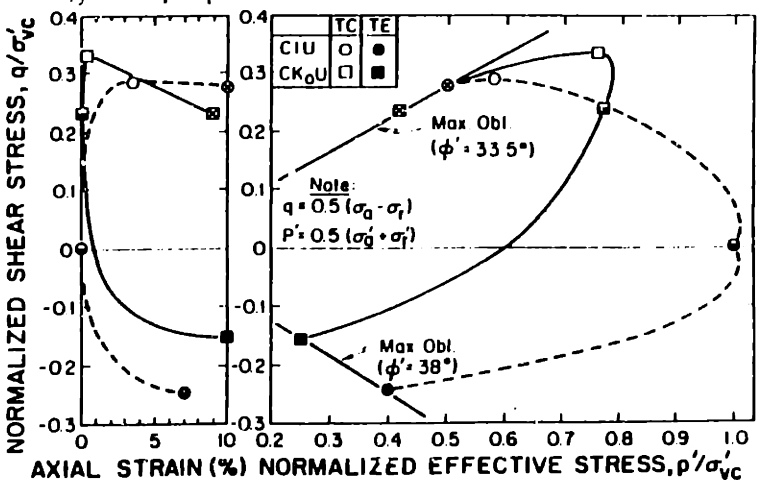

Figure 2.1 Undrained Stress Strain Behavior for Ko and Isotropic Consolidation of OCR = 1 Resedimented Boston Blue Clay (Germaine and Ladd, 1988)

Because the tests were controlled manually, the early methods of K_o consolidation were very labor intensive. For K_o consolidation, the axial and volumetric strains need to be balanced to keep a constant specimen area. So after each small increment, the area of the specimen is evaluated and value of K_c modified to correct the area. This required twenty to thirty increments to reach the desired stress state, equivalent to twenty to thirty days. This testing time was far too long, especially for commercial labs, so simplified methods were introduced to save time. One such method alternated between hydrostatic increments and shear increments, both easy to perform and shown in Figure 2.2. Even using a simplified method, the stress path should cross the yield surface at the correct point to keep the structure of the soil the same as it would be following the correct stress path. Therefore path B in the figure is preferred over path C.

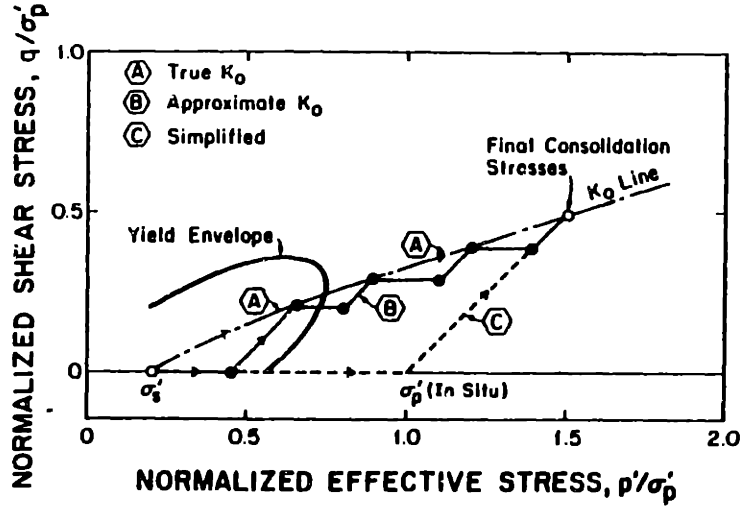

Figure 2.2 Techniques for Ko Consolidation (Germaine and Ladd, 1988)

The introduction of computer control in testing greatly improved the possibilities during the consolidation phase. While loading the specimen at a constant rate, a computer can control the cell pressure and pore pressure. With continuous feedback, the computer can constantly monitor the axial and volumetric strains and adjust the cell pressure while keeping the pore pressure constant to balance these strains.

The consolidation rate is chosen conservatively to allow complete dissipation of excess pore pressures. This may be unnecessarily slow however, and several issues should be examined to

allow shorter testing times. First is to better understand the factors controlling excess pore pressure generation such as rate, height, and drainage conditions. The presence of filter drains on the specimen has a large impact but needs to be quantified. In addition, the shear behavior should be examined to determine the influence of partial drainage during consolidation on the shear strength.

There are two alternate methods available in the literature for prediction of pore pressures during continuous loading. The first was developed for the constant rate of strain consolidation test (Smith and Wahls, 1969 and Wissa et al, 1971) designed as an alternative to the incremental oedometer. This analysis is for typical one dimensional flow and linearly relates the excess pore pressure at the base of the specimen to the strain rate and hydraulic conductivity of the soil. The second method is based on a modification to the conventional consolidation equations (Gibson and Henkel, 1954 and Bishop and Gibson, 1963). These equations predict that the excess pore pressure is related to the coefficient of consolidation and the loading rate. This second method has the advantage that terms are included to consider the case of both vertical and radial drainage due to filter drains and also considers the effectiveness of the drains.

The goal in choosing the rate for drained shear is to provide adequate time for water movement through the specimen so that the pore pressure everywhere is equal to the backpressure. This is controlled by how quickly flow may occur (a property of the material) and the location of the closest drainage surface (whether there is filter paper to allow radial drainage). Performing the test too quickly results in excess pore pressure in the center of the specimen and leads to errors in the measured strength and effective stress failure envelope. Performing the test slower than necessary causes negligible errors however it is always preferable to minimize testing times.

In choosing undrained shear rates, sufficient time must be provided to allow pore pressure equilibration within the specimen. Pore pressure variations are primarily caused by frictional ends. End restraint causes dead zones in the ends of the specimen and as load is applied, the pore pressure in this zone approaches the total stress applied. Therefore, water must migrate to equilibrate pore pressures within the specimen (Germaine and Ladd, 1988).

The move to K_o consolidation has eliminated the option of using the consolidation data to compute the shear rate based on existing methods. Even with incremental K_o loading, the small LIR required to prevent premature shear failures invalidates the use of the Taylor square root of time method due to the excessive amounts of secondary compression. Therefore, the strain rate for shear is based on conservative estimates of the coefficient of consolidation and the effectiveness of the drainage conditions. This does not adjust for specific test conditions as with the methods that will be discussed in the following section and forces the selection of conservatively low strain rates.

2.2 Incremental Hydrostatic Consolidation

The conventional method to perform triaxial tests was based on incremental hydrostatic consolidation followed by shear. Properties measured during the last increment of consolidation could then be used to calculate either the drained or undrained shear rate. The incremental consolidation was performed as in the oedometer test with a large load increment ratio (LIR). Measurements of volume change were taken over time and, for simplicity, analyzed using an approximation of the Taylor square root of time construction. In a plot of volume change against $\sqrt{t}$ as shown in Figure 2.3, the initial portion is a straight line, regardless of drainage condition. The intersection of this line with a horizontal line representing 100% consolidation provides t_{100}. The large LIR guaranteed that primary consolidation dominates over secondary compression deformations, and hence the Taylor construction always yields a value for the end of consolidation (Bishop & Henkel, 1962).

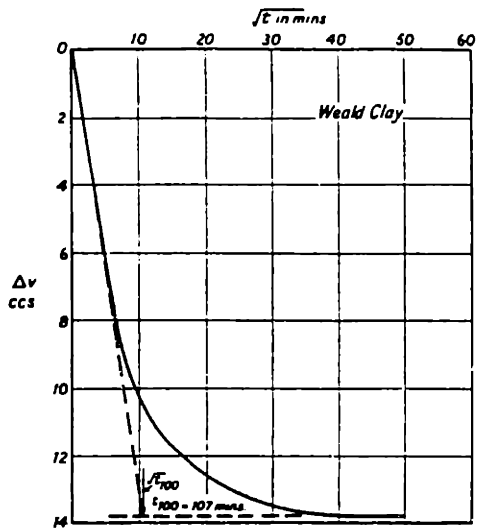

Figure 2.3 Approximation of the Taylor Square Root of Time Construction

Table 2.1 (h=½ height of specimen, R=radius of specimen) summarizes expressions of the coefficient of consolidation, C_v, in terms of t_{100} for various drainage conditions, allowing easy calculation of C_v with the t_{100} estimated from Figure 2.3.

Drainage Conditions	C_v	C_v ($h = 2R$)
One end only	$\frac{\pi h^2}{t_{100}}$	
Both ends	$\frac{\pi h^2}{4t_{100}}$	
Radial boundary only	$\frac{\pi R^2}{16t_{100}}$	$\frac{\pi h^2}{64t_{100}}$
Both ends and radial boundary	$\frac{\pi h^2}{4t_{100}}\left[\frac{1}{(1+2h/R)^2}\right]$	$\frac{\pi h^2}{100t_{100}}$

Table 2.1 Expressions for Coefficient of Consolidation in Terms of t_{100}

With the value of C_v calculated from the last step of the consolidation phase, the approximate time to failure for drained shear may be calculated. The theory of consolidation has been applied to this problem by Gibson and Henkel (1954) and Bishop and Gibson (1963). Details of these theories relevant to pore pressure generation under various drainage conditions will be discussed in Section 2.3.2. Taking only the first part of the more complete solution, neglecting the

exponential terms that contribute to the initial transient portion, the average degree of consolidation is expressed as:

$$\overline{U}_f = 1 - \frac{h^2}{\eta C_v t_f} \qquad \text{Equation 2.1}$$

where h = ½ height of specimen
η = a factor depending on drainage conditions at the specimen boundaries (Table 2.2)
C_v = coefficient of consolidation
t_f = time to failure

Drainage Conditions	η
One end only	0.75
Both ends	3.0
Radial boundary only	32.0
One end and radial boundary	35.8
Both ends and radial boundary	40.4

Table 2.2 Values of η for Various Drainage Conditions

Bishop and Henkel (1962) compare results from drained tests to the theoretical expressions used above and show that there is little change in strength at a degree of consolidation greater than 95% (actually perhaps even 90%). Using 95%, the time to failure may then be written as:

$$t_f = \frac{h^2}{\eta C_v 0.05} = \frac{20h^2}{\eta C_v} \qquad \text{Equation 2.2}$$

In order to choose an appropriate rate based on t_f, the strain at failure needs to approximated. The failure strain depends on OCR, consolidation stress state, and test stress path. For isotropically consolidated tests in compression loading, strains typically range from 20% to 25% for normally consolidated specimens and is only a few percent for specimens at high OCR. Bishop & Henkel (1962) provide a table summarizing strain at failure for various types of soil, but some previous knowledge of the soil is preferable.

In calculating the values of η, it has been assumed that for radial drainage the specimen height is twice the diameter. It is also assumed that the drains are fully effective, meaning that they are continuous around the specimen and infinitely permeable, making the water pressure at the drainage boundary zero. In reality, this is often not an accurate assumption since radial drainage is occurring through thin filter paper drains. These drains only cover part of the curved surface and have a finite hydraulic conductivity.

To address the problem of not having fully effective radial drainage, Bishop and Gibson (1963) have examined the effect on the calculated value of coefficient of consolidation and time to failure as determined from the Taylor square root of time method. They define a parameter ν to describe the effectiveness of the drains, taking into account the relative hydraulic conductivity of the drains and soil and the geometry of the system:

$$\nu = \frac{\pi^2}{4} \frac{k_p}{k_r} \frac{R\delta}{h^2} \qquad \text{Equation 2.3}$$

where k_p = hydraulic conductivity of the filter paper
k_r = hydraulic conductivity of the soil in the radial direction
R = radius of the specimen
δ = thickness of the filter paper drain

This is then entered into a more complete expression for the average degree of consolidation to calculate the true time to failure, $t_{f\ \text{actual}}$. Table 2.3 (Bishop and Henkel, 1962) summarizes the effect of drainage conditions on testing time, where $t_{f\ \text{calculated}}$ is the apparent time to failure calculated assuming the drains are fully effective. The table also includes a comparison of the coefficient of consolidation calculated assuming infinitely permeable drains to that calculated to account for the effectiveness.

ν	$C_{v\ calculated}/C_{v\ actual}$ I. Drainage to one end plus radial	$C_{v\ calculated}/C_{v\ actual}$ II. Drainage to both ends plus radial	$t_{f\ calculated}/t_{f\ actual}$ For Case II
∞	1.00	1.00	1.00
100	0.834	0.953	1.02
10	0.341	0.674	1.18
5	0.212	0.515	1.23
1	0.064	0.208	1.25

Table 2.3 Effect of Drainage Conditions on Calculated Time to Failure

As the effectiveness of the drains decreases, there is more error in the computed values of C_v. Because this method does not compute the true values of C_v, it is important to note that they should never be used as field values, they are a tool for choosing strain rate only. The conventional method results in low values of C_v, leading to slower than required rates during the shear phase of the test. This is an acceptable error that does not cause significant changes in the measured strength.

The method for choosing the strain rate for drained shear is essentially the same process. The strain rate is controlled by the time required for equalization of non-uniform pore pressures, however this value is not easily calculated to support the theory. A theoretical relationship obtained by Gibson (Bishop and Henkel, 1962) is shown in Figure 2.4 and relates the degree of equalization to the time factor T. The degree of equalization is defined as $1 - p/p_o$, where p_o is the difference in pore pressure between the middle and the ends of the specimen at a given strain with no redistribution and p is the difference in a test taking a time t to reach this strain.

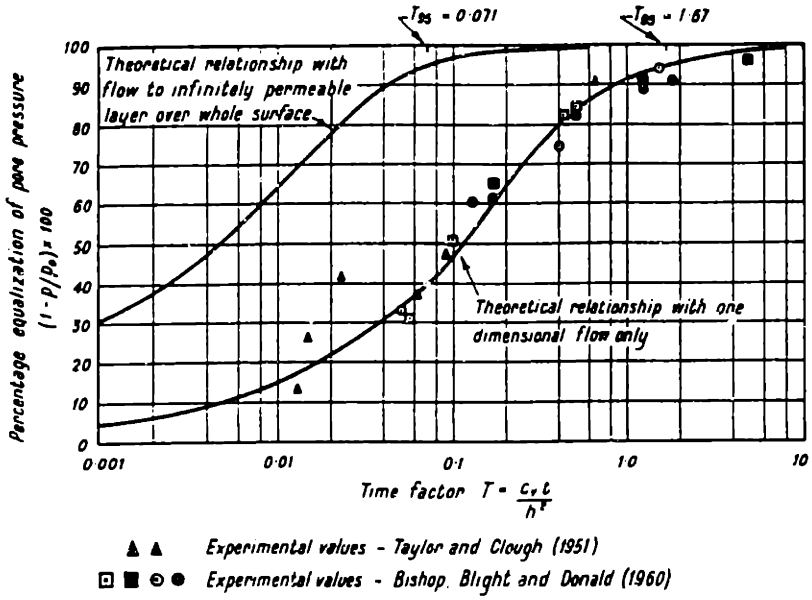

Figure 2.4 Equalization in the Undrained Test (Bishop and Henkel, 1962)

This relationship was formulated based on the following assumptions:

1) The rate of loading is constant.
2) The non-uniformity of pore pressure is parabolic over the height of the specimen.
3) The difference in pore pressure is proportional to the magnitude of the stress increment.
4) The coefficients of consolidation and of swelling are the same.

Ideally, a time factor should be chosen so that the degree of equalization approaches 100% (Bishop, Blight, and Donald 1960). Choosing 95% leads to a time factor of 1.67 for the case of no radial drainage and 0.071 for tests with radial drainage. With a value of C_v calculated as in the drained test, the undrained testing time may be calculated from the time factor.

Difficulty arises in measuring p_0 because tests must be performed at very high strain rates to achieve no redistribution. Instead, a number of tests are run at suitable rates and the theoretical degree of pore pressure equalization is plotted against the observed difference in pore pressure. The observed difference is then extrapolated to a theoretical degree of equilization of zero to obtain p_0.

Tests have been run by Taylor and Clough (1951) and Bishop, Blight, and Donald (1960) with no radial drainage. Little information on these tests is provided by Bishop and Henkel (1962), but the results are included in Figure 2.4 and show reasonable agreement with the theoretical relationship. A similar relationship for the case of fully effective drainage over the entire curved surface is also shown in the figure. Tests with drains referred to by Bishop and Henkel run at Imperial College do not exhibit the unequalized pressures predicted, however this may be due to a connection between the measurement locations by the drainage paper. This suggests that the drains may not be effective during undrained shear.

As with the drained test, the approximate strain to failure is required. The strain to failure is a function on the type of consolidation, type of loading, and overconsolidation ratio. Typically the strain increases with the consolidation stress ratio ($\sigma'_{hc}/\sigma'_{vc}$), OCR, and shear in extension (Germaine and Ladd, 1988).

Using the coefficient of consolidation calculated from the last increment during consolidation for choosing both the drained and undrained shear rates has several advantages. The consolidation occurs at an optimal rate and the shear rate is automatically adjusted to the particular specimen conditions. In effect, the method accounts for the consolidation properties of the specific specimen and the effectiveness of the drainage conditions.

2.3 Continuous K_o Consolidation

2.3.1 Constant Rate of Strain Consolidation Theory

Until the early 1970's, the consolidation characteristics of cohesive soils were determined primarily from the incremental oedometer test. Because the increments are typically left on for longer than necessary (24 hours rather than to the end of primary which may occur in a matter of minutes), this test is frequently time consuming and may take several weeks to run. In addition, because a load increment ratio (LIR) of one is typically used, there are large gaps between data points, and the results may not adequately define certain S-shaped compression curves associated with sensitive clays. Using a smaller LIR to better define the compression curve often results in

a Type III settlement curve, making it difficult to define the time to primary and therefore the value of C_v.

One alternative to the incremental test is the constant rate of strain consolidation (CRS) test. This test is run on approximately the same size specimen as in the incremental oedometer, similarly trimmed into a rigid ring. It is completed in only a few days and provides a continuous compression curve. Because the test has new boundary conditions, it requires a different analysis than that used for the incremental oedometer. Smith and Wahls (1969) and Wissa et al (1971) have related both the coefficient of consolidation and the hydraulic conductivity to quantities measured during the test. The relationship of most interest to this research is that relating excess pore water pressure to the strain rate and hydraulic conductivity. This is more difficult at the beginning of the test due to the transient condition that develops immediately as the piston is set in motion. Wissa et al (1971) derive an expression to model the transient portion and show that it is insignificant after a time factor of 0.5.

Figure 2.5 shows a schematic of the general purpose consolidometer developed by Wissa at MIT. The test specimen held inside a stainless steel ring rests directly on a fine ceramic stone epoxied into the base. The specimen is typically loaded at a constant rate of strain by moving the piston with a gear driven load frame. During the test the excess pore pressure at the base of the specimen is measured by a transducer connected through the porous stone, the pressure at the top of the specimen is measured through another transducer outside the apparatus, the load is measured by an external load cell, and the displacement is measured by an LVDT on the piston. Section 3.2 includes a complete description of the apparatus and some recent modifications to the equipment.

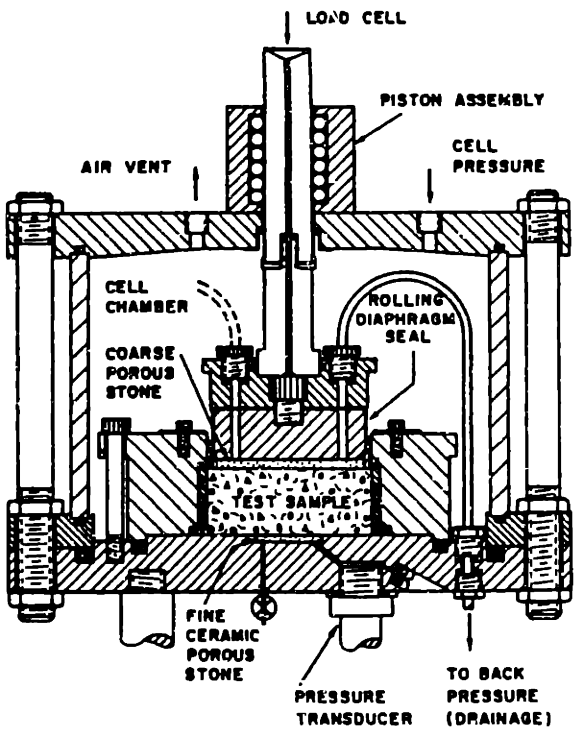

Figure 2.5 MIT General Purpose Consolidometer

2.3.1.1 Smith and Wahls

The first solutions for the CRS test were developed by Smith and Wahls (1969) and apply only to the steady state portion of the test that is reached after the transient portion has dissipated. Their formulation is very similar to the Terzaghi one-dimensional theory, making some but not all of the Terzaghi assumptions. The following are assumed:

1) The soil is both homogeneous and saturated.

2) Both the water and the solids are incompressible relative to the soil skeleton.

3) Darcy's law is valid for flow through the soil.

4) The soil is laterally confined and drainage occurs only in the vertical direction.

5) Both the total and effective stresses are uniform along a horizontal plane, i.e., stress differentials occur only between different horizontal planes.

6) Infinitesimal strains exist.

They use the basic equation for consolidation based on the continuity of flow through a soil element:

$$\frac{\partial}{\partial z}\left(\frac{k}{\gamma_w}\frac{\partial u}{\partial z}\right)=\frac{1}{1+e}\frac{\partial e}{\partial t} \qquad \text{Equation 2.4}$$

where z = vertical coordinate of the point
k = hydraulic conductivity
γ_w = unit weight of water
u = excess pore water pressure
t = time
e = void ratio

In order to solve this nonlinear, partial differential equation, they further assume that the hydraulic conductivity is a function of the average void ratio and is therefore independent of z. They also assume that because there are no lateral strains and the strain rate is constant, the volumetric rate of change is also a constant, making $\partial e/\partial t$ constant. The final assumption is that the void ratio of the soil varies linearly with depth. The final expression for the excess pore water pressure at the base of the specimen is a function of hydraulic conductivity and rate of change of the average void ratio only:

$$u_{base} = \frac{1}{2}\frac{sH^2\gamma_w}{k(1+\bar{e})} \qquad \text{Equation 2.5}$$

where u_{base} = excess pore water pressure measured at the base
s = rate of change of the average void ratio
H = height of specimen
$\bar{e}$ = average void ratio

2.3.1.2 Wissa et al

Wissa et al (1971) developed a more general solution that includes the initial transient behavior, making the following assumptions:

1) Infinitesimal strains exist.
2) The coefficient of consolidation, C_v, is independent of depth at any time.
3) Deformation and flow occur in the vertical direction only.
4) Both the water and solids are incompressible relative to the soil skeleton.
5) The soil is completely saturated.

They then write the governing equation for consolidation in terms of strain rather than stress as done by Smith and Wahls:

$$C_v\frac{\partial^2\varepsilon}{\partial z^2} = \frac{\partial\varepsilon}{\partial t} \qquad \text{Equation 2.6}$$

where $C_v = k/\gamma_w m_v$

ε = vertical strain
m_v = coefficient of volume compressibility

The solution to this equation (in Appendix of Wissa et al, 1971) gives the strain at any point and time within the specimen as:

$$\varepsilon(X,T_v) = rt\left[1 + F(X,T_v)\right] \qquad \text{Equation 2.7}$$

where $X = z/H$
H = height of specimen
$T_v = C_v t/H^2$

$$F(X,T_v) = \frac{1}{6T_v}\left(2 - 6X + 3X^2\right) - \frac{2}{\pi^2 T_v}\sum_{n=1}^{\infty}\frac{\cos n\pi X}{n^2}\exp\left(-n^2\pi^2 T_v\right)$$

The two components of the strain equation help explain what happens during the test. The first part of the equation, rt, represents the average imposed strain, or what the case would be if the strains were the same everywhere in the specimen. The second part, F, is made up of two parts. The first represents the deviation of the strain with position from the average strain in the steady state case. It is this deviation that provides the gradient necessary for a constant flow of pore fluid. The second part is the transient term describing the decay of the initial discontinuities present as the test is started. Figure 2.6 shows the deviation from the average strain as a function of depth for various times in the test. This illustrates that for times greater than T_v = 0.5, the transient component is insignificant.

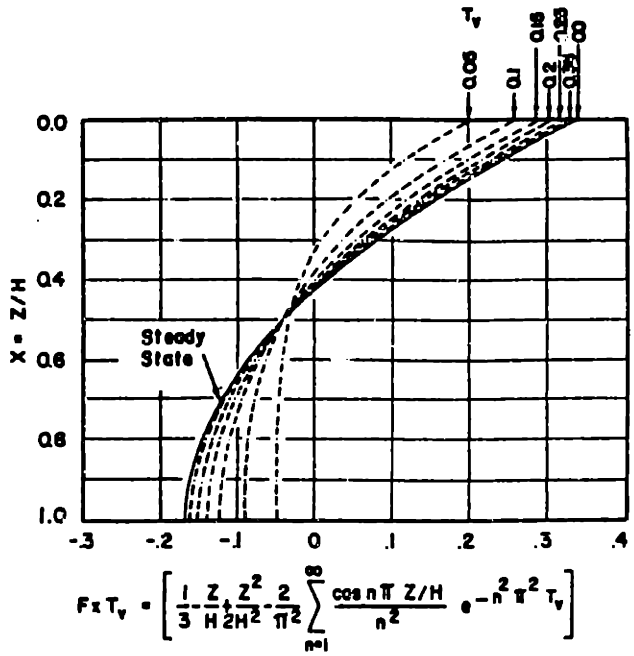

Figure 2.6 Deviation of Strain from Average (Wissa et al, 1971)

The solutions described above have not assumed a form for the stress strain relationship. In order to interpret the data from the test (after the transient portion has dissipated), it is necessary to assume a form for the stress strain relationship. Wissa et al provides solutions for two different possibilities.

The first assumes that the soil is linear, so the effective stress strain relation is defined by a constant coefficient of volume compressibility, m_v. This leads to the following solution:

$$u_{base} = \frac{1}{2}\frac{rH^2\gamma_w}{k} \qquad \text{Equation 2.8}$$

The variable r in this case is the strain rate rather than the rate of change of void ratio as used in the equation by Smith and Wahls. Smith and Wahls have the term $(1+\bar{e})$ in the denominator of their equation. If this were instead $(1+e_0)$, the two equations would be identical. But this slight difference causes little change in the values computed. The average effective stress for the linear case is then defined as:

$$\sigma'_{v_{ave}} = \sigma_v - \frac{2}{3}u \qquad \text{Equation 2.9}$$

The second reasonable assumption for the effective stress strain relation is of nonlinear soil where:

$$-\frac{d\varepsilon}{d\left(\log \sigma_v\right)} = C_c$$ Equation 2.10

This leads to the following equation for coefficient of consolidation:

$$C_v = -\frac{H^2 \log\left(\frac{\sigma_{v2}}{\sigma^{v1}}\right)}{2\Delta t \log\left(1 - \frac{u_{base}}{\sigma_v}\right)}$$ Equation 2.11

The hydraulic conductivity is then calculated as $k = c_v m_v \gamma_w$. The effective stress equation is also changed, but with the excess pore pressures typically generated (0.1% of σ_v) the effective stress decreases by only 1% from that calculated by linear theory. The equation is:

$$\sigma'_{v_{use}} = \left(\sigma_v^3 - 2\sigma_v^2 u + \sigma_v u^2\right)^{1/3}$$ Equation 2.12

2.3.2 Conventional Consolidation Equations

The alternative to the CRS test analysis is presented by Gibson and Henkel (1954) and Bishop and Gibson (1963). The theory was derived for analysis of drained shear under continuous loading. This analysis uses Terzaghi's consolidation equation relating pore pressure to position and time, adding an additional term to generate pore pressure with time. Unlike the equations for the CRS, the results predict that the degree of consolidation is related to the loading rate and coefficient of consolidation.

This analysis is focused on finding a prediction of excess pore pressure dissipation during the drained triaxial test. Although shear tests have different deformation conditions than K_o consolidation (shear has lateral spreading while consolidation does not), the expressions derived by Gibson and Henkel (1954) should be applicable to both cases since the solutions consider small strains only.

The analysis starts with the general theory of consolidation developed by Biot coupling pore pressure and compressibility:

$$k\nabla^2 u + \frac{\partial \Delta}{\partial t} = 0$$ Equation 2.13

where u = excess pore water pressure

t = time
k = hydraulic conductivity
Δ = volume change per unit volume

To solve the equation in terms of pore pressure only, the compressibility is related to changes in effective stress by Skempton's equation. Separating the effective stress into changes in pore pressure and changes in total stress provides two terms: $\partial u/\partial t$, and a second term that is still a function of changes in total stress. Assuming that the generation of excess pore pressure is proportional to the increase in total stress replaces the total stress term with a term $\partial u_o/\partial t$. It is then assumed that the total stress increases at a constant rate and hence $\partial u_o/\partial t$ is replaced with a constant $\overline{R}$, providing the following equation:

$$C_t \nabla^2 u = \frac{\partial u}{\partial t} - \overline{R} \qquad \text{Equation 2.14}$$

where C_t is the consolidation coefficient relevant to this type of test. $\overline{R}$ is the rate at which the pore water pressure, u_o, would increase with time in an undrained test. Figure 2.7 shows hypothetical curves for a consolidated, undrained test at a constant rate of strain. These curves relate the pore pressure and deviator stress ($\Delta\sigma_1 - \Delta\sigma_3$) to axial strain. Idealized, the pore pressure increases at a constant rate, $\partial u_o/\partial t$, up to a maximum at the time of failure and then remains constant (along with the deviator stress).

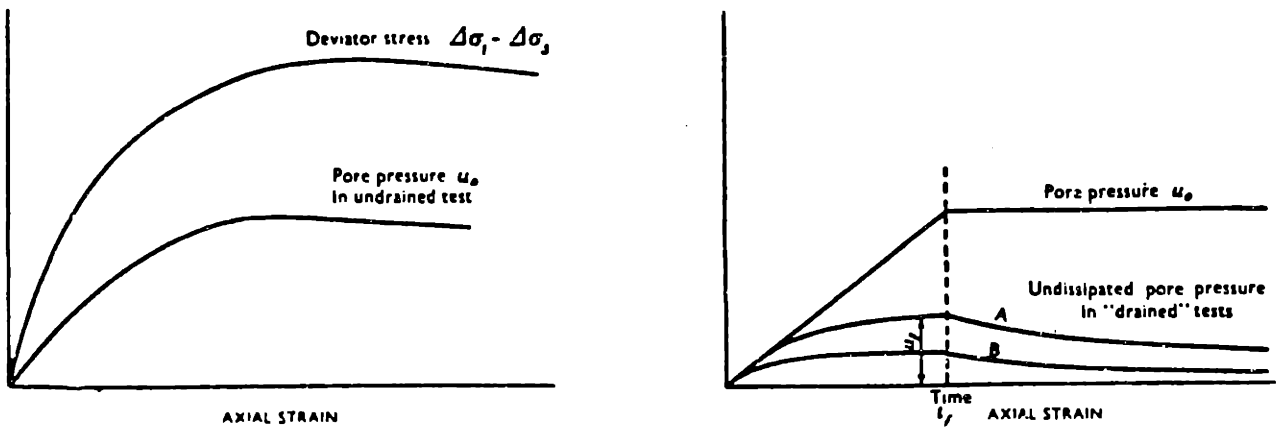

Figure 2.7 Pore Pressure Generation in Triaxial Tests (Gibson and Henkel, 1954)

Equation 2.14 has been solved, relating the average value of the undissipated pore pressure over the specimen to the total time from start of loading for different drainage boundary conditions.

The solution is fairly involved and is shown in Gibson and Henkel (1954). Neglecting the exponential terms provides the following equation for the degree of consolidation as a function of time:

$$U = 1 - \frac{h^2}{\eta C_v t} \qquad \text{Equation 2.15}$$

Equation 2.15 is the same as Equation 2.1 but generalized to any increment in time from the start of loading rather than to the time of failure only. As before, η varies for the drainage conditions (refer to Table 2.2 for values).

This equation completely ignores the series that includes the exponential terms. To determine when this is a reasonable simplification, the data from one constant rate of strain consolidation test was considered. C_v was calculated based on Equation 2.15, then calculated including the first term of the series. The results are presented in Figure 2.8. The results are identical after a time factor of 2, indicating that the equation may correctly be used after this point.

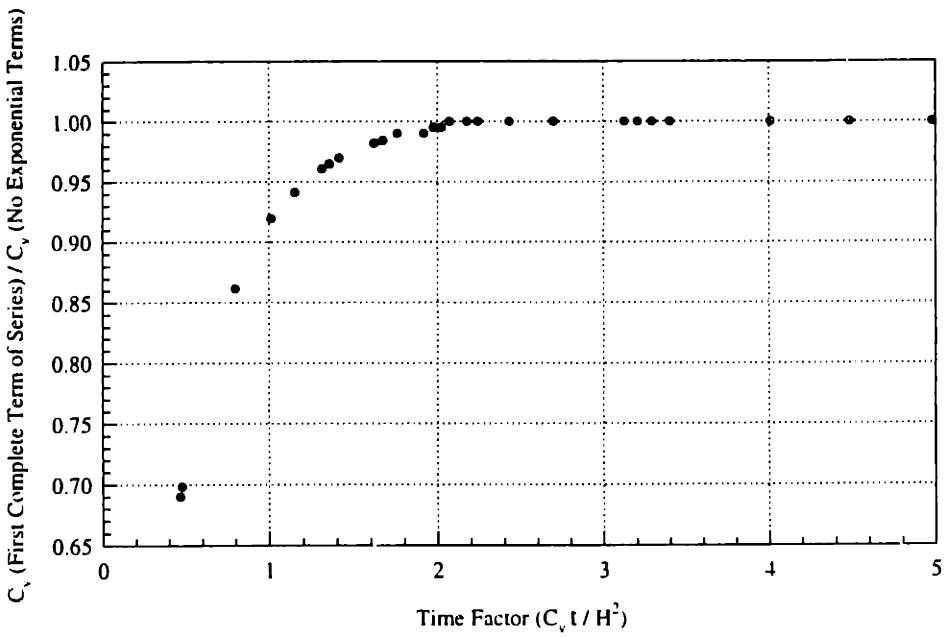

Figure 2.8 Effect of First Term of Series on Coefficient of Consolidation

This equation should also be relevant to K_o consolidation for a given increment in stress from the start of loading. The application of the theory to K_o consolidation is actually simpler than the

case used for the above solution. For K_o consolidation, the pore pressure generated in a test if there were no drainage is exactly equal to the change in applied load rather than some fraction of the deviator stress as shown in Figure 2.7, making u_o easy to estimate. As with the drained test, the rate of pore pressure increase, $\overline{R}$, is assumed to be constant.

2.4 Influence of Side Drains

The following section discusses some specific details regarding the common applications of side drains and the standard corrections required. The filter drains are commonly placed between the curved surface of low hydraulic conductivity specimens and the membrane. This significantly shortens the drainage path during both consolidation and drained shear by allowing radial flow in addition to vertical flow, allowing routine tests to be run in acceptable lengths of time. If the drains had infinite hydraulic conductivity, the drained test in compression could be performed more than ten times faster. Undrained shear testing times are also decreased because the drains accelerate the equalization of pore pressures. The drains, however, have a finite hydraulic conductivity and do not typically cover the entire curved surface. There are equations for effectiveness of the drainage system that try to account for this, however more investigation is needed to understand the effects of partial coverage.

2.4.1 Geometry

Ideally, the most efficient application of side drains would be a continuous porous jacket enclosing the specimen, as tried by Jurgenson in 1934, providing continuous drainage through all surfaces of the specimen. The measured deviator stress, however, is significantly affected by the strength of the drains, making it necessary to instead use a series of drainage strips.

For standard 1.5 inch diameter specimens in compression, Bishop and Henkel (1962) suggest using a jacket, shown in Figure 2.9, cut with a razor from a single piece of filter paper. This jacket is wrapped around the specimen, overlapping the porous disks at either end. At MIT however, eight separate ¼ inch by 3 ½ inch strips are placed on the specimen vertically. For extension tests, the effect on strength is more critical, so five ¼ inch by 8 inch strips are wrapped spirally around the specimen. Both layouts are shown in Figure 2.10. Cuts are made half way

across the strips every centimeter from alternating sides and placed on the specimen at an inclination of 1:1.5. This inclination is chosen so that the drains do not affect radial deformation of the specimen (Berre, 1982). In both cases, the strips are soaked in water, then tucked between the rubber sleeves and the pedestal prior to setup. Once the stones and specimen are placed on the pedestal and the top cap set in place, the filter strips are extended along the specimen and tucked between the top cap and rubber sleeve.

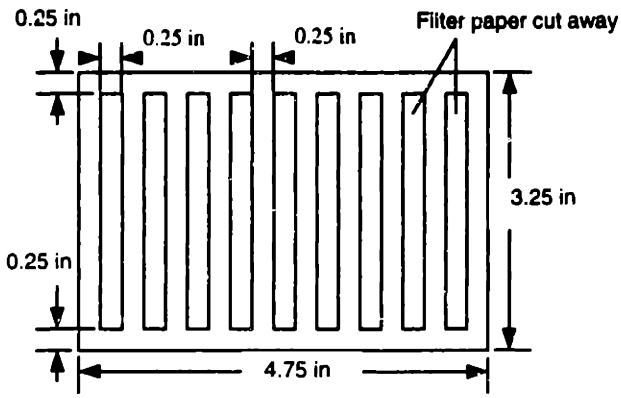

Figure 2.9 Drainage Jacket Used by Bishop and Henkel (1962)

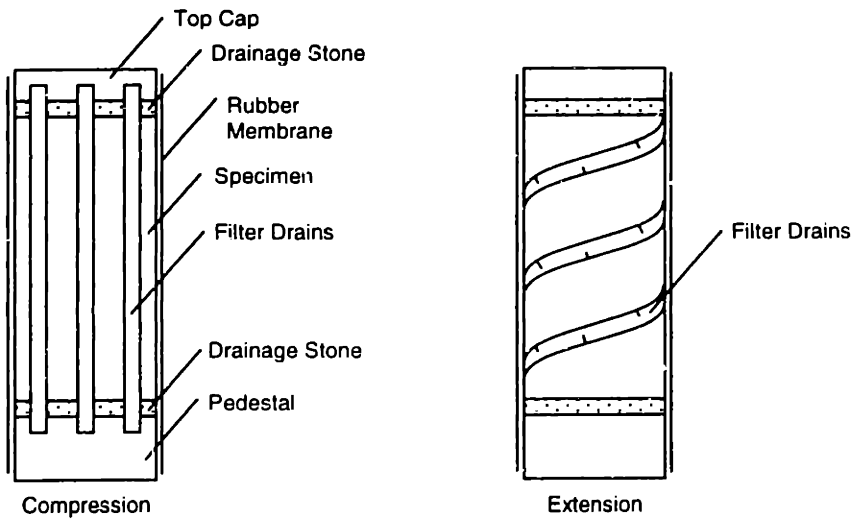

Figure 2.10 Filter Paper Layout for Compression and Extension

The type of paper used should not soften in water so that it will maintain a drainage path and also may be easily removed at the end of the test. Whatman 54 is most common, although this may be too stiff for use with soft clays due to problems with buckling. In cases with especially soft

soil and hard filter paper it is possible for the paper to buckle and penetrate into the soil resulting in a reduction in strength (Olson and Kiefer, 1963). An alternative is using a softer paper, such as Whatman 1, but this tears easily (during setup for instance) and may be difficult to remove from the specimen after testing.

2.4.2 Filter Drain Resistance

There has been little recent research about the compressive resistance of the side drains used in triaxial strength tests. It is generally accepted that vertical filter drains carry some of the vertical load applied to the specimen and spiral drains carry no load (Germaine and Ladd, 1988). However, the distribution of this load with strain and the magnitude of the maximum value are highly approximate. In conventional practice, it is assumed that the filter drains carry linearly increasing load with axial strain, reaching a maximum value at 2 to 3 % strain expressed by:

$$\Delta\sigma_{ufp} = K_{fp}(P/A_s) \qquad \text{Equation 2.16}$$

where $\Delta\sigma_{ufp}$ = maximum correction to axial stress for compressive strength of filter paper drains
K_{fp} = load per perimeter of filter paper
P = length of perimeter covered by filter paper
A_s = specimen area

In order to determine the value of K_{fp}, comparative tests were performed with and without filter paper drains. Results referred to by Bishop and Henkel (1962) for triaxial specimens with ¼ inch Whatman 54 strips lead to a value of K_{fp} of 0.19 kg/cm. Other tests at the University of California have been run on plane strain specimens with Whatman 54 paper and result in a value of 0.13 kg/cm (Duncan and Seed, 1967). This difference in K_{fp} may be due to the confining nature of drains in triaxial tests, while drains in plane strain tests can carry load only through column action.

More recent observations (R.S.Ladd, 1998), however, suggest that the corrections are not adequate and that more research is necessary in order to eliminate the errors in strength caused by the presence of the filter drains. The behavior of the drains appears to be a function of the stiffness of the specimen based on the observation that wrinkles may penetrate into the soil, away from the soil or be totally suppressed. Drains are assumed to buckle at 2 to 3% axial strain, yet

during K_o consolidation testing no wrinkles are observed even though the specimen is at 10% strain. Finally, comparison tests of Gulf of Mexico clay on specimens having vertical and spiral filter drains yield different K_o values after the drain corrections are applied to the data. All the above information suggests that the current correction is missing important elements of the drain behavior.

2.4.3 Filter Drain Hydraulic Conductivity

The hydraulic conductivity of the filter paper is an important factor in defining the effectiveness of a drain system (see Equation 2.3). Bishop and Gibson (1963) refer to results from tests done by D.L. Webb at Imperial College. No details are included, however other sources assume that this refers to Whatman 54 filter paper. The following table relates the filter paper hydraulic conductivity for flow along the length of a strip to the confining stress. Complete characterization of the hydraulic conductivity over the conditions experienced in the triaxial test is an important subject for this research.

Confining Stress (psi)	Hydraulic Conductivity (cm/s)
4.5	1.7×10^{-3}
10	8.7×10^{-4}
30	3.2×10^{-4}
100	5.4×10^{-5}
300	1.1×10^{-5}
950	1.0×10^{-6}

Table 2.4 Filter Paper Hydraulic Conductivity as Reported by Bishop and Gibson (1963)

Chapter 3 Equipment and Procedures

3.1 Resedimented Boston Blue Clay

Resedimented Boston Blue Clay (RBBC) was used for this research in order to provide a uniform material with constant and known properties between all tests. The natural material is a lean illitic glacio-marine clay of low to medium sensitivity deposited in the Boston basin. Germaine (1982) developed a resedimentation technique to produce saturated, uniform b··ches of BBC. The process has been modified by a number of researchers, with the most recent procedures best described by Seah (1990). In addition to being a uniform material with established properties, RBBC has the advantage that its behavior is representative of natural, uncemented clay deposits. Therefore, trends in behavior may be generalized to properties of many natural deposits with adjustment to specific site conditions.

3.1.1 Batching Procedure

The material for the batch of RBBC used in this research is part of Series IV, obtained in 1992 from the base of an excavation for MIT's Biology Building (Building 68). The natural material was retrieved from a depth of approximately 12 meters with overconsolidation ratio from 1.3 to 4.3. Softened with tap water, the material was mixed into a thick slurry and passed through a #10 US standard sieve to remove all large soil particles, wood, and shells. The slurry was then oven dried and ground to a powder with 95% passing a #100 US sieve. This stock powder is stored in sealed 40 gallon containers until it is used to make blocks of resedimented material (Cauble, 1996). The remainder of the resedimentation process is divided into four stages: sedimentation, consolidation, extrusion, and trimming.

The equipment used for mixing and sedimentation is shown in Figure 3.1. Under a vacuum, 15 kg of oven-dried powder and 15 kg of deaired, distilled water are added alternately in small quantities to the mixing chamber. Approximately 100 gm of sodium chloride (a flocculant) and 2 ml of phenol (a bacterial growth inhibitor) are also added to the slurry during initial steps of the process. Throughout the addition of all components, the upper chamber is isolated from the lower chamber, and the mixing blades are rotating at approximately 60 rpm. With all ingredients

added, the slurry, at roughly 100 % water content, is mixed for 30 minutes at 120 rpm. Finally, while still under a vacuum, the two chambers are connected and the slurry is sprayed through the lower free-fall chamber into the consolidometer.

At this point the vacuum is released, the free-fall chamber is removed, and the consolidation process begins. The slurry is incrementally loaded with a load increment ratio (LIR) of 1 up to a maximum stress of 1 ksc, then unloaded to 0.25 ksc to produce an OCR of 4. This is done in 7 loading increments, each left on for 48 hours to allow full primary consolidation, beginning with the application of 0.0156 ksc. Figure 3.2 shows the loading geometries required at different stress levels. At very low stresses, it is necessary to have a pulley and counterweights to compensate for the weight of the piston. Once the increment is larger than the weight of the piston and attachments, weights are set directly on the piston. Finally, for stresses over 0.125 ksc the consolidometer is moved into a loading frame where the load is applied by a pressure chamber. During the entire consolidation process, the vertical deformation is measured by a displacement transducer, and once in the load frame, the force is measured by a load cell.

Several methods are reported for the extrusion procedure. For the batch used in this research, the tie rods and bolts were removed such that the piston, steel chamber, and porous base were independent of each other. The piston was then held in place, trying not to apply excessive pressure to the soil, while the chamber was pulled vertically away from the soil. This leaves the final soil cake resting on the porous base. In general it is believed that the RBBC is characterized by low sample disturbance because at an OCR of 4, the soil is very close to a hydrostatic stress state, resulting in minimal shear strains from removal of the sample from the chamber (Santagata, 1994).

Finally, the sample is cut in several large pieces, being careful that the soil is always supported by plexiglass and not moved by hand. The size of these smaller pieces depends on the expected tests, so some planning is required to maximize the number of specimens obtained from each batch. Each piece of soil is wrapped with plastic wrap, a layer of a 1:1 mixture of paraffin wax and petroleum jelly, a second layer of plastic, and a second layer of the wax mixture. Ideally the

pieces are stored in a humid room at 90 – 100 % relative humidity with stable temperature, keeping the water content constant until they are used for testing.

3.1.2 Index Properties

Material index tests are a useful way to compare properties between series and batches of RBBC and also provide a measure of quality control. Because RBBC has been used so extensively at MIT, a large database of both index and engineering properties exists, and it is beneficial to be able to compare the current batch to the database. Table 3.1 summarizes index tests run on batches from Series IV RBBC, while Table 3.2 summarizes index tests run on batches from the previous three series (Cauble, 1996).

Measurements of specific gravity were not run for this research, however the value has been fairly consistent between batches. Results from previous series range from 2.75 to 2.785, although Cauble reports a higher value of 2.81 for Series IV. An average value of 2.78 was chosen for this research.

Figure 3.3 shows Atterberg limits reported by Cauble (1996) for Series IV RBBC. One set was run on the current batch (No. 420) to confirm that the batch is typical of this series. The plastic limit is $w_p = 22.6\%$, the liquid limit is $w_l = 45.2\%$, and the plasticity limit is $I_p = 22.6\%$. Data are included in the Appendix. These are within the standard deviation of the values reported by Cauble: $w_p = 23.5 \pm 1.1\%$, $w_l = 46.1 \pm 0.9\%$, and $I_p = 22.7 \pm 1.4\%$. This difference measured between the current batch and the values reported by Cauble may simply be due to operator variability and it is well within the acceptable range of results specified by ASTM.

Figure 3.4 shows grain size distribution curves for 5 different batches from Series IV and also includes a curve for the powder alone before sedimentation. The data are very consistent, with an average clay fraction of $58 \pm 1.2\%$. Salt content, measured by conductivity and calibrated against a KCL standard, was 11.6 ± 1.5 g/l (Cauble 1996). The salt content should be adjusted during batching to reach a concentration of 16 g/l to control clay fabric. Recent batches, however, have not been properly adjusted, resulting in the lower value reported by Cauble.

Table 3.2 includes values of salt content in previous research, ranging from from 2 g/l to 35 g/l. Organic content by loss on ignition was 4.4% for this series, however these data are not available for previous series (Cauble 1996).

Engineering properties of RBBC relating to consolidation will be discussed in Chapter 4 and play an important role in this research. For more detailed summary of the material properties, see Santagata (1998).

3.2 Constant Rate of Strain Apparatus

3.2.1 Wissa Consolidometer

A general purpose consolidometer was developed at MIT by Wissa et al (1971). This device provided more flexibility in testing than the conventional incremental oedometer test. With the new apparatus, specimens could be saturated at constant volume under a backpressure, then loaded with no lateral strains by three different methods: under incremental loads, at a constant rate of strain, or at a constant rate of stress. The same equipment is used for this research although it has been modified as described in the following sections.

A schematic of the original consolidometer is shown in Figure 3.5. Figure 3.6 shows the same device with the recent modifications. Formerly, the device had two separate chambers, the cell chamber and the test specimen chamber. The two were hydraulically isolated from each other by a rolling diaphragm seal connected between the loading cap and the outer retaining ring. With this arrangement, the specimen could be loaded incrementally by increasing the cell pressure in increments or by externally loading the piston using a hanger and weights or an air jack. It could be loaded at a constant rate of stress by increasing the cell pressure at a constant rate. Finally it could be loaded at a constant rate of strain by a gear driven load frame moving the piston at a constant velocity. However, with the retaining ring and the top cap connected by the diaphragm, large seating errors occurred. The problem was solved by the removal of the diaphragm, although constant rate of stress consolidation is no longer possible.

Originally, drainage occurred through a coarse porous stone epoxied to the underside of the top loading cap. This was connected to drainage lines leading to valves in the base plate, and onto a twin burette volume change apparatus to monitor flow. With the removal of the diaphragm seal, the top of the specimen is directly open to the cell chamber pressure. The loading cap was also modified to be permanently attached to the piston. In addition, the stone is no longer attached, allowing it to be boiled or placed in ultrasound for cleaning and saturation. The drainage lines were removed, and the cell chamber pressure is now controlled through the opening in the base plate where the top drainage lines were previously connected. Mercury pots are raised vertically to increase the pressure and are connected to a mercury water interface leading to the chamber.

The excess pore pressure is measured on the bottom face of the specimen through the base of the apparatus. A high air-entry ceramic porous stone is epoxied into a recess in the center of the base plate. A small hole connects the stone to the pressure transducer, and another small hole serves as a vent when connecting the transducer. The pore pressure measuring system has very low volume compressibility, making response time short, though it is very important that the system be completely saturated.

The specimen is trimmed into a thin walled stainless steel retaining ring using a removable knife-edge shoe cutter. Monofilament nylon is placed on the top of the specimen, however there is no filter paper on the bottom, and the specimen ring and specimen are placed directly on the ceramic stone in the base. A sturdier outer retaining ring is fit over the specimen ring and the two are sealed together by an o-ring at the base. Another o-ring seals the outer ring to the base plate, and finally the chamber is bolted to the base plate and sealed by a third o-ring. The loading platen is moved up until the piston is in contact with the load cell and a small seating load applied. The chamber is then filled with water and connected to the manifold. Backpressure saturation is performed in small increments to a pressure of 4 ksc, maintaining a constant specimen height throughout the process. After allowing the system to equilibrate overnight, a constant rate of strain is applied by a gear controlled motor. Once to the desired load or strain, the load is transferred to an air jack, and left on for 24 hours to allow secondary compression before unloading. The central data acquisition computer records the axial displacement, load, pore pressure, and chamber pressure for test interpretation.

A detailed procedure for setting up and running the constant rate of strain consolidation test in the modified consolidometer is included in the Appendix. Information on running the test in the original device can be found in Wissa et al, 1971.

3.2.2 Apparatus Compressibility

The apparatus deflects due to both changes in cell pressure and axial load. This compressibility needs to be quantified in order to calculate the correct height of the specimen during both saturation and consolidation. As the chamber pressure is increased during backpressure saturation, corrections are made manually to the piston position to keep the height of the specimen constant at the initial height. Step by step procedures for height adjustments during saturation are included in the Appendix. The loading deflections are primarily required to correctly compute the height of the specimen during data reduction of the consolidation phase of the test.

For evaluating compressibility, the device was set up with a steel dummy, assumed to be incompressible, the top porous stone, and the top filter paper, made of monofilament nylon. For calculating the compressibility due to changes in cell pressure, a seating load of 1 kg was applied before filling the cell with water. A cell pressure of 0.5 ksc was then applied, and the piston manually adjusted until the load applied to the dummy was again 1 kg. At this point the cell pressure and the displacement are measured. This was repeated for cell pressures up to 4 ksc. The slope of the line fit through the pressure displacement data provides the apparatus compressibility: $\delta_c = 0.001*\sigma_c$, where δ_c is the deflection in centimeters due to change in cell pressure and σ_c is the cell pressure in ksc. Figure 3.7 show the plots of these data. The process was repeated again at a seating load of 10 kg, and the resulting data gave approximately the same slope, indicating that the compressibility is not affected by seating load.

For the deflection due to loading, the device was again set up with the steel dummy, stones, and filter paper. The cell pressure was set to 4 ksc, and the device loaded and unloaded twice at a constant displacement rate while measuring the load and deflection. In a plot of net force

(corrected for cell pressure and piston weight) vs deflection, shown in Figure 3.7, a power function best fit the data, with the deflection: $\delta_l = 0.0031*(\text{load})^{0.2351}$, where δ_l is the deflection in centimeters due to loading, load (in kg) = load measured by load cell – $A_p*\sigma_c + W_p$, A_p is the area of the piston, and W_p is the weight of the piston. Calibrations and compressibility equations are summarized in Table 3.3.

3.2.3 Data Interpretation

A number of useful engineering properties are derived from the CRS data with very little effort on the part of the researcher (unlike the time consuming constructions required for interpretation of incremental oedometer data). The derivations of equations based on linear theory are discussed in Chapter 2 and lead to the following equations for hydraulic conductivity, coefficient of consolidation, and effective stress:

$$k = \frac{rH^2\gamma_w}{2u_e} \qquad C_v = \frac{H^2}{2u_e}\left(\frac{\Delta\sigma_v}{\Delta t}\right) \qquad \sigma'_{v_{ave}} = \sigma_v - \frac{2}{3}u_e$$

where k = hydraulic conductivity (cm/s)
r = strain rate (s^{-1})
H = height of specimen at given increment in time (cm)
γ_w = unit weight of water (kg/cm^3)
u_e = excess pore pressure measured at base of specimen (ksc)
C_v = coefficient of consolidation (cm^2/s)
$(\Delta\sigma_v/\Delta t)$ = rate of stress change (ksc/s)
σ'_{vave} = average effective stress (ksc)
σ_v = applied total stress (ksc)

A BASIC computer program calculates these values over each increment of the input data file. The program also includes calculations of apparatus compressibility to provide the correct specimen height. Variations in the measurements due to noise cause large variations in the calculated values of strain rate and stress rate. This variation becomes worse with more frequent readings. To remove this error the program puts a linear regression through a range of data specified by the user to provide a more accurate value of strain rate and stress rate for use in the hydraulic conductivity and coefficient of consolidation calculations. The window, however, starts with the data before loading has started, and continues through once loading is stopped.

Therefore the hydraulic conductivity and coefficient of consolidation data must be truncated over half of the specified strain for the window on either end of loading. The data at the start of loading must also be checked to see that the transient portion is over. As discussed in Chapter 2, the transient component is insignificant after a time factor of 0.5. The time factor for the initial data should be calculated and anything below 0.5 truncated.

One important point in the reduction of the CRS data is that the excess pore pressure in the first line of data is zero. When performing the test, the data acquisition readings should begin before loading while the system is fully backpressured with zero excess pore pressure. Then a zero value for the pore pressure transducer should be backcalculated so that the pore pressure exactly equals the cell pressure in the first line of data. This correction is necessary because the transducers are slightly nonlinear and the cell pressure and pore pressure measurements may be slightly different at the end of saturation while the true pressures are the same.

3.3 Triaxial Apparatus

3.3.1 Standard MIT Triaxial Apparatus

The standard MIT automated stress path triaxial apparatus is used for the majority of this research. The equipment is used in two different capacities, one in measuring the hydraulic conductivity of the filter paper and the other in measuring excess pore pressure during K_o consolidation. Each required some modification to the basic apparatus. The standard setup is described here, with the modifications explained in Section 3.3.2 and Section 3.3.3.

The triaxial equipment consists of the following main components: the triaxial cell, load frame, two pressure/volume control devices, motor control box, control computer, and central data acquisition system. Figure 3.8 is a schematic depicting the interaction of each of these elements.

The triaxial cell is shown in Figure 3.9. Pressure transducers located on the base measure the pore pressure and cell pressure with very little system compliance. The load applied to the specimen is measured directly by an internal load cell, an improvement over external measurements that included piston friction. The cell is filled with silicon oil (a nonconductive

fluid), allowing electronics inside the cell and preventing the diffusion of air and water through the membrane into the specimen. The displacement is measured by an external direct current LVDT, and the volumetric change is also measured by an LVDT on the piston of the pore pressure control device.

The triaxial cell is mounted on a Wykeham Farrance load frame inside a temperature controlled enclosure. Maintaining a constant temperature is especially important to the stability of the Kulite pressure transducer described in Section 3.3.3. The pore pressure and cell pressure lines are connected to two pressure/volume control devices. There are DC motors with tachometers on the load frame and two pressure/volume control devices. The computer sends a command signal to each of the motor controllers depending on the requirements of the motor and the specified pressure, force, or displacement.

The computer control is a fairly recent development, primarily implemented by Sheehan (1988). The control is carried out by a BASIC computer program that performs the initial pressure up, backpressure saturation, consolidation along any stress path, and shear in either compression or extension. The transducer measurements and input voltage are sent to the control computer and converted to engineering units. These units are compared to target values specified by the BASIC program. Based on the difference between the current and the target values, the computer sends a signal to the motor control box to adjust the motors.

This is an important improvement, allowing accurate K_o consolidation at a constant rate of vertical displacement. In this procedure, the axial motor loads at a constant rate while the computer calculates the axial and volumetric strains. The cell pressure is changed as a results of a difference between the two strains, then the pore pressure/volume controller responds to keep the pore pressure the same.

The transducer readings and input voltage are also read by the central data acquisition system and stored in a data file. The system consists of an IBM compatible PC interfaced with an expanded channel Hewlett-Packard HP3497A data acquisition unit capable of monitoring 150 channels throughout the laboratory. The system uses a high integrating analog to digital

converter with autoranging capability to produce a precision of one microvolt and a range of 1000 volts. Data is stored at a trigger rate of up to 1 Hz (allowing 1 to 2 second readings).

3.3.2 Constant Flow Modification

When applying the equations for effectiveness of a filter drain system, it is necessary for the hydraulic conductivity of the filter drains to be well defined over a range of stress conditions. In order to completely characterize the conductivity, the triaxial equipment was modified to allow constant flow tests on the drains.

Equipment was added to the system to provide a constant pressure at the top of the specimen. A manually controlled air pressure is applied to an air water interface in a closed chamber. The water line from the chamber is then connected to the auxiliary connection to the top drainage lines of the specimen. This keeps a constant head at the top of the specimen, regardless of the pressure at the base or the surrounding cell pressure.

During triaxial tests with soil, water must drain from the specimen into the filter drains and flow along the length of the paper to the stones. Therefore, the hydraulic conductivity is measured for flow along the length of the filter paper. Figure 3.10 illustrates the setup and the flow of water through the drains. To make this measurement, a lucite dummy, approximately the length of a standard triaxial specimen, is wrapped with continuous filter paper, the ends of the paper extending approximately 5 mm beyond each end of the dummy. When setup, this allows the paper to cover the stones completely. In contrast to the standard triaxial tests, the filter paper is left dry during setup. Although more difficult to saturate, the dry paper is easier to handle, making setup smoother and the paper less likely to tear (especially a problem with the soft Whatman 1). Both the top and bottom porous stones are set on a paper towel to remove excess water, and the bottom stone is placed on the pedestal with the membranes prepared at the base. The dummy/filter paper unit is set on the stone with the paper covering or extending slightly beyond the stone. The second stone is set on top of the dummy, again with the paper covering it. The top cap is then set and locked in place. The top and bottom rubber sleeves are flipped over the paper, holding it in place. By this time the paper has started to pull water from the stones and

is partially wet. Now in place, more water may be sprayed onto the paper to completely saturate it. Finally, the membranes are rolled up and secured with o-rings.

The system is then backpressure saturated to force any air in the system into solution. In this case, the pressure is increased to 4 ksc ensuring that there are no air bubbles. During this phase, both the top and bottom drainage are connected to the pore pressure control. Although the computer can control the load on the specimen, or dummy in this case, the load and deflection are not important. Therefore the piston is locked in place and axial motor control turned off. The only measurements of concern are the pore pressure at the base, the constant pore pressure at the top, the cell pressure, and the volume change (which more importantly provides the flow rate).

Once saturated, the air pressure applied to the pressure chamber is increased to equal the existing pore pressure (4 ksc). The pore motor is turned off and the top drainage line is opened to the pressure chamber. The pressure chamber is now maintaining a constant pressure throughout the filter paper and stones. Once in equilibrium, reached in only a few seconds, the pressure is measured through the transducer in the base of the specimen. At this point, the pore motor is turned on manual control, forcing steady flow through the bottom stone, along the paper on the side of the dummy, back into the top stone, and out the top drainage line into the pressure chamber (water is drained from the chamber after every few tests). The flow causes a pressure gradient from the bottom to the top of the paper. It is assumed that the pressure at the top of the paper is equal to that in the pressure chamber and although it is not measured throughout the test, it is assumed that it is steady and equal to the equilibrium pressure measured in the base at the beginning and end of the conductivity measurement when no flow is occurring. The pressure at the bottom of the paper is measured through the base during the test and is approximately steady after an initial transient period. Detailed procedures are included in the Appendix.

The interpretation of these tests is based directly on Darcy's Law: $K = \frac{Q}{iA} = \frac{Q}{\frac{h}{L}A}$

where Q = flow rate (cm^3/s)
i = gradient
A = cross section of drains (cm^2)

h = head loss (cm)
L = length of specimen (cm)

A spreadsheet is set up to calculate the pore pressure and volume change with time through each test. The flow rate is constant and estimated by a linear fit through the volume vs time data. The pressure at the top of the paper is equal to the equilibrium pressure measured before and after flow. The pressure at the bottom of the paper is taken as an average during the period when flow occurs. This difference is converted to a head loss in centimeters. There are also head losses through the system alone with no filter paper present. These losses were quantified by performing tests with a zero length specimen (a piece of thin rubber only to separate the stones). The data is summarized in Chapter 4. The system head losses are accounted for by subtracting the zero length measures from the full length data at the same confining stress. The cross sectional area of the paper is simply the perimeter based on the diameter measurement of the lucite dummy multiplied by the measured thickness. The length is defined as the length of the dummy rather than the full length of the paper assuming that flow passes into the stones once reaching the ends of the dummy. At each confining pressure, three tests are run with varying gradients achieved by varying flow rate.

3.3.3 Modified Base with Excess Pore Pressure Measurement

In order to evaluate the effectiveness of drains and existing models for analysis, it is necessary to measure the maximum excess pore pressures in triaxial soil specimens during consolidation. This requires equipment to measure the pore pressure in the center of the soil without causing disturbance.

A modified triaxial base was used which allowed a removable bottom pedestal. The base and pedestal are illustrated in Figure 3.11. The base has two outside connections, for the cell pressure and the pore pressure. The tubing connected to the cell pressure port forms a T, with one line connected to the pressure volume controller to control the cell pressure during the test and the other passing through a valve to the silicon oil supply used for filling the cell. The pore pressure connection goes to the top drainage lines only, with this base there is no bottom drainage. This is connected to a pressure/volume controller to maintain the pore pressure during

the test. The base is held above the loading platform by four supports. The pedestal is attached to the base with four bolts and sealed by an o-ring. Both the base and the pedestal have an opening through the center to allow a probe to pass through into the specimen.

The excess pore pressure in the specimen is measured by a stainless steel hypodermic needle probe developed by Cauble (1996) inserted through the bottom of the specimen. The needle has an inside diameter of 0.023 cm and has a 0.2 cm long porous stone press fitted into the tip. The tube is soldered to a stainless steel transducer block. Figure 3.12 illustrates the probe and transducer assembly. The probe is connected to the pedestal by a threaded brass connector and sealed with a small o-ring.

A major issue in this type of system is the response time of the probe. Cauble (1996) has a thorough discussion on the factors controlling response time and the theoretical equations derived for prediction. Essentially, a very small but finite amount of volume must enter the probe to deflect the face of the transducer and cause a change in output. The compliance of the probe system is defined as the change in volume divided by the change in pressure measured. In water, the time for the fluid to enter the transducer through the probe is controlled primarily by the geometry of the measuring system, the compliance, and the hydraulic conductivity of the porous stone in the tip of the probe. The following solution was derived by Henderson (1994) for a unit step pressure increase:

$$\frac{P_o}{P_a} = \left(1 - e^{-bt}\right) \qquad b = \frac{kA}{\gamma_w LM} \qquad M = \frac{\Delta V(t)}{\Delta P(t)}$$

where P_o = probe output pressure
P_a = applied pressure
t = time
k = probe tip hydraulic conductivity
A = probe tip cross-sectional area
L = probe tip length
M = probe system compliance
$\Delta V(t)$ = change in volume of probe system
$\Delta P(t)$ = change in probe system pressure

More important for this research is the response time of the probe in soil. In this case the controlling factors are the geometry, the compliance, and the hydraulic conductivity of the soil. A theoretical solution based on closed form solutions for pore pressure probes with rigid spherical porous inclusion stones in an elastic soil follows (DeJosselin De Jong, 1953; Gibson, 1963; Kutter et al, 1990):

$$\frac{P_o}{P_a} = \left(1 - e^{-dt}\right) \qquad d = \frac{4\pi r k_s}{\gamma_w M} \qquad M = \frac{\Delta V(t)}{\Delta P(t)}$$

where r = radius of the porous tip
k_s = soil hydraulic conductivity

The only aspect possible to control in this case is compliance, more specifically the transducer face diameter and deflection. The three types of transducers previously used with the needle probe are Data Instruments, Cooper, and Kulite. Table 3.5 summarizes the important physical characteristics of each. Data Instruments is most commonly used for pressure measurements in the laboratory and is therefore readily available, however it has a large face diameter and thus a slower response time. The Kulite has the smallest face diameter, leading to a quicker response time. In soil with a hydraulic conductivity of 1.4×10^{-7} cm/s, the calculated response time of the Kulite probe at 95% of the applied pressure was 1 second vs 212 seconds for the Data Instruments (Cauble 1996). Initially tests were run using the Data Instruments transducer, however the response time of the system was not adequate and the transducer was replaced with a Kulite pressure transducer.

The specimen rests directly on the pedestal, with no bottom drainage. Using a specimen half the height of a standard triaxial specimen, the pore pressure generated at the base is equivalent to that in the center of the standard size specimen with drainage through both ends. Therefore, the probe is positioned so the tip is even with the pedestal (but slightly above so the probe has good contact with the soil). To allow the piston to reach the shorter specimen, the plexiglass chamber and support posts are replaced with shorter equipment (available from early tests before the use of an internal load cell). The test is controlled and instrumented the same as a standard triaxial test, but with the pore pressure controlled through the top drainage lines only. The additional probe pressure measurement is sent to central data acquisition but not to the personal computer controlling the test. The Appendix includes a detailed procedure for test setup and execution.

An Excel macro developed by Kurt Sjoblom is used to reduce the data. This provides void ratio, strain, stress, and stress path conditions based on standard definitions of these quantities. Both filter drain corrections and membrane corrections are applied to the axial load and membrane corrections to the radial stresses. The user may choose three different options for the area correction: cylindrical, parabolic, or bulging. The equation for the average effective stress was changed to account for the excess pore pressure. Calculations of hydraulic conductivity and coefficient of consolidation based on the probe pressure measurement for tests with no radial drainage are also added. The calculation of the strain rate and stress rate used for the hydraulic conductivity and coefficient of consolidation are slightly different in this program than in the CRS reduction program. The rates are calculated incrementally and then the rates for the five surrounding increments are averaged for a given increment. The equations used in the modifications of effective stress, hydraulic conductivity, and coefficient of consolidation were taken from the CRS test analysis. Similar to the CRS test reduction, the zero value for the Kulite transducer is backcalculated so the excess pore pressure is zero at the start of consolidation. There is much more noise in this transducer however, so using the first line of data only is not adequate. Instead an average value of excess pore pressure from the end of the backpressure saturation data is taken. The zero value of the transducer is then changed to set this average equal to zero.

Year	Researcher	Source Batch	G_s	w_l	w_p	I_p	Clay Frac. <2μm (%)	Organic Content	Salt (g/l)
1994	Zriek	powder	2.78	46.4	22.5	23.9	60.1	4.4	
1994	Sinfield	402		46.8	22.4	24.4			
		403		47.2	23.3	23.9			
1996	Cauble	powder	2.81						
		401		46.7	21.8	24.9			
		404		47.4	21.9	25.5			10.4
		405		45.2	22.1	23.1			10
		406		45.0	22.6	22.4	57.5		12.5
		407		44.6	23.0	21.6	57.8		13.1
		408		44.7	23.9	20.8	58.7		10.1
		409		45.4	24.0	21.4	56.8		13
		410		46.6	25.0	21.6			13.4
		411		46.7	24.5	22.2	56.9		10.2
		413		45.5	24.3	21.2			9.7
		414		46.3	24.3	22.0			12
		415		46.1	24.7	21.4			10.5
		416		46.7	24.0	22.7			12.9
		417		47.2	24.5	22.7			13.2
1998	Santagata	418							
		419							
1998	this research	420		45.2	22.6	22.6			
	average	powder, 401-411 413-420	2.80	46.1 ±0.9	23.4 ±1.1	22.7 ±1.4	58.0 ±1.2	4.4	11.6 ±1.5

Table 3.1 Index Properties of Resedimented Boston Blue Clay from Series IV (after Cauble, 1996)

Year	Researcher	Series	Source Batch	G_s	w_l	w_p	I_p	Clay Frac. <2μm (%)	Salt (g/l)
1961	Bailey	Ia	MIT	2.77	30.0	17.5	12.5	40	2-3
			1139		34.7	17.7	17.0		35
1963	Jackson				36.2	19.5	16.7		16.7
1964	Varallyay		S4		32.6	19.5	13.1		
			S5		33.3	20.4	12.9	35	16.8
			S6		32.8	20.3	12.5		16
1965	Ladd, R.S.	Ib		2.77	45.0	22.0	23.0		16
1965	Preston		S1	2.77	45.6	23.4	22.2	35	24
1965	Braathen		S2	2.77	45.4	23.1	22.3		22
1967	Dickey				34.5	23.9	19.6		
1970	Kinner		100	2.78	43.5	19.6	23.9	50	
			150		43.5	19.6	23.9		
			200		38.1	17.8	20.3	52	8
			300		39.7	21.6	18.1		10
			400		39.4	21.3	18.1	52	10
			800		41.5	19.5	22.0	48	16
			900		41.2	18.7	22.5	54	16
			1000		41.1	19.5	22.6	58	16
			1100		42.0	20.6	21.4		16
			1200		40.2	18.6	21.6	48	16
			M101		40.7	19.6	21.1	52	
			M104		40.3	19.6	20.7		
			M107		41.3	19.6	21.7		
			M200		42.3	18.5	23.8	52	
			M400		39.8	18.9	20.9	47	
1971	Ladd et al.		160	2.78	38.1	17.8	20.3		8
			1300		42.1	22.1	20.0		16
			1500		43.8	20.6	23.2		16
1984	Bensari	II	105	2.75	47.6	23.3	24.3		16
			111	2.75	47.1	24.9	22.2		16
1985	O'Neill		105-112	2.78	41.3	22.1	19.2	52	16
1989	Seah	III	200-207	2.78	45.2	21.7	23.5	58	16
1991	Sheahan		210,214, 216		45.6	21.4	24.2		
1993	Cauble		217-218	2.78	37.0	21.3	15.7		
1994	Santagata		219-220		40.4	20.9	19.5		

Table 3.2 Index Properties of Resedimented Boston Blue Clay from Series I -- III (after Cauble, 1996)

	Value	r^2
Piston		
Area (cm^2)	3.37	0.99999
Weight (kg)	2.04	
Calibration Factor		
Cell (ksc/v/v)	-707.824	0.999992
Pore (ksc/v/v)	-700.075	0.999992
Displacement (cm/v/v)	2.548751	0.99999
Load (kg/v/v)	26987.236	0.99991
Compressibility		
Cell (cm)	$0.001*\sigma_c$	0.96
Axial Load (cm)	$0.0031*load^{0.2351}$	0.9990

σ_c = cell pressure (ksc)

load = load measured by load cell - $A_p*\sigma_c + W_p$ (kg)

Table 3.3 Constant Rate of Strain Calibration Factors

	Value	r^2
Calibration Factor		
Cell (ksc/v/v)	-702.9853	
Pore (ksc/v/v)	705.107	0.999992
Probe (ksc/v/v)	4626	0.99997
Volume (cm3/v/v)	7.07173	0.99998
Displacement (cm/v/v)	2.0282	0.99996
Load (kg/v/v)	6404.29	0.99999

Table 3.4 Triaxial Apparatus Calibration Factors

Transducer Diaphragm	Kulite	Cooper	Data Instruments
diameter, cm	0.39	0.55	1.59
area, cm^2	0.12	0.24	1.98
thickness, cm	0.016	0.013	0.042
*deflection $cm^5 p_a(t)/N$	1.68×10^{-6}	8.92×10^{-6}	3.72×10^{-4}

*$p_a(t)$ = applied pressure

Table 3.5 Important Physical Characteristics of the Three Probe Transducers (Cauble, 1996)

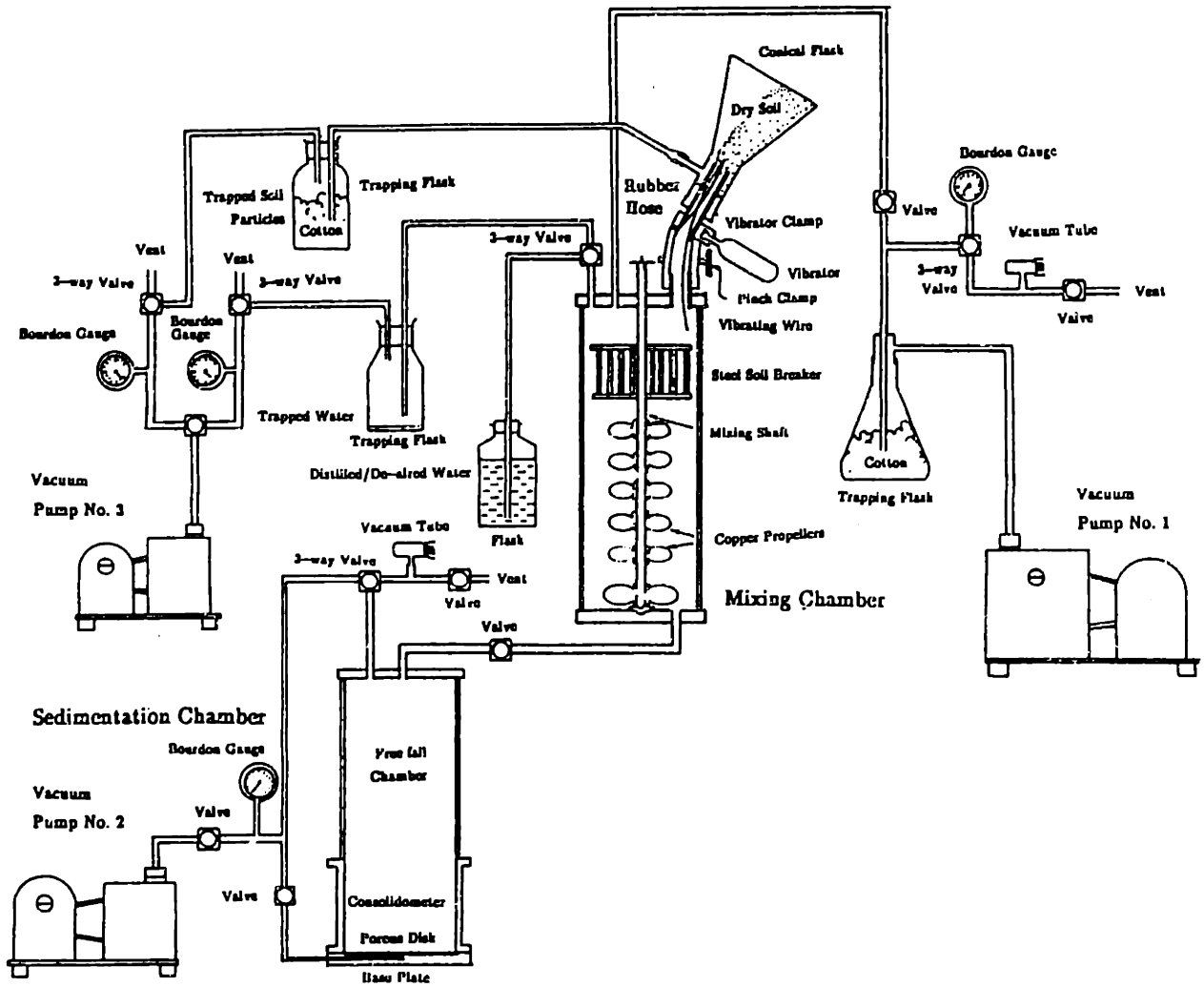

Figure 3.1 Preparation of Resedimented Boston Blue Clay (Seah, 1990)

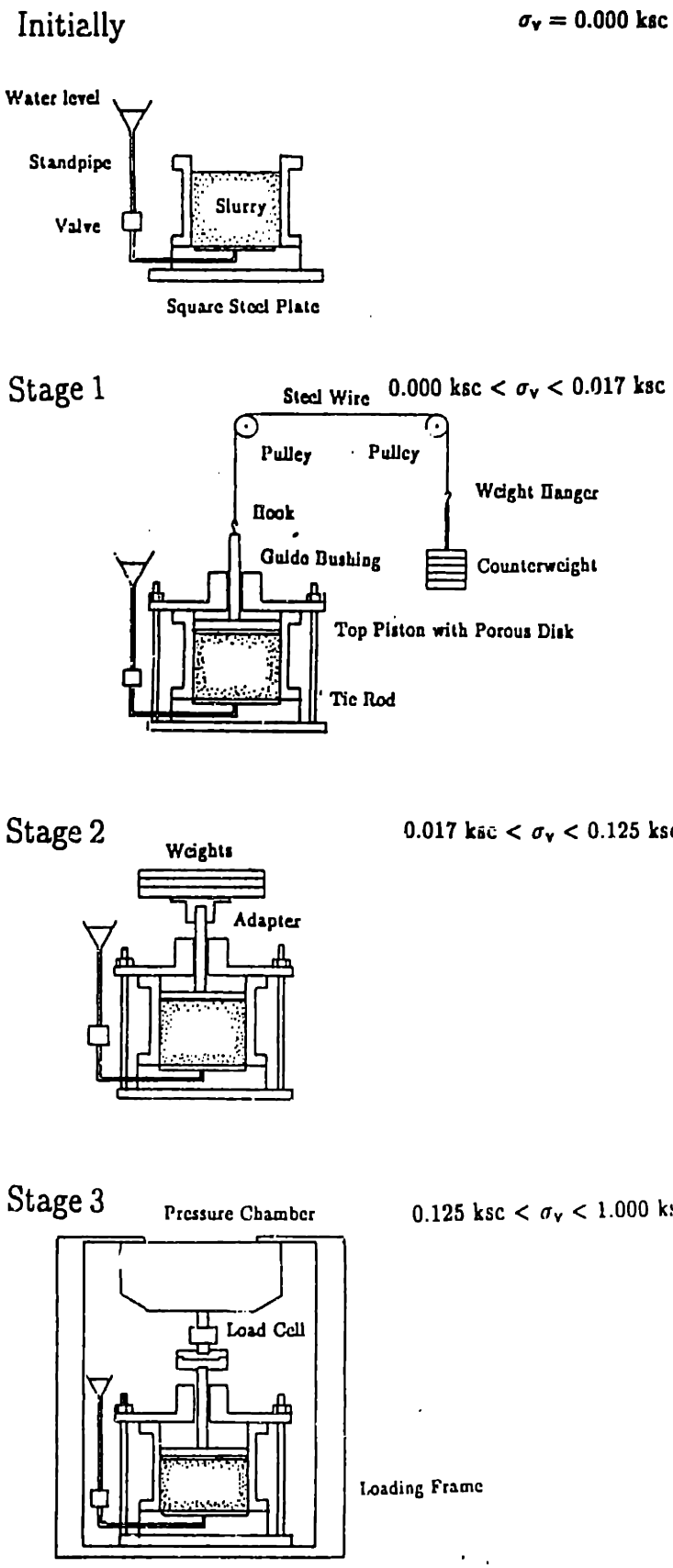

Figure 3.2 Consolidation Process of Resedimented Boston Blue Clay (Seah, 1990)

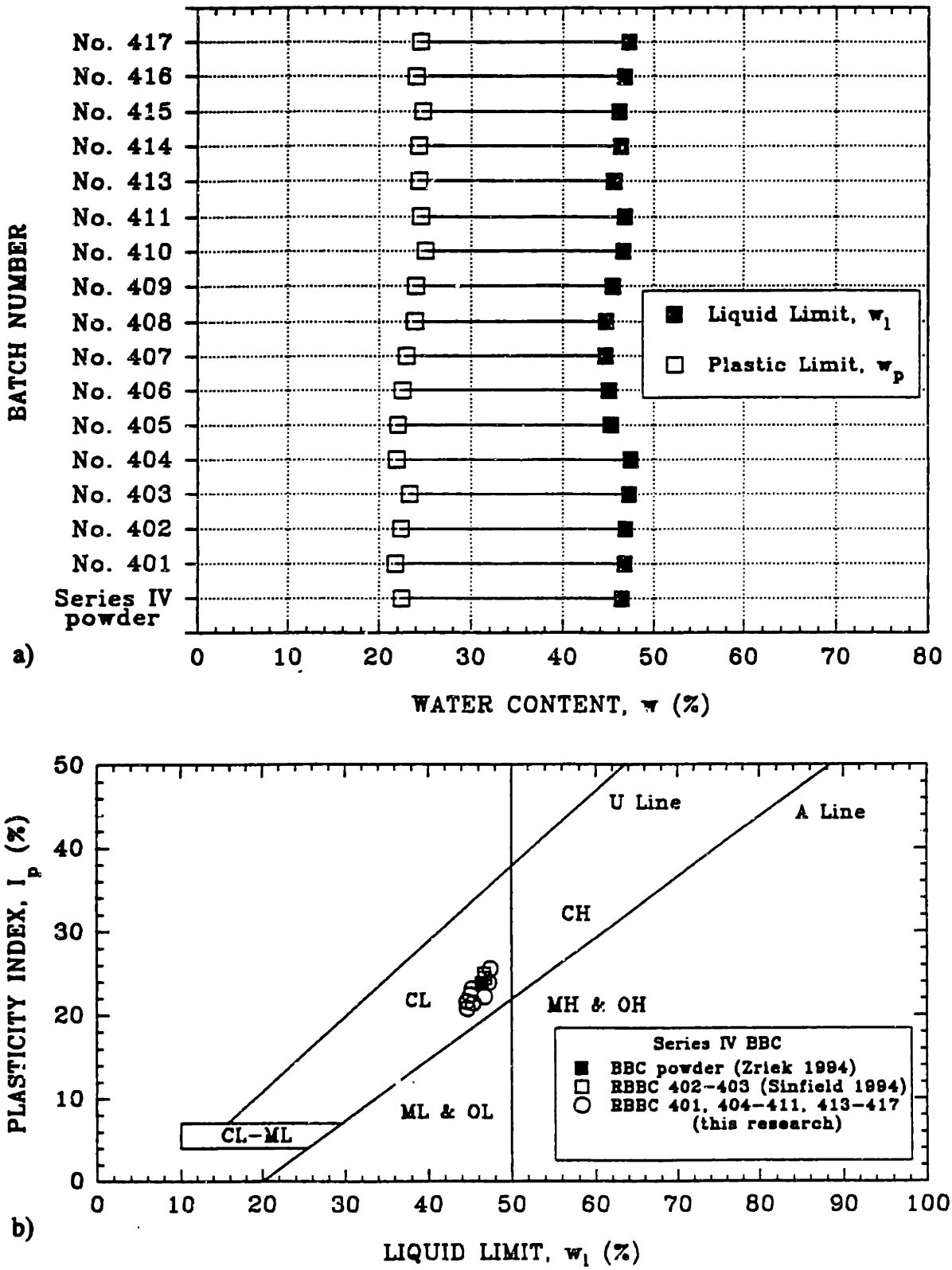

Figure 3.3 Atterberg Limits for Series IV Boston Blue Clay (Cauble, 1996)
a) Plastic and Liquid Limits
b) Plasticity Chart

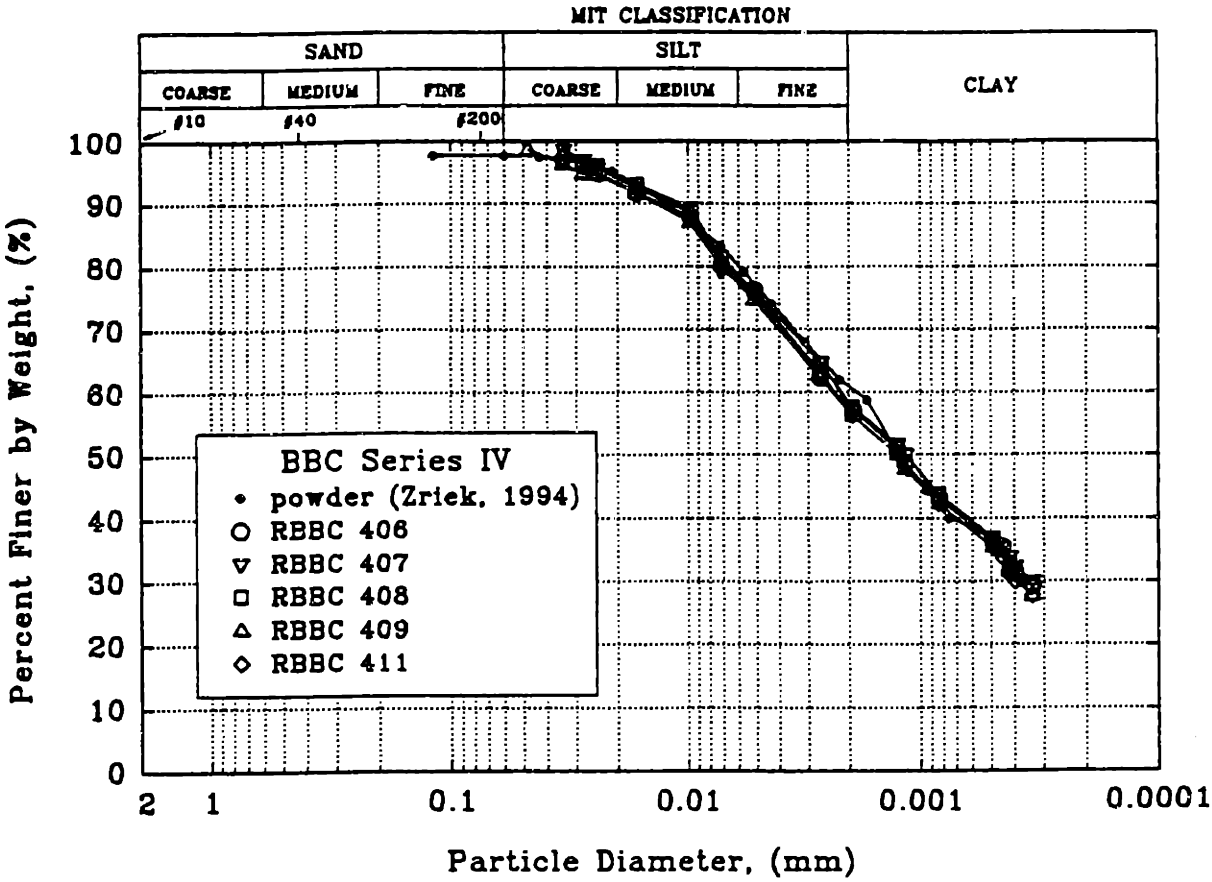

Figure 3.4 Grain Size Distribution of Series IV Boston Blue Clay (Cauble, 1996)

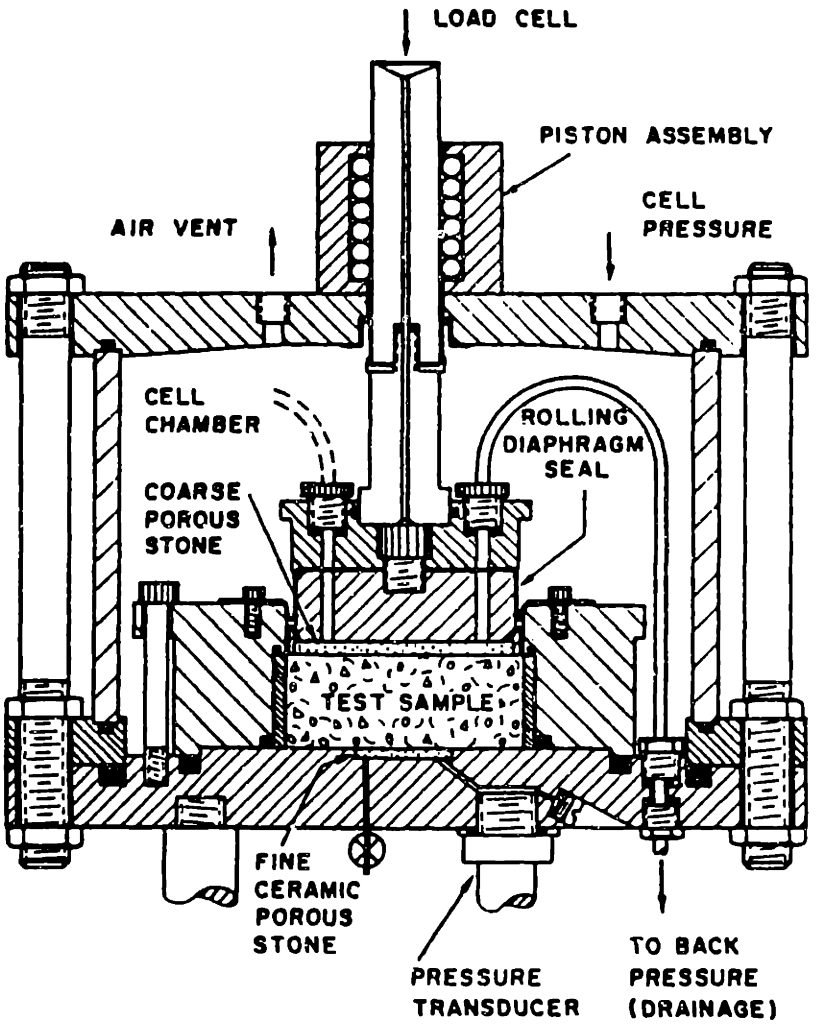

Figure 3.5 Original MIT General Purpose Consolidometer (Wissa et al, 1971)

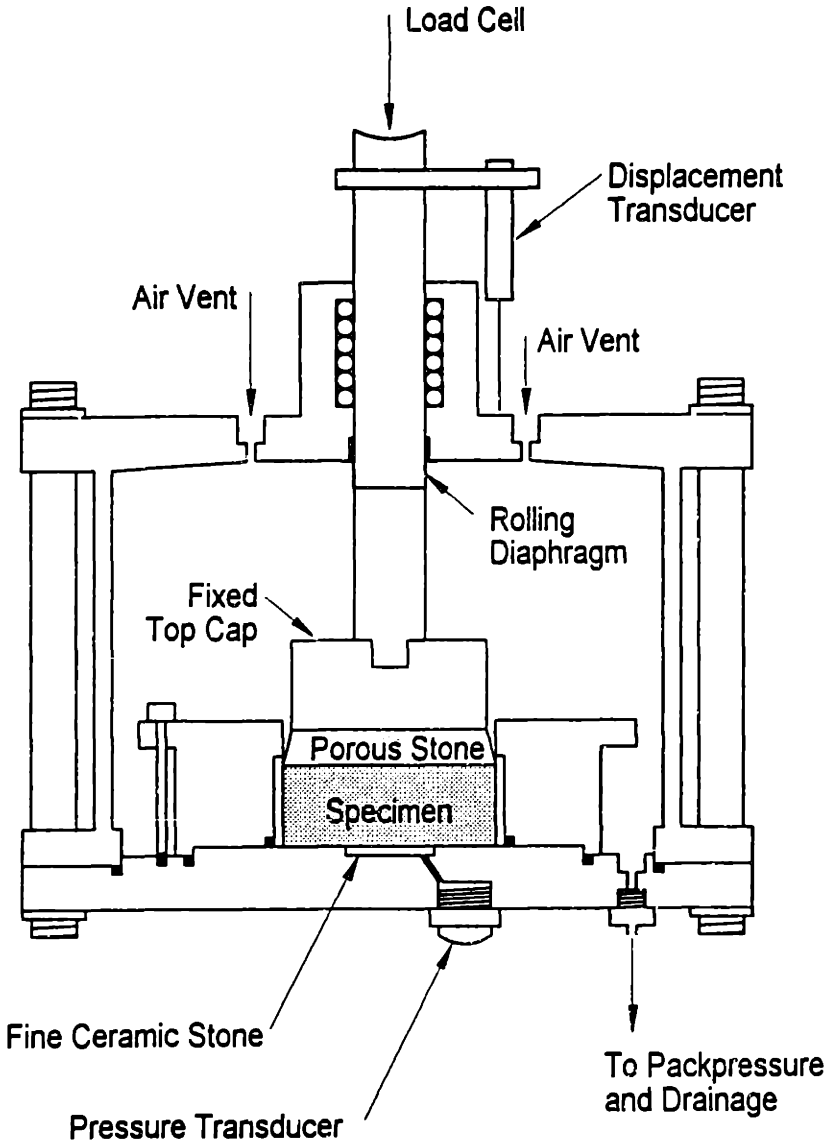

Figure 3.6 Modified Constant Rate of Strain Consolidometer

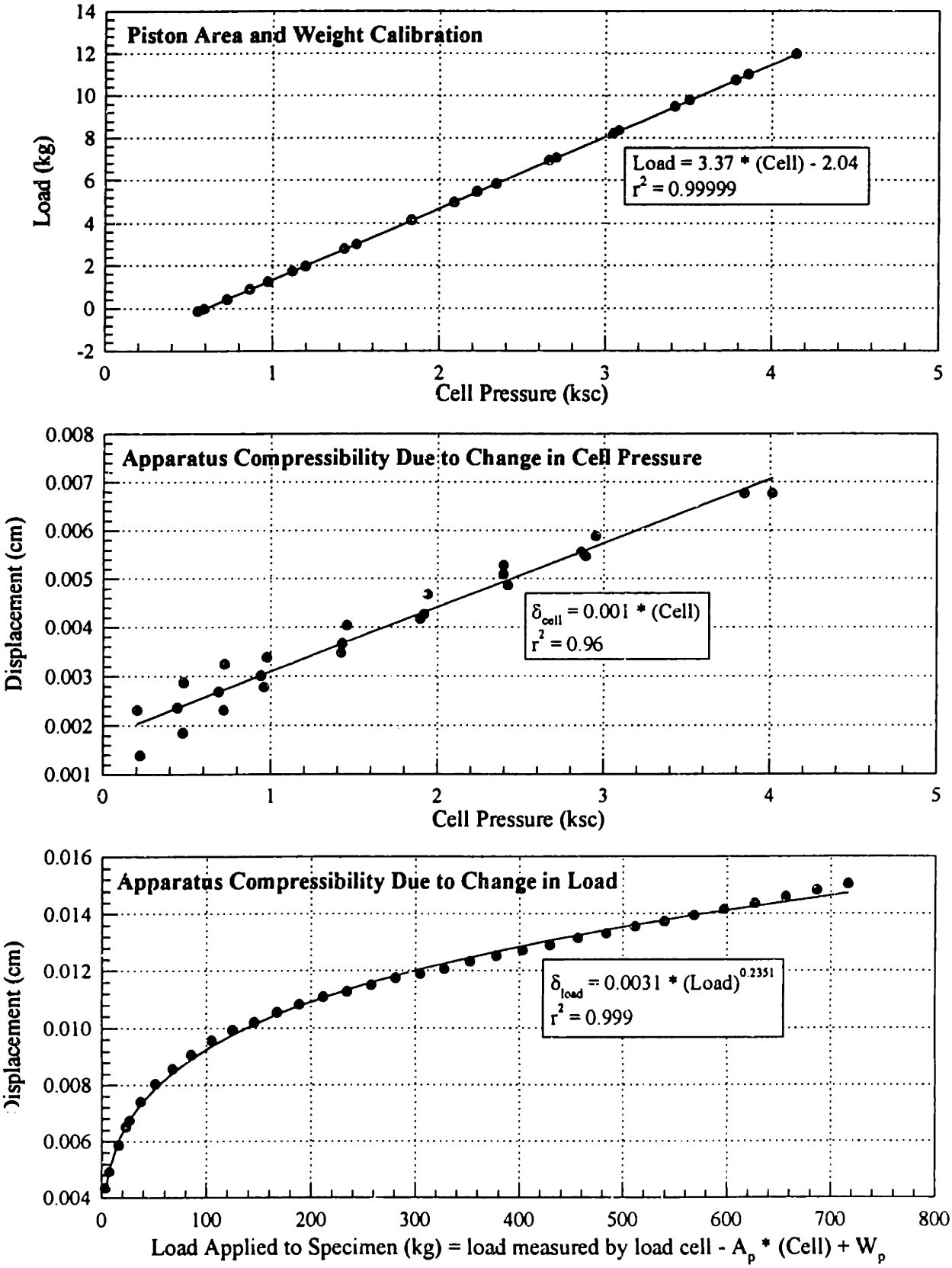

Figure 3.7 Calibration and Compressibility Curves for Constant Rate of Strain Device

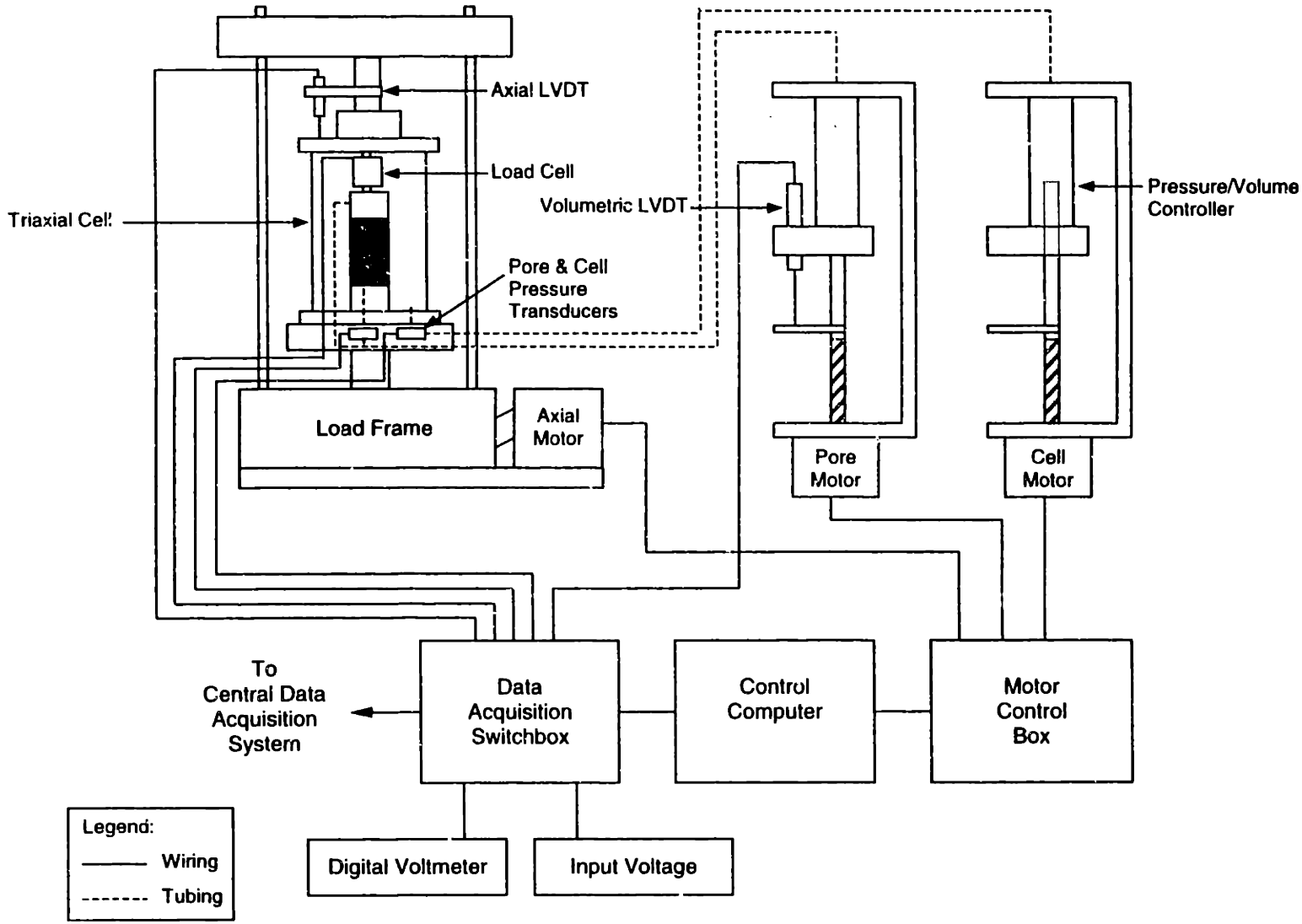

Figure 3.8 Schematic Representation of the MIT Automated Stress Path Triaxial Apparatus

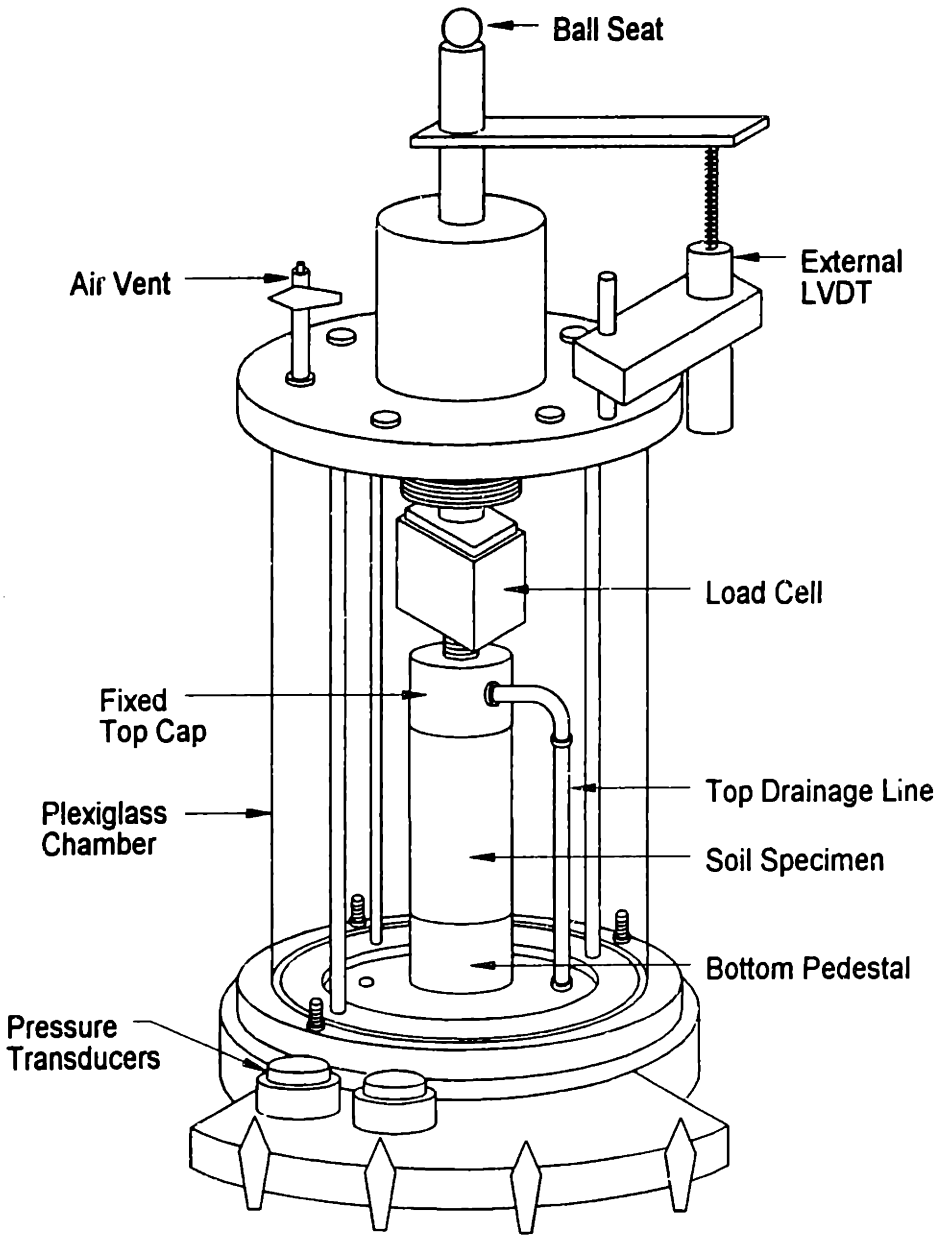

Figure 3.9 Triaxial Cell

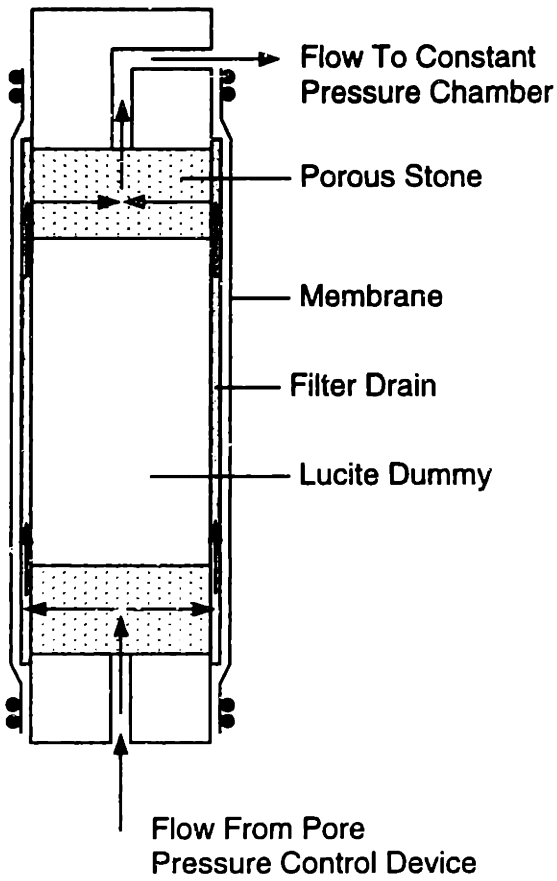

Figure 3.10 Test Configuration to Measure Filter Drain Hydraulic Conductivity

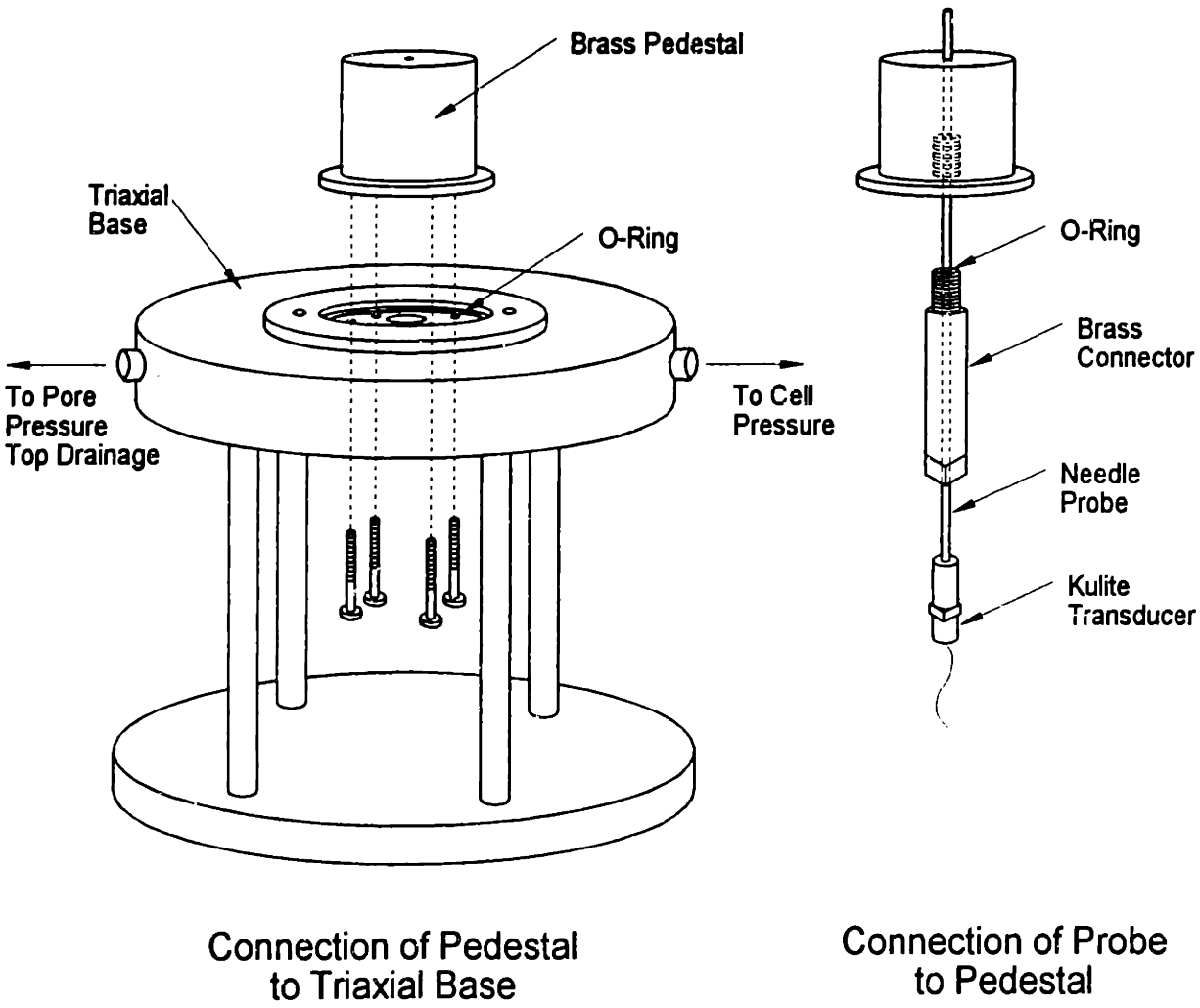

Figure 3.11 Modified Triaxial Base to Measure Excess Pore Pressure

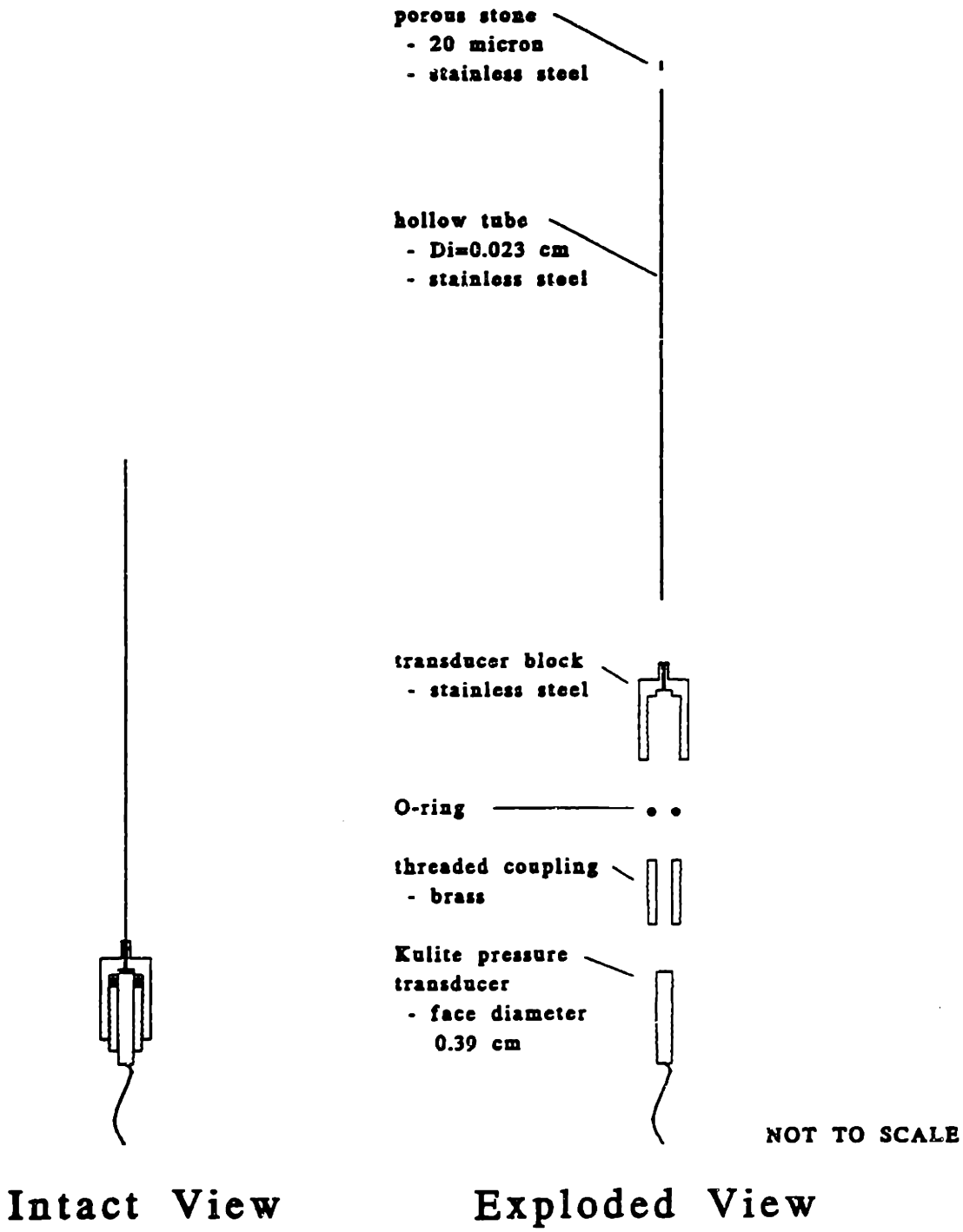

Figure 3.12 Pore Pressure Probe with Kulite Transducer (Cauble, 1996)

Chapter 4 Test Results

4.1 Filter Paper Hydraulic Conductivity

4.1.1 Initial Tests

The objective of the first phase of this research was to characterize the hydraulic conductivity of the filter paper under the range of conditions that it would be subjected to in a triaxial test on soil. Therefore it must be defined as a function of confining stress, flow rate, total volume through the paper, and load history.

Considerable time was spent performing trial tests to determine which of these factors controlled the hydraulic conductivity of the paper. Table 4.1 summarizes all of the tests in this research program. It became apparent that there was an initial decrease in hydraulic conductivity until a steady value was reached. These first tests were run over a number of days with varying flow rates and confining stresses. Because so many factors were changing, it was not clear if the decrease was due to a change in the paper with time or with total volume through the paper. To determine the cause, steady flow was forced through the paper immediately after saturation at a low flow rate and under a constant confining stress.

Figure 4.1 and Figure 4.2 plot results from this type of test on both Whatman 1 and Whatman 54 filter paper. The hydraulic conductivity of the paper decreases with total flow, quickly at first then approaches a constant value after approximately 30 cm^3 of water have passed through the paper. Because the hydraulic conductivity approaches a steady value, the tests indicate that it is volume and not time that is affecting the behavior of the paper. Both types of filter paper had similar behavior, although the starting point was different for each. The Whatman 1 changed from 6.2×10^{-4} to 4.2×10^{-4} cm/s (32%) while the Whatman 54 changed from 3.8×10^{-3} to 2.2×10^{-3} cm/s (42%), a slightly larger percentage change.

There are a total of four tests on Whatman 1 that confirm this trend (including the one plotted in Figure 4.1). There is considerable variability, however, between the tests. The following is a summary of starting and ending hydraulic conductivities. All tests were on Whatman 1 at a

confining stress of 0.5 ksc. There was only the one test (plotted in Figure 4.2) on Whatman 54, and all tests were run to steady state at a confining stress of 0.5 ksc, none started at higher stress levels.

Trial Number	Starting K (cm/s)	Ending K (cm/s)
1	$7.3x10^{-4}$	$3.9x10^{-4}$
2	$5.0x10^{-4}$	$3.4x10^{-4}$
6	$5.0x10^{-4}$	$2.5x10^{-4}$
7	$6.2x10^{-4}$	$4.2x10^{-4}$

In order to examine the trends with confining stress and load history, water was flushed through the paper until a steady state was reached after each new setup. Although this is a much larger volume than would flow through the drainage paper during a standard triaxial test, it was the only way to separate the other variables from the trends with total flow. The values of hydraulic conductivity measured here may therefore be lower than actual values during testing, but they will have the correct trends with a slight offset due to the initial flushing of water.

4.1.2 System Losses

Tests were run to evaluate the head losses through the system with no filter paper present. Initially these tests were run with a piece of stiff rubber separating the two porous stones and a short piece of filter paper to allow flow around the rubber. These tests, however, provided unreasonably high head losses, sometimes more than the losses measured through the full length of filter paper. The rubber may have been cutting into the thin strip of filter paper, allowing almost no channel for flow around the rubber. This possibility led to the current method of measuring losses, using a thin flexible rubber sheet between the two stones to prevent cutting of the filter paper. In addition to the filter paper, a drainage cloth was also added between the filter paper and the membrane, providing very easy flow from the bottom stone to the top stone.

At each confining stress, head loss was measured at different flow rates. There was very little change in head with change in flow rate, therefore an average value of head was chosen for each

confining stress, independent of rate. Figure 4.3 presents data from a confining stress of 0.5 ksc. This was the first flow through the system, so the first flow rate was run for a longer time to ensure that the head was not changing with flow. Satisfied that there was a constant head, the other two flow rates were run for shorter periods of time. All three yielded almost identical data.

As with the tests on filter paper, the system loss tests followed an unload reload cycle, and the losses are dependent on the cycle. The data followed a clear trend with the exception of the first point at 0.5 ksc. A value of 11.5 cm head loss was measured, but this was greater than the following head loss of 9.5 cm at a higher confining stress. Therefore the data from the full length filter paper tests were examined. At each confining pressure in the full tests, the head loss at three different flow rates was measured. Extrapolating this data to zero flow should agree with the system head loss measured. Figure 4.4 is the data for a confining pressure of 0.5 ksc on the full length of Whatman 54 filter paper. The intercept with the head loss axis is approximately 8 cm. Similar plots for two trials on Whatman 1 filter paper provide the same intercept. This indicates that a value of 8 cm is the system head loss at 0.5 ksc rather than the initially measured 11.5 cm.

The other values of head loss measured roughly agree with those estimated from the filter paper data, so they were used as measured. This data is presented in Figure 4.5. Initially the system head losses increase with increasing confining pressure. The unloading portion of the curve, however, is unusual. As the confining pressure is decreased, the system losses continue to increase, the opposite of the expected behavior. The cause of this is still not clear. The data from the first flow through the system (Figure 4.3) seemed to establish that head was fairly constant with time and flow, so this should not be the cause. Perhaps there is another factor not considered by this research.

4.1.3 Filter Paper Hydraulic Conductivity

The first factor controlling hydraulic conductivity is total flow, discussed above. The second factor is confining pressure. As expected, the conductivity decreases with increase in confining pressure. However, as with soil, the behavior is affected by stress history. Figure 4.6 and Figure

4.7 show the results from tests on both Whatman 1 and Whatman 54 including an unload reload cycle. Each of these points is an average of three different flow rates. The different rates provided very repeatable values and the standard deviation at each stress is included in Table 4.2.

Also clear from the tests on Whatman 1, is that variability in the filter paper is an important factor. From numbers quoted above for the starting and ending values of hydraulic conductivity during the flushing phase, there is a range from $7.3x10^{-4}$ to $5.0x10^{-4}$ cm/s in starting values and a range from $2.5x10^{-4}$ to $4.2x10^{-4}$ cm/s in ending values. This is also apparent in the two curves shown in Figure 4.6. The filter paper for these two tests was actually taken from the same sheet and there is still a large variability. The values tend to converge at higher stress levels, with the last points almost identical.

The results from the first time loading portion of the tests are compared to values quoted by Bishop and Gibson (1963) in Figure 4.8. It is not clear what type of paper Bishop and Gibson refer to, the values fall between those measured for Whatman 1 and Whatman 54. The trend in the quoted values is quite different than measured values, perhaps as a result of the flushing procedure used in this research. Semi-log equations fit well through the measured data, and these equations are used later to define changes in the hydraulic conductivity of the paper throughout K_o consolidation tests in the triaxial apparatus. Table 4.2 summarizes the data and provides the equations.

4.2 Constant Rate of Strain Consolidation in the Wissa Consolidometer

4.2.1 Linear Theory

Seven constant rate of strain consolidation tests were performed on Resedimented Boston Blue Clay in the Wissa consolidometer. The results from these tests, analyzed using linear theory, are summarized in Table 4.3 and plotted in Figures 4.9 through 4.11. The first test was run at 0.84 %/hr, the standard rate used on low plasticity clays. This generates excess pore pressures ranging from 0.05 ksc to 0.2 ksc, magnitudes that are accurately read by the transducer but are not large enough to cause high exit gradients or unusual pore pressure distributions. This test

provides a compression curve, hydraulic conductivity variation with void ratio, and coefficient of consolidation variation with stress. These are used as a base for comparison to later tests.

A second test was performed at this rate, with a pause in loading at an effective stress of 6 ksc to allow the excess pore pressure to dissipate. Loading was then resumed at the same rate. This test will be used to determine if the equations used for drained shear may also be applied to K_o consolidation. As discussed in Chapter 2, these equations indicate that the pore pressure generation is load history dependent. According to this theory, the pore pressure curve will be different after the pause in loading than the curve with continuous loading.

Three fast tests were performed at rates varying from 1.35 %/hr to 12.71 %/hr. These tests will determine how changes in strain rate change the generation of excess pore pressure. They will also examine the application of the standard Wissa equations for hydraulic conductivity and coefficient of consolidation under vastly different rate and pore pressure conditions.

Finally, two very slow tests were run at 0.15 %/hr and 0.07 %/hr. These tests had almost no excess pore pressure and show that there is not a large secondary effect in the compression curves. Because the pressures are so low however, it is not possible to compute hydraulic conductivity or coefficient of consolidation.

The first point to note from these tests is the initial specimen conditions, summarized in Table 4.3. Tests performed prior to this research contained inconsistencies in initial void ratio and lead to saturation values below 100%. The calculations were based on the initial volume measurement, initial total mass, and final mass of solids. The error occurred in the volume measurement. The height of the specimen was taken as the difference between the height of the sample ring and the height of the recess tool. The recess tool however may not have been entirely flat or the sample ring not seated completely, making the calculated height greater than the actual specimen height. To correct this, the distance from the top of the ring to the specimen was measured directly and this provided very consistent results in the initial state of the soil. For the CRS tests, the average initial water content is 44.23% ±0.15%, initial void ratio is 1.206 ±0.006, and saturation is 100.9% ±0.4%.

The second finding is that there is a very narrow band including the compression curves for all seven tests shown in Figure 4.9. As expected, the faster tests are shifted very slightly to the right. The average maximum past pressure is 1.31 ksc by the Cassagrande method (C) and 1.18 ksc by the strain energy method (SE). The values measured for the test run at 12.71 %/hr are 1.52 ksc (C) and 1.35 ksc (SE) compared to those from the test at 0.07 %/hr of 1.28 ksc (C) and 1.15 ksc (SE). This is an interesting discovery: changing the strain rate by two orders of magnitude changes the maximum past pressure by only 0.2 to 0.24 ksc. This confirms the strain rate effect predicted by Leroueil et al (1985) that the preconsolidation pressure changes by 10 to 15% per logarithm cycle of strain rate.

Examining the hydraulic conductivity curves in Figure 4.9 again reveals that the data fall within a narrow band. The consistency of the relationship between void ratio and hydraulic conductivity implies that the equations used here effectively capture the behavior of the excess pore pressure. There is more variability in the initial data, possibly a result of space between the soil and the specimen ring. As load is applied, this gap may be sealed and the data becomes consistent.

Not surprisingly, the only test which is outside the band of data is that run at 12.71 %/hr. This implies that the pore pressure distribution through the specimen may be different and that the equations no longer apply at such high rates. These tests may allow us to determine at what point the equations are no longer valid. Examining the test at 4.02%/hr more closely shows that it begins to deviate from the trend at a void ratio of 0.95. Turning to the curves of the excess pore pressure shown in Figure 4.11 provides a value of 0.5 ksc. This is equivalent to a gradient of almost 250, where we would no longer expect laminar flow. This is very useful information in deciding what pore pressures are acceptable for analysis.

The coefficient of consolidation curves shown in Figure 4.10, have very good agreement once the soil is normally consolidated. The faster tests appear to hit the straight line portion at slightly higher stresses, but after 2 ksc, all are consistent. This initial variability may simply be a function of the initial stiffness of the material and not related to rate. The pore pressure curves in

Figure 4.11 all have the same shape but with higher values at faster strain rates. The initial portion of each curve has an unusual trend. There is a quick increase in pressure, followed by a drop to almost zero. From that point, pore pressures are generated consistently through the test.

4.2.2 Nonlinear Theory

Three of the tests (0.84 %/hr, 4.02 %/hr, and 12.71 %/hr) were also reduced using the nonlinear theory. The compression curves are nearly identical to those using linear theory for all three tests, with a very slight shift to the left in the fast test (by a maximum of 0.04 ksc). As mentioned in Chapter 2, this difference may be easily calculated, excess pore pressure 10% of the total stress causes only a 1% change in effective stress calculated.

The coefficient of consolidation curves are shown in Figure 4.12. The curves for the two slower rates are almost identical, however there is a clear decrease in the curve for the fast test. This shifts the curve outside the narrow band of results reported by the linear theory.

The hydraulic conductivity curves are shown in Figure 4.13. Again the slower two tests yield very similar results to the linear theory. The results for the fast test, however, are decreased significantly, moving them even further away from the range of results for the other tests. The hydraulic conductivity in this theory is calculated directly from the coefficient of consolidation and coefficient of volume compressibility. As expected, because the compression curves are constant but the coefficient of consolidation decreases (by 15% for instance at a void ratio of 1.0), the hydraulic conductivity also decreases (by approximately 15% at a void ratio of 1.0). The nonlinear theory clearly makes the results less repeatable, particularly in the fast test. Because the linear theory reduction provided more consistent results between various strain rates, this was the analysis chosen for presentation and comparison of results.

4.3 K_o Consolidation in Triaxial Apparatus

4.3.1 Response Time of Probe

The most difficult issue to resolve in the triaxial testing phase of the research was the selection of a probe configuration with adequate response time. The factors controlling response time and the theoretical equations derived for prediction were discussed in Section 3.3.3. The factor that could be controlled was face diameter and deflection of the transducer. Although the Kulite transducer clearly has the shortest response time, it also has a number of problems. The transducer has poor stability, is strongly affected by temperature changes, and often has grounding problems, frequently causing short circuits.

Because of the better response time, the first tests were run using a Kulite transducer. Unfortunately the particular transducer used did have a grounding problem and the data was useless. In addition to the short, the transducer had a much larger capacity than the test needed, leading to very poor resolution.

The K_o consolidation tests take approximately one day to perform, so the slower response time of the Data Instruments transducer may have been acceptable in exchange for the increased stability and reliability. Approximately ten tests were run with this transducer. These tests had compression curves that generally agreed with those measured in the Wissa device. The slope of the hydraulic conductivity curves (coefficient of hydraulic conductivity) also agreed with those measured from the Wissa device, however the curves were shifted to the right. Believing this to be the result of not having adequate lateral confinement of the specimen, tests were run forcing higher confining pressures to see if this corrected the curve. There was little effect. Faster tests were also performed, but this only shifted the curves farther to the right, the opposite trend observed in the faster CRS tests. Finally, as should have been done from the beginning, the response time was examined during the B value check after saturation. The drainage lines are closed and a cell pressure of 0.5 ksc applied to the specimen. If properly saturated, the pore pressure responds and also increases by 0.5 ksc. During the pressure increase, both the pore pressure transducer and the probe transducer were monitored. Figure 4.14 shows the response of the two transducers. The second plot in this figure shows the ratio of the change in probe

pressure to the change in pore pressure. This should approach a value of one when the probe has completely responded. The figure shows that even after the cell pressure has been applied for over one minute, the probe has only reached 45 percent of the actual pressure in the soil. This is an unacceptably slow response time, and explains the disparities between the triaxial tests and the CRS tests.

This discovery forced returning to the Kulite transducer. A new transducer was used, and although it still had a higher capacity than required, it was relatively stable and properly grounded. A typical response time curve during the B value check is shown in Figure 4.15. There is a very slight lag in the response of the probe, but is a negligible problem for these tests.

After running one test with the new probe, another test was setup immediately without ultrasounding the probe. This test resulted in a poor response, although still a huge improvement over the Data Instruments. Figure 4.16 presents these data. As expected, the hydraulic conductivity from this test was shifted to the right. The slower response is believed to be the result of either clogging of the porous stone in the tip of the probe or of the probe no longer being completely saturated. To prevent both of these possibilities, the probe was suspended in the ultrasound prior to each test, removing any air or soil that may have entered the probe during the previous test. The response time was checked for the remainder of the tests and always had an acceptable response.

4.3.2 Triaxial System Modifications

There were also a number of tests run to solve problems with the computer control. Because the tests consolidate to such high stresses and the specimens are so small, the gain rate previously used for pore pressure control caused too much response in the soil. If the pressure was slightly lower than the target, a large amount of water was forced into the specimen causing the pressure to overshoot the target. This lead to pressure variations from 3 ksc to 5 ksc while trying to maintain 4 ksc. However, the gain required to prevent this behavior caused sluggish response during initial backpressure saturation because at this point the system needs a larger volume of water to cause a given change in stress. Specifying one gain rate during pressure up (a value of

0.2) and a higher gain (to impose less voltage change for a given change in stress) during consolidation (a value of 0.4) solved the problem.

One more problem caused by consolidating to such large strains was that the volumetric LVDT did not have a large enough stroke to stay in range throughout the tests on taller specimens. For these tests it was necessary to stop loading and reset the LVDT. Data from the first tall sample in the triaxial apparatus was lost over 5 ksc. Once out of range, the area is no longer kept constant by the computer and the stress path does not follow the K_o line. Procedures for doing this are in the Appendix.

4.3.3 Tests with No Radial Drainage

With the equipment working properly, a total of seven tests were run with no radial drainage to confirm that the triaxial apparatus provided results comparable to those from the Wissa consolidometer. Tests are summarized in Table 4.4. Three of these specimens were approximately the same height as those in the CRS test, 2.35 cm, which is extremely short compared to standard triaxial specimens. The remainder of the specimens varied in height up to roughly twice the height of the CRS specimen, 4.5 cm. The tests with varying height were examined to confirm that the equations used for the CRS test also apply to taller samples.

The initial specimen conditions for the triaxial tests were very similar to those for the CRS tests. The average water content is 43.84%, initial void ratio is 1.210, and saturation is 101.0% compared to 44.23%, 1.206, and 100.9% respectively in the CRS tests. The void ratio and saturation conditions are very similar, implying that the soil has little variability. The water content, however, is slightly lower than the standard deviation of the CRS tests. This implies that there is some bias in the trimming methods.

Results are plotted in Figures 4.17 through 4.20, with shaded areas indicating the range of results from the CRS tests in the Wissa apparatus. There is excellent agreement with measured data from the CRS tests, apparent in the compression curves, hydraulic conductivity, and coefficient of consolidation data shown in Figure 4.17 and 4.18. This agreement implies that the equations

used in this reduction (by Wissa et al, 1971) properly account for the strain rate and height. Examining the range of results for the hydraulic conductivity compared to the range of results from the CRS shows that the CRS has much greater variability in the initial portion while the triaxial data has a consistently narrow band. This suggests that the side seals in the CRS once the test is running. The pore pressure curves are shown in Figure 4.19, and are the subject of discussion in Chapter 5. The stress paths in Figure 4.20 fall within a narrow band, and once normally consolidated, the lateral stress coefficient is also fairly repeatable, showing a steady increase with stress.

4.3.4 Tests with Varying Radial Drainage Conditions

Once convinced that the results were repeatable and had good agreement with the CRS tests, eight more tests were run with varying radial drainage conditions. These are summarized in Table 4.5. All of these tests were on specimens approximately 4 cm tall. This is half the height of a standard triaxial test but equivalent to the full height sample due to the one ended drainage condition. Most of the tests were run at 1 %/hr (numbers 460, 461, 463, 464, 467, and 469), with one run at 1.5 %/hr (number 472) and 2 %/hr (number 462) to examine the rate effect with radial drainage. Two tests were run with the standard radial drainage condition: eight ¼ inch strips of Whatman 54 filter paper. Three tests were run with complete coverage of Whatman 54 and one with eight 1/8 inch strips of Whatman 54. These tests will be used to examine how the drain coverage effects the reduction of excess pore pressure. Two unusual tests were run to improve the effectiveness of the drains. One was setup with the standard eight strips of ¼ inch Whatman 54, but with a thick string added between the filter paper and the membrane. This provides an almost infinite hydraulic conductivity along the length of the specimen in contrast to the conductivity of the filter paper alone. One final test was performed to examine whether the filter paper has limited drainage in the radial direction. Instead of strips of filter paper, eight ¼ inch strips of monofilament nylon were placed around the specimen, again with string between the nylon and the membrane. This provides very good drainage radially through the nylon and good drainage along the length of the specimen through the string.

The results of these tests are presented in Figures 4.21 through 4.23. The previous tests with no radial drainage included plots of hydraulic conductivity and coefficient of consolidation. Now with radial drainage, there are no well defined equations to calculate these properties. Figure 4.21 compares the compression curves to those with no radial drainage, in terms of both void ratio and strain. These tests do not have as narrow a band as the previous triaxial tests, but this is expected since there is more variability in the setup conditions. There is also no clear trend in the curves with respect to either strain rate or filter paper conditions. The test with the largest values of strain during loading had ¼ inch strips of Whatman 54 with string (number 467). The curve with the lowest values of strain had 1/8 inch strips of Whatman 54 (number 464). The remainder of the tests essentially are the same.

Some of the variability is due to the uncertainty in the amount of axial stress the filter paper drains carry. The axial stress was corrected using a maximum of 0.16 kg/cm at 2% strain. For the tests with unusual drainage conditions (nylon or string), the same correction was applied based on the perimeter of filter paper present, but no additional correction was made for the string. The load carried by drains is examined in Chapter 5, although there is no clear solution. Figure 4.22 shows the pore pressure curves, but again these will be discussed in Chapter 5.

Figure 4.23 compares the stress paths and lateral stress coefficients. Interestingly, there is a clear trend in these curves. The increase in filter paper perimeter causes a steeper stress path and a lower lateral stress coefficient. Because there should be no change in the area of the specimen during true K_c consolidation, the change in the radial stress condition is not expected. This implies that there may be some small radial strain in these tests or that the filter paper has a confining behavior. The final radial dimensions were measured for the tests with radial drainage and included in the summary table. The tests with complete coverage of filter paper had radial strains of 0.97%, 0.98%, and 0.82%, those with ¼ inch strips had strains of 0.66% and 0.77%, and the test with only 1/8 strips had a strain of –0.09%. So there is a clear trend: with increase in filter paper perimeter there is an increase in radial strain and a decrease in lateral stress coefficient.

Test Number	Type of Test	Description
Trial 1	filter paper K	Type of paper unknown. Initial test to examine controlling factors.
Trial 2	filter paper K	Whatman 1. Backpressure to only 2 ksc.
Trial 3	system loss	Thick rubber sheet, losses higher than in filter paper K tests.
Trial 4	system loss	
Trial 5	system loss	
Trial 6	filter paper K	Whatman 1. Used in analysis.
Trial 7	filter paper K	
Trial 8	system loss	Thin rubber sheet, losses still very high.
Trial 9	system loss	Thin rubber sheet, added drainage cloth. Used in Analysis.
Trial 10	filter paper K	Whatman 1. Mistake in saturation, confining pressures too high.
Trial 11	filter paper K	Whatman 54. Used in analysis.
CRS 238	CRS	Used in analysis.
CRS 239	CRS	
CRS 241	CRS	
CRS 242	CRS	
CRS 243	CRS	
CRS 244	CRS	
CRS 250	CRS	
TX 431	Ko Consol.	Kulite transducer short.
TX 434	Ko Consol.	DI transducer. Poor computer control.
TX 435	Ko Consol.	
TX 436	Ko Consol.	
TX 437	Ko Consol.	DI transducer. Terrible computer control.
TX 439	Ko Consol.	DI transducer. Improved computer control.
TX 440	Ko Consol.	DI transducer. Noticeable bulging.
TX 441	Ko Consol.	DI transducer. Good control but still poor response.
TX 443	Ko Consol.	
TX 444	Ko Consol.	
TX 446	Ko Consol.	
TX 447	Ko Consol.	
TX 448	Ko Consol.	
TX 449	Ko Consol.	
TX 450	Ko Consol.	
TX 451	Ko Consol.	DI transducer w/ sheet of nylon across bottom to provide more area for drainage to probe.
TX 452	Ko Consol.	Kulite transducer. Average response. Used in analysis.
TX 453	Ko Consol.	Kulite transducer. Poor response. Pore pressure data ignored.
TX 454	Ko Consol.	Kulite transducer. Average response. Used in analysis.
TX 456	Ko Consol.	Kulite transducer. Good response. Data only to 5 ksc. Used in analysis.
TX 457	Ko Consol.	Kulite transducer. V. good response. Used in analysis.
TX 458	Ko Consol.	Kulite transducer. Excessive bulging.
TX 460	Ko Consol.	Kulite transducer. V. good response. Filter paper present. Used in analysis.
TX 461	Ko Consol.	
TX 462	Ko Consol.	
TX 463	Ko Consol.	
TX 464	Ko Consol.	
TX 465	Ko Consol.	Kulite transducer. V. good response. Used in analysis.
TX 467	Ko Consol.	Kulite transducer. V. good response. Filter paper present. Used in analysis.
TX 469	Ko Consol.	
TX 472	Ko Consol.	

Table 4.1 Overview of Testing Program

Trial #	Type	Confining Stress (ksc)	Hydraulic Conductivity (cm/s)	System Losses (cm)	Standard Deviation	Best Fit Equation to First Time Loading Data	r^2
6	Whatman 1	0.47	2.53E-04		6.7E-06	$K = \exp\left(\frac{\sigma' + 14.78}{-1.85}\right)$	0.997
		0.95	2.10E-04		3.0E-06		
		1.93	1.15E-04		4.4E-06		
		0.95	1.52E-04		3.9E-06		
		0.45	1.89E-04		1.7E-05		
		0.94	1.77E-04		4.9E-06		
		1.93	1.21E-04		4.3E-06		
		2.90	7.03E-05		7.4E-06		
7	Whatman 1	0.45	4.95E-04		1.4E-05	$K = \exp\left(\frac{\sigma' + 9.04}{-1.25}\right)$	0.998
		0.94	3.40E-04		1.5E-05		
		1.91	1.45E-04		1.1E-06		
		0.93	1.88E-04		7.0E-06		
		0.43	3.19E-04		3.4E-05		
		0.93	2.40E-04		1.7E-05		
		1.90	1.38E-04		2.5E-06		
		2.87	7.32E-05		4.3E-06		
9	System Loss	0.49		8.0	*		
		1.00		9.5	0.91		
		2.00		12.1	0.64		
		0.99		13.4	0.45		
		0.49		14.1	0.32		
		0.98		15.0	0.67		
		2.00		17.2	1.2		
		3.00		19.0	1.8		
11	Whatman 54	0.50	1.53E-03		2.3E-05	$K = \exp\left(\frac{\sigma' + 7.97}{-1.33}\right)$	0.998
		0.99	1.13E-03		7.7E-05		
		1.97	5.93E-04		7.0E-05		
		0.99	7.03E-04		5.3E-06		
		0.49	8.99E-04		2.1E-05		
		0.97	7.48E-04		5.9E-05		
		1.98	4.49E-04		5.3E-05		
		2.95	2.68E-04		6.4E-06		

* Taken from linear regression through data from first confining stress of Trial 6. $r^2 = 0.9998$.

Table 4.2 Summary of Constant Flow Tests for Measurement of Filter Paper Hydraulic Conductivity

Test Information			Index	Specimen Data		Compression Results			Pore Pressure	Hydraulic Conductivity	
Test #	Height (cm) Rate (%/hr)	u_b (ksc)	W_n (%) SD	W_n (%) S_i (%)	e_i	σ'_p C σ'_p SE	C_c* $e_{\sigma'v = 2ksc}$	$e_{\sigma'v = 4ksc}$ $e_{\sigma'v = 8ksc}$	$u/\sigma_{e=1.1}$ $u/\sigma_{e=0.95}$	C_k* $K_{e=1.1}$	$K_{e=0.95}$ $K_{e=0.8}$
CRS238	2.36 0.84	3.92	41.92 1.16	44.29 100.5	1.212	1.23 1.12	0.360 1.073	0.965 0.856	0.034 0.022	0.493 1.04E-07	5.16E-08 2.56E-08
CRS239	2.35 0.85	3.95	40.93 0.49	44.40 100.7	1.213	1.23 1.06	0.364 1.070	0.961 0.851	0.033 0.023	0.463 1.10E-07	5.23E-08 2.48E-08
CRS241	2.34 1.35	3.90	41.42 0.52	44.20 100.9	1.205	1.28 1.16	0.373 1.072	0.960 0.848	0.048 0.034	0.473 1.14E-07	5.51E-08 2.66E-08
CRS242	2.35 12.71	3.91	39.98 0.31	44.00 100.9	1.199	1.52 1.35	0.376 1.084	0.971 0.857	0.360 0.300	0.430 1.03E-07	4.63E-08 2.07E-08
CRS243	2.35 4.02	4.02	40.56 0.22	44.26 101.3	1.201	1.42 1.28	0.387 1.084	0.968 0.851	0.119 0.102	0.405 1.20E-07	5.13E-08 2.19E-08
CRS244	2.36 0.15	3.89	41.12 0.23	44.23 † 100.4	1.212	1.19 1.12	0.360 1.070	0.962 0.854	0.0051 0.0040	low excess pore pressures, large scatter in K	
CRS250	2.35 0.07	3.87	39.84 0.60	44.23 † 101.4	1.200	1.28 1.15	0.369 1.066	0.955 0.844	0.0024 0.0020	low excess pore pressures, large scatter in K	
Average		3.92	40.82	44.23 100.9	1.206	1.31 1.18	0.370 1.074	0.963 0.852		0.453 1.10E-7	5.13E-8 2.39E-8
Standard Deviation			0.75	0.15 0.4	0.006	0.12 0.10	0.010 0.007	0.005 0.005		0.035 7E-9	3.2E-9 2.5E-9

* Both C_c and C_k estimated from an effective stress of 3 ksc to the end of loading.

† Initial mass of water unavailable, average water content of 44.23% assumed for calculation.

Table 4.3 Summary of Constant Rate of Strain Consolidation Results in the Wissa Apparatus

Test Information				Index	Specimen Data		Compression Results			Pore Pressure	Hydraulic Conductivity		Saturation
Test # Depth	Height (cm) Rate (%/hr)	Drainage Condition	u_b (ksc)	W_n (%) SD	W_n (%) S_i (%)	e_i	σ'_p C σ'_p SE	C_c* $e_{\sigma'v=2ksc}$	$e_{\sigma'v=4ksc}$ $e_{\sigma'v=8ksc}$	u/σ $_{vm1.1}$ u/σ $_{vm0.95}$	C_k* $K_{vm1.1}$	$K_{vm0.95}$ $K_{vm0.8}$	δ vol probe response
TX452 top	2.28 3.28	no filter paper	4.06	41.56 0.66	43.69 101.4	1.201	1.25 1.10	0.359 1.064	0.956 0.848	0.114 0.078	0.467 1.13E-7	5.39E-8 2.57E-8	0.70 average
TX453 top/mid	2.38 1.54	no filter paper	4.06	40.87 0.44	43.73 101.1	1.206	1.16 1.06	0.357 1.067	0.959 0.852	ignore	ignore		0.59 poor
TX454 top	3.34 1.53	no filter paper	4.06	41.57 0.51	44.07 100.6	1.221	1.10 0.98	0.370 1.070	0.958 0.847	0.120 0.078	0.495 1.03E-7	5.14E-8 2.56E-8	0.69 average
TX456 ' mid	4.46 0.82	no filter paper	4.04	40.30 3.43	43.97 101.2	1.212	1.21 1.07	0.384 1.073	0.958 0.842	0.108 0.068	0.520 1.12E-7	5.75E-8 2.96E-8	0.59 good
TX457 top	4.05 1.04	no filter paper	4.10	41.89 2.01	44.28 101.8	1.213	1.20 1.08	0.366 1.066	0.955 0.845	0.110 0.078	0.487 1.07E-7	5.27E-8 2.59E-8	0.44 v. good
TX458 bottom	2.39 0.82	no filter paper	3.98	40.90 2.91	43.5 100.5	1.207	excessive bulging during test, low Kc, inconsistent Wcf, indicates leak			ignore	ignore		0.53 v. good
TX465 top	4.06 1.48	no filter paper	4.12	41.86 0.66	43.57 100.6	1.208	1.30 1.15	0.375 1.078	0.965 0.853	0.101 0.140	0.477 1.12E-7	5.41E-8 2.62E-8	0.50 v. good
Average			4.06	41.28	43.84 101.0	1.210	1.20 1.07	0.369 1.070	0.959 0.848		0.489 1.09E-7	5.39E-8 2.66E-8	
Standard Deviation			0.04	0.60	0.28 0.5	0.006	0.07 0.06	0.010 0.005	0.004 0.004		0.020 4E-9	2.3E-9 1.7E-9	

* Both C_c and C_k estimated from an effective stress of 3 ksc to the end of loading.

' Only have data up to 5 ksc

Table 4.4 Summary of K_o Consolidation Results in the Triaxial Apparatus with No Radial Drainage

Test Information				Index	Specimen Data		Compression Results			Pore Pressure	Saturation	Final
Test # Depth	Height (cm) Rate (%/hr)	Drainage Condition	u_b (ksc)	W_n (%) SD	W_n (%) S_i (%)	e_i	σ'_p C σ'_p SE	C_c* $e_{\sigma'v = 2ksc}$	$e_{\sigma'v = 4ksc}$ $e_{\sigma'v = 8ksc}$	$u/\sigma_{v=1.1}$ $u/\sigma_{v=0.95}$	δ vol probe response	Radial Strain (%)
TX460	3.81	8 x 1/4"	4.00	39.67	43.96	1.207	1.19	0.364	0.943	0.015	0.93	0.66
bottom	1.13	Wh. 54		1.32	101.6		0.98	1.052	0.833	0.012	v. good	
TX461	4.08	8 x 1/4"	3.99	40.97	44.17	1.224	1.16	0.381	0.956	0.009	0.73	0.77
top	1.00	Wh. 54		2.43	100.6		1.02	1.071	0.842	0.010	v. good	
TX462	4.04	continuous	4.00	41.09	44.12	1.217	1.21	0.381	0.952	0.020	0.68	0.98
bottom	1.96	Wh. 54		1.79	101.1		1.01	1.066	0.837	0.018	v. good	
TX463	4.07	continuous	4.01	41.85	44.03	1.208	1.33	0.411	0.949	0.005	0.92	0.97
top	1.01	Wh. 54		1.62	101.6		1.18	1.072	0.825	0.005	v. good	
TX464	4.06	8 x 1/8"	4.03	41.06	43.73	1.208	1.08	0.365	0.961	0.022	0.60	-0.09
bottom	1.02	Wh. 54		1.52	100.9		1.06	1.071	0.851	0.016	v. good	
TX467	4.08	8 x 1/4"	4.01	40.25	44.05	1.217	1.00	0.375	0.937	0.010	0.98	0.85
bottom	1.01	Wh 54+string		1.31	100.9		0.94	1.050	0.824	0.008	v. good	
TX469	4.03	8x1/4"	4.02	40.76	43.98	1.220	1.23	0.384	0.953	0.009	0.67	0.36
top	1.01	nylon+string		2.54	100.5		1.08	1.068	0.837	0.013	v. good	
TX 472	4.07	continuous	4.03	40.34	43.90	1.212	1.11	0.388	0.949	0.011	0.84	0.82
bottom	1.48	Wh. 54		2.22	101.0		1.04	1.066	0.832	0.01	v. good	
Average			4.01	40.75	43.99	1.214	1.16	0.381	0.950			
					101.0		1.04	1.065	0.835			
Standard Deviation			0.01	0.66	0.14	0.006	0.10	0.015	0.007			
					0.4		0.07	0.009	0.009			

* C_c estimated from an effective stress of 3 ksc to the end of loading.

Table 4.5 Summary of K_o Consolidation Results in the Triaxial Apparatus with Varying Radial Drainage Conditions

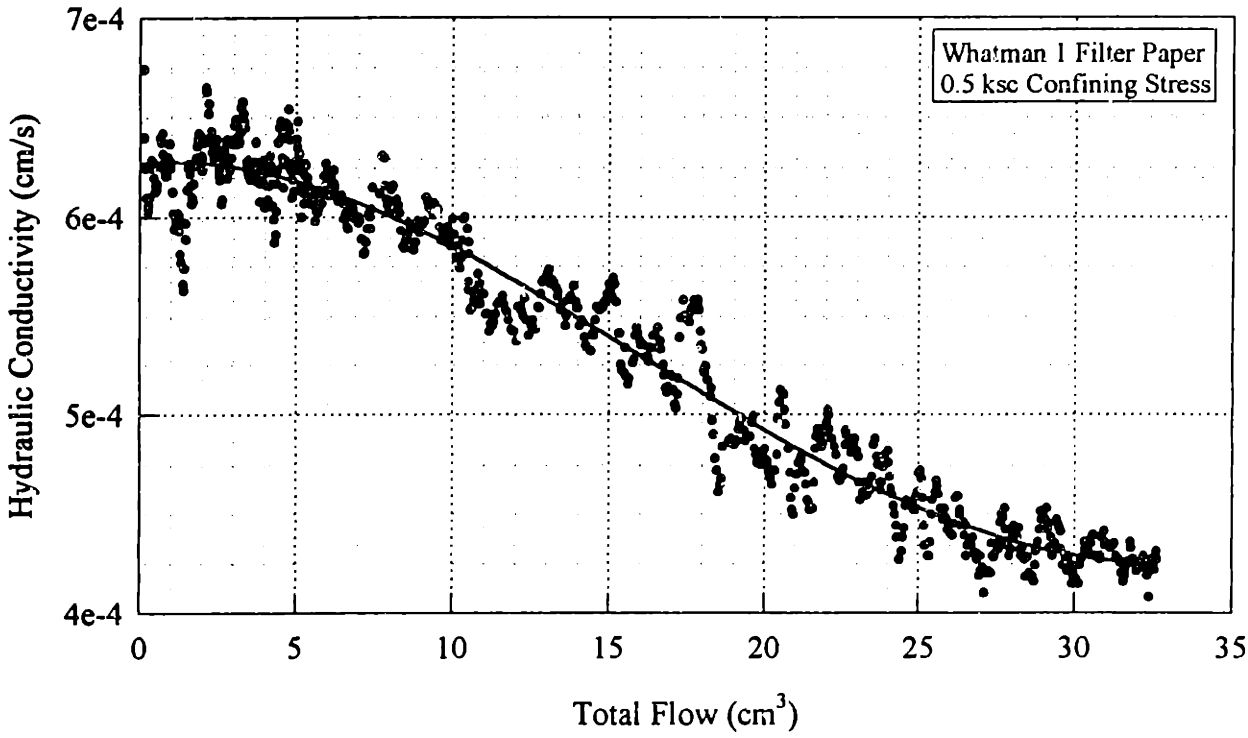

Figure 4.1 Variation of Hydraulic Conductivity with Total Flow in Whatman 1

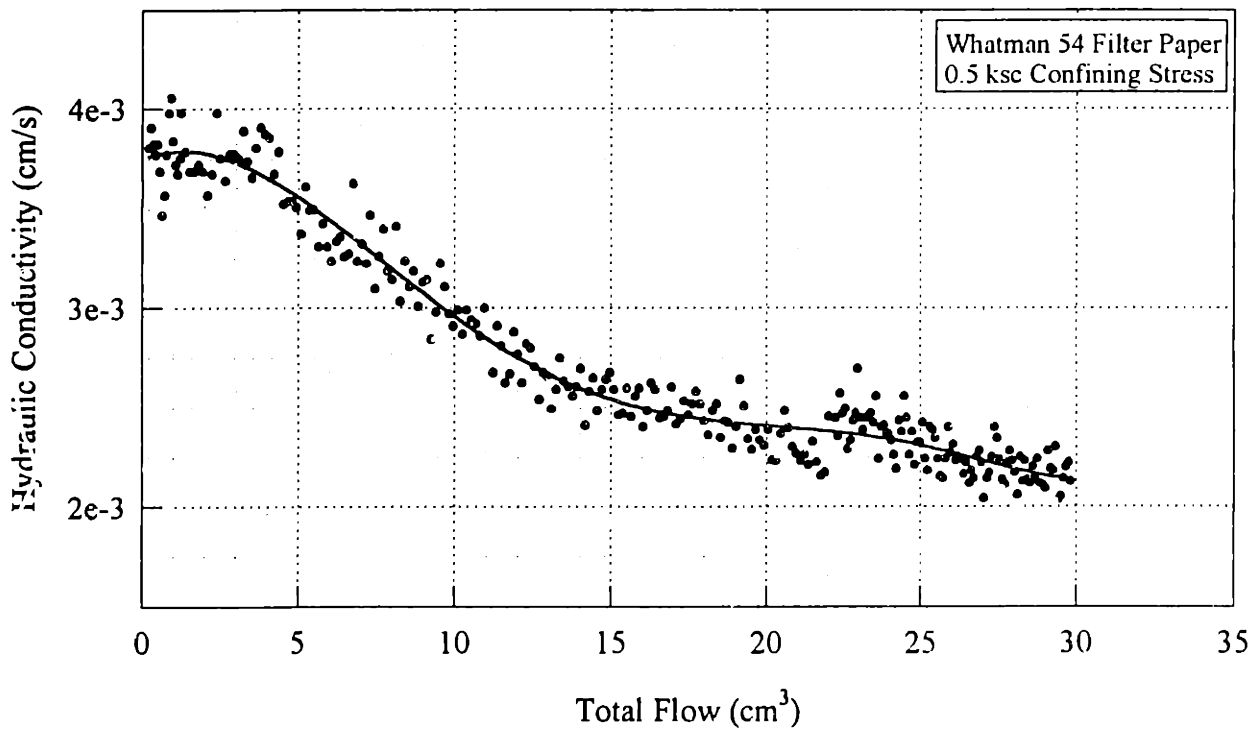

Figure 4.2 Variation of Hydraulic Conductivity with Total Flow in Whatman 54

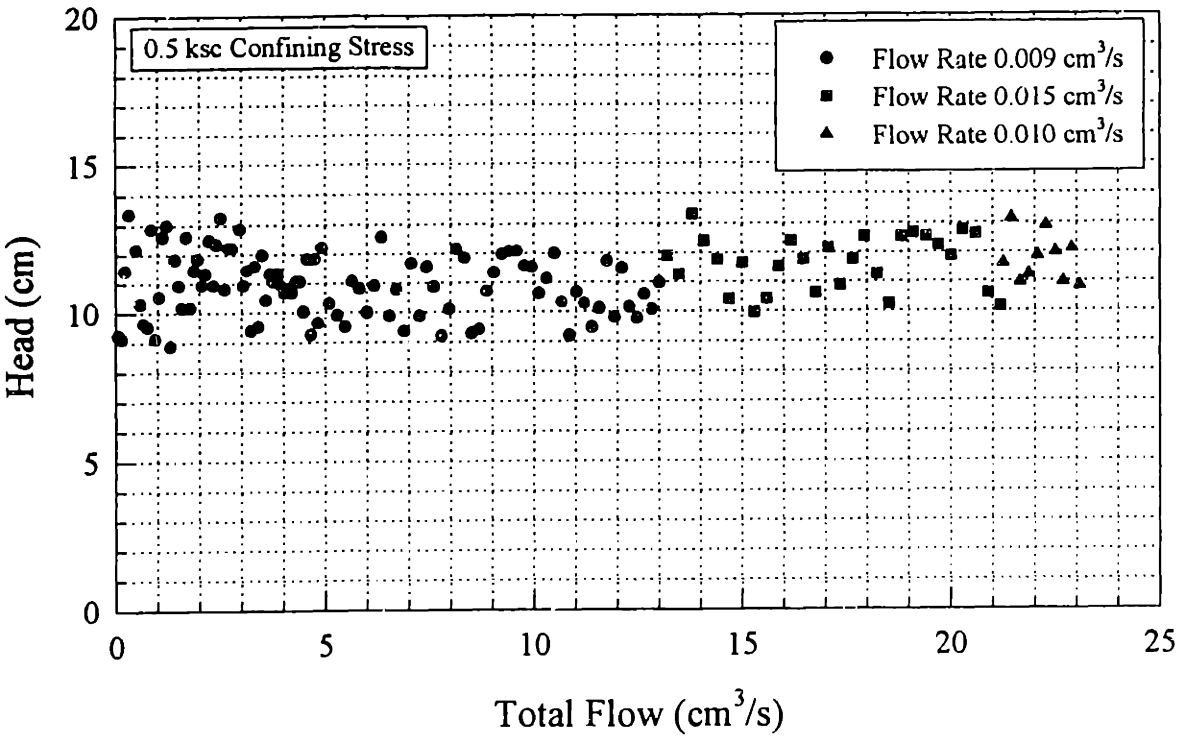

Figure 4.3 System Head Losses with Varying Flow Rate

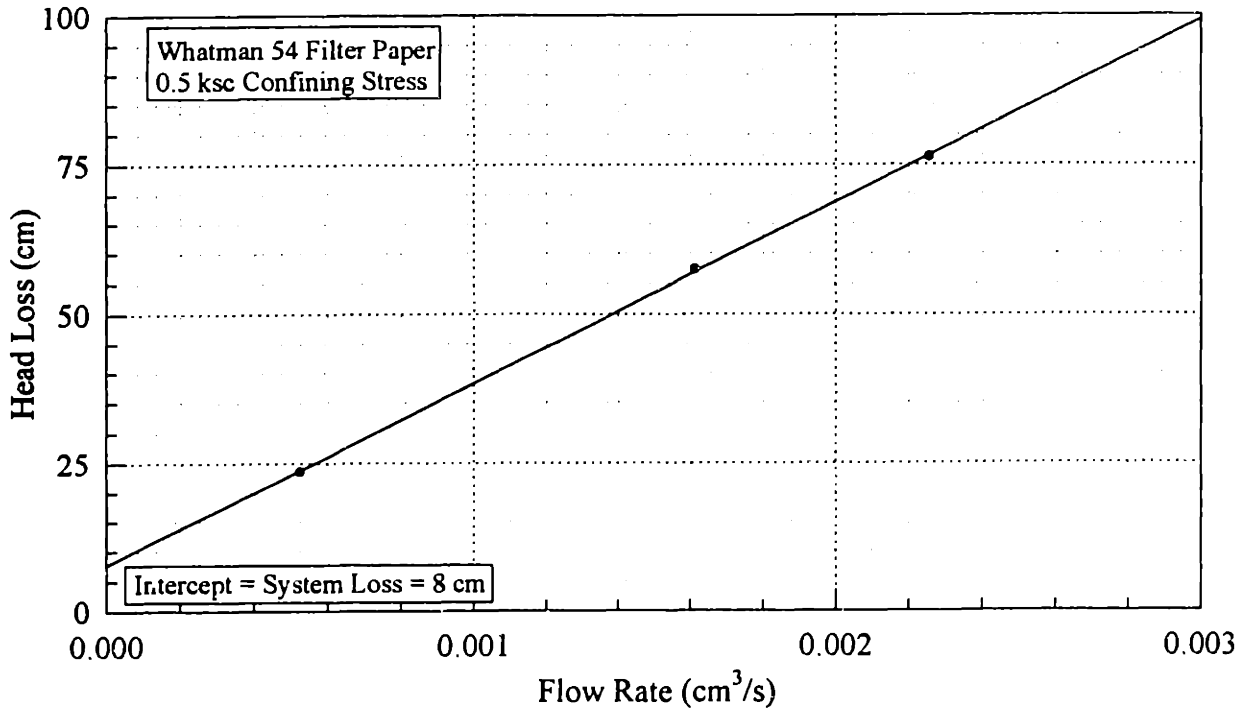

Figure 4.4 Determination of System Losses at 0.5 ksc Confining Stress

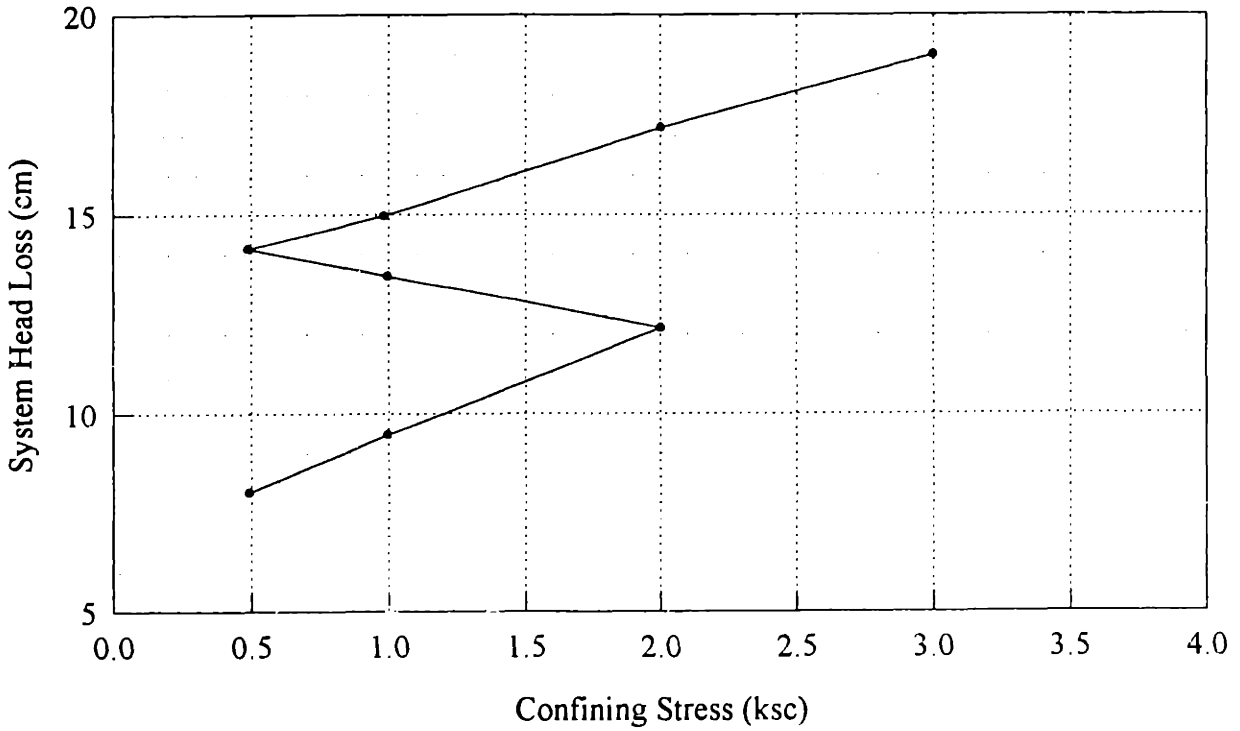

Figure 4.5 System Head Losses with Unload Reload Cycle

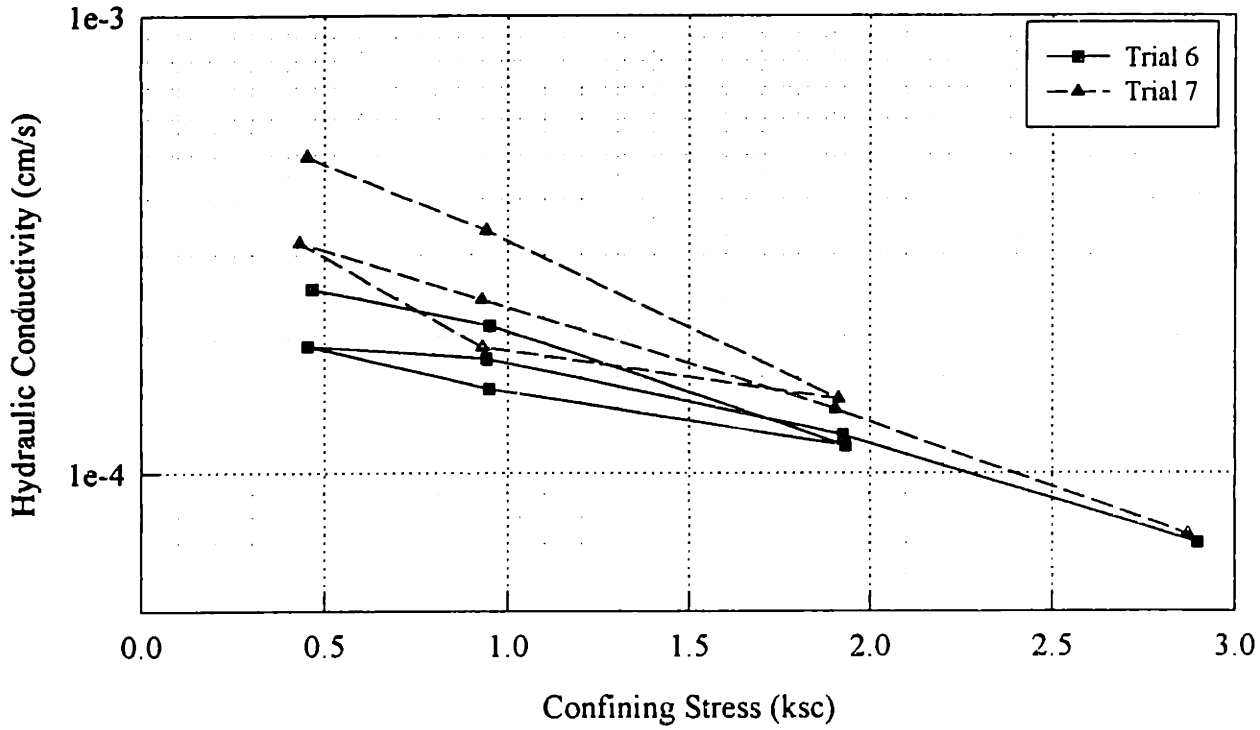

Figure 4.6 Whatman 1 Filter Paper Hydraulic Conductivity with Unload Reload Cycle

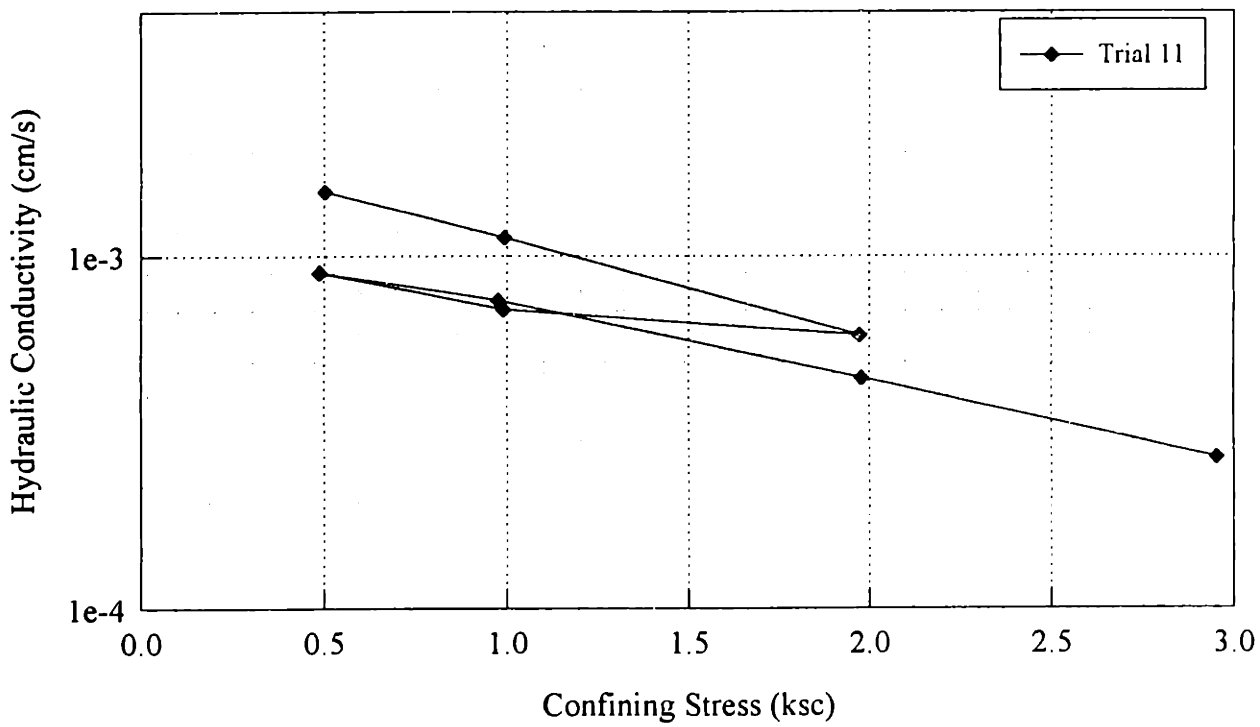

Figure 4.7 Whatman 54 Filter Paper Hydraulic Conductivity with Unload Reload Cycle

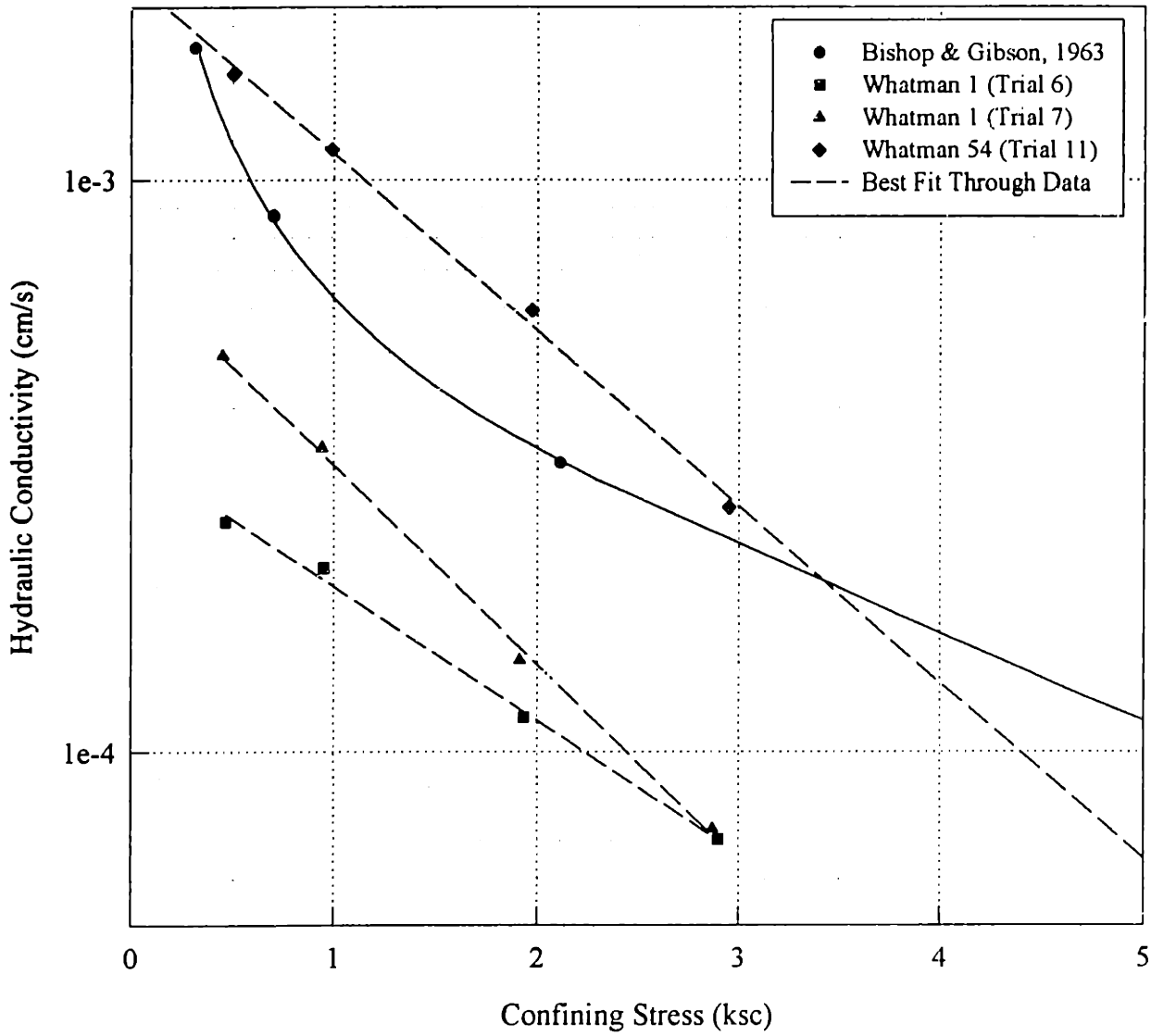

Figure 4.8 Filter Paper Hydraulic Conductivity under First Time Loading

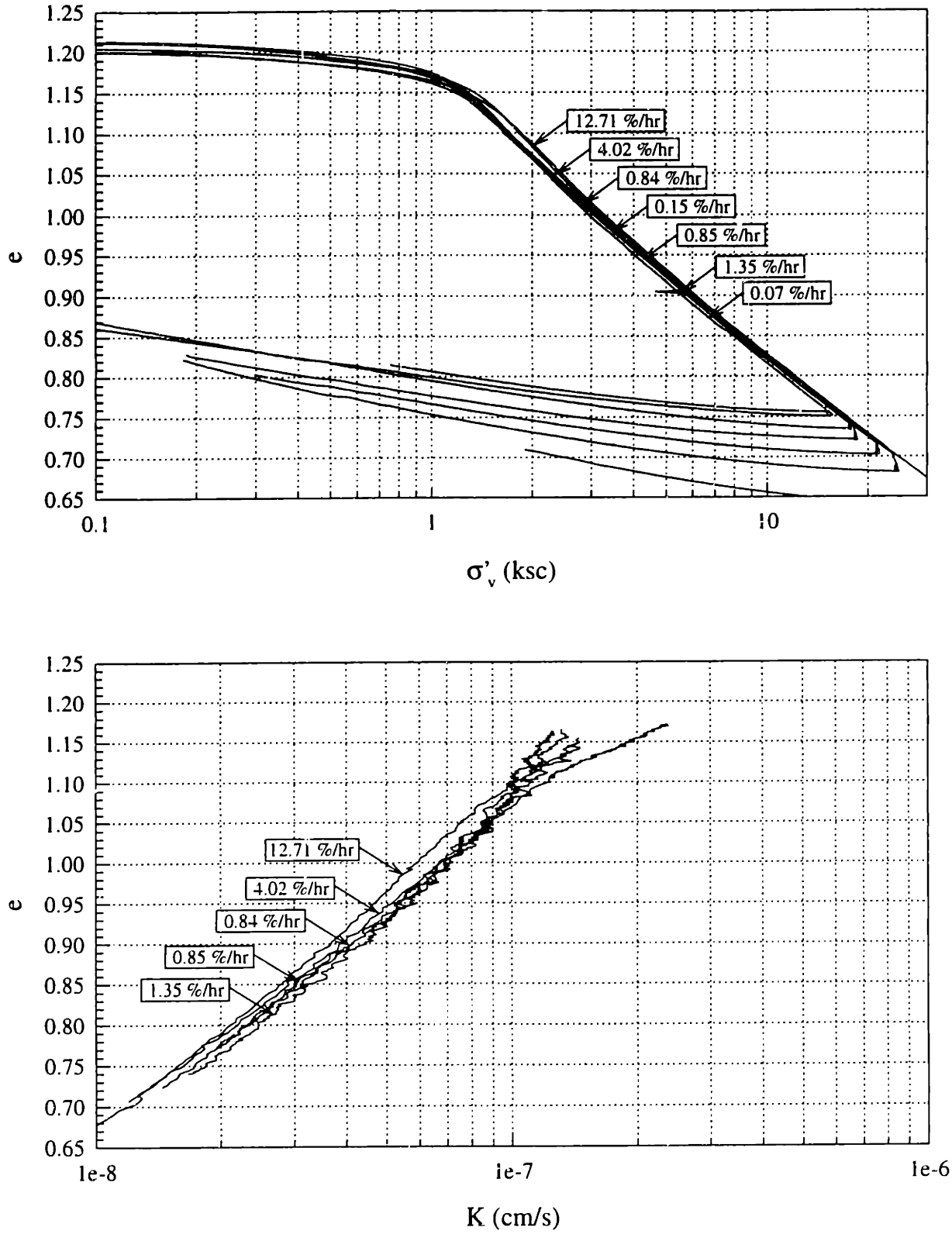

Figure 4.9 Constant Rate of Strain Consolidation Results in the Wissa Apparatus: (a) Compression Curves; (b) Hydraulic Conductivity

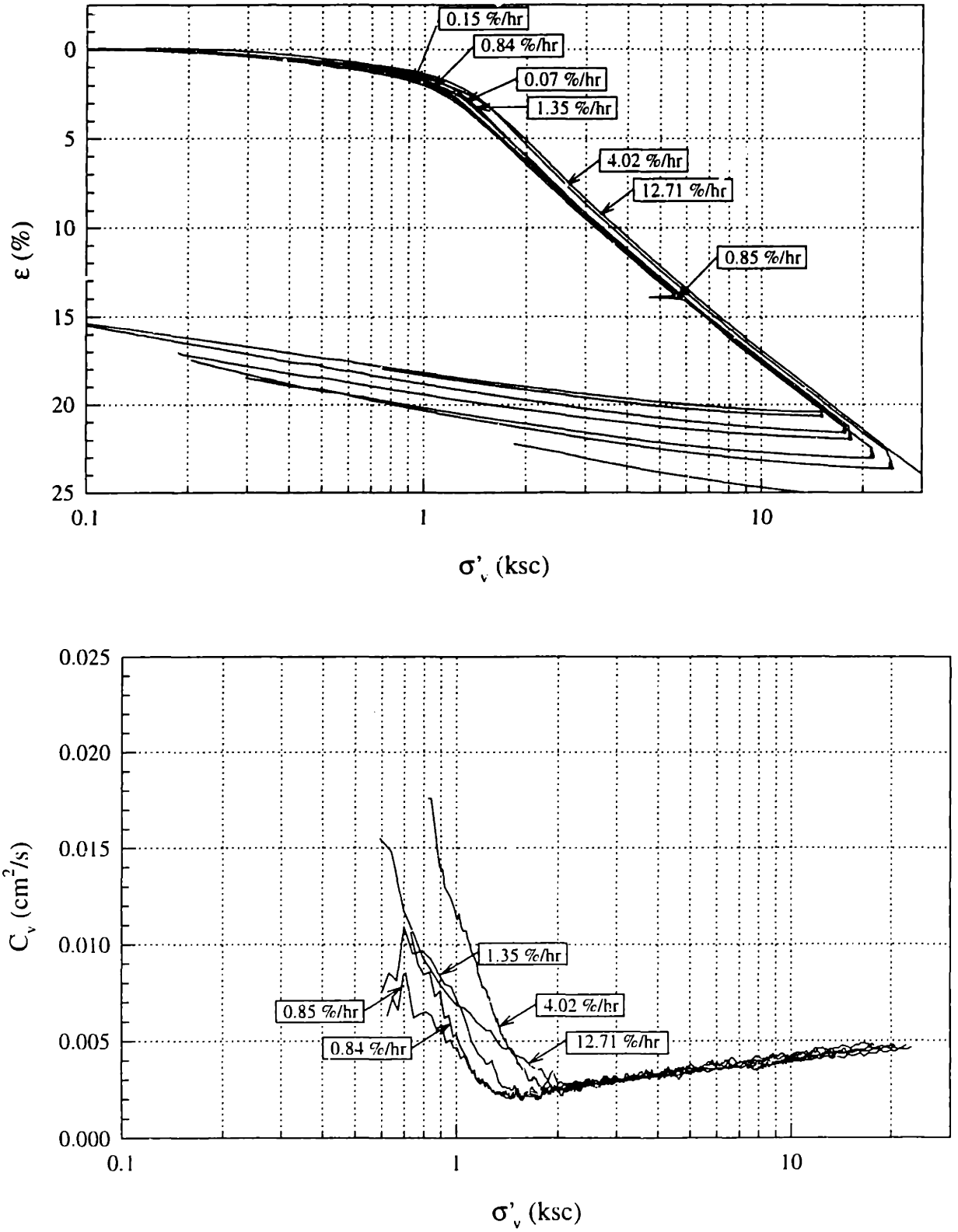

Figure 4.10 Constant Rate of Strain Consolidation Results in the Wissa Apparatus: (a) Compression Curves; (b) Coefficient of Consolidation

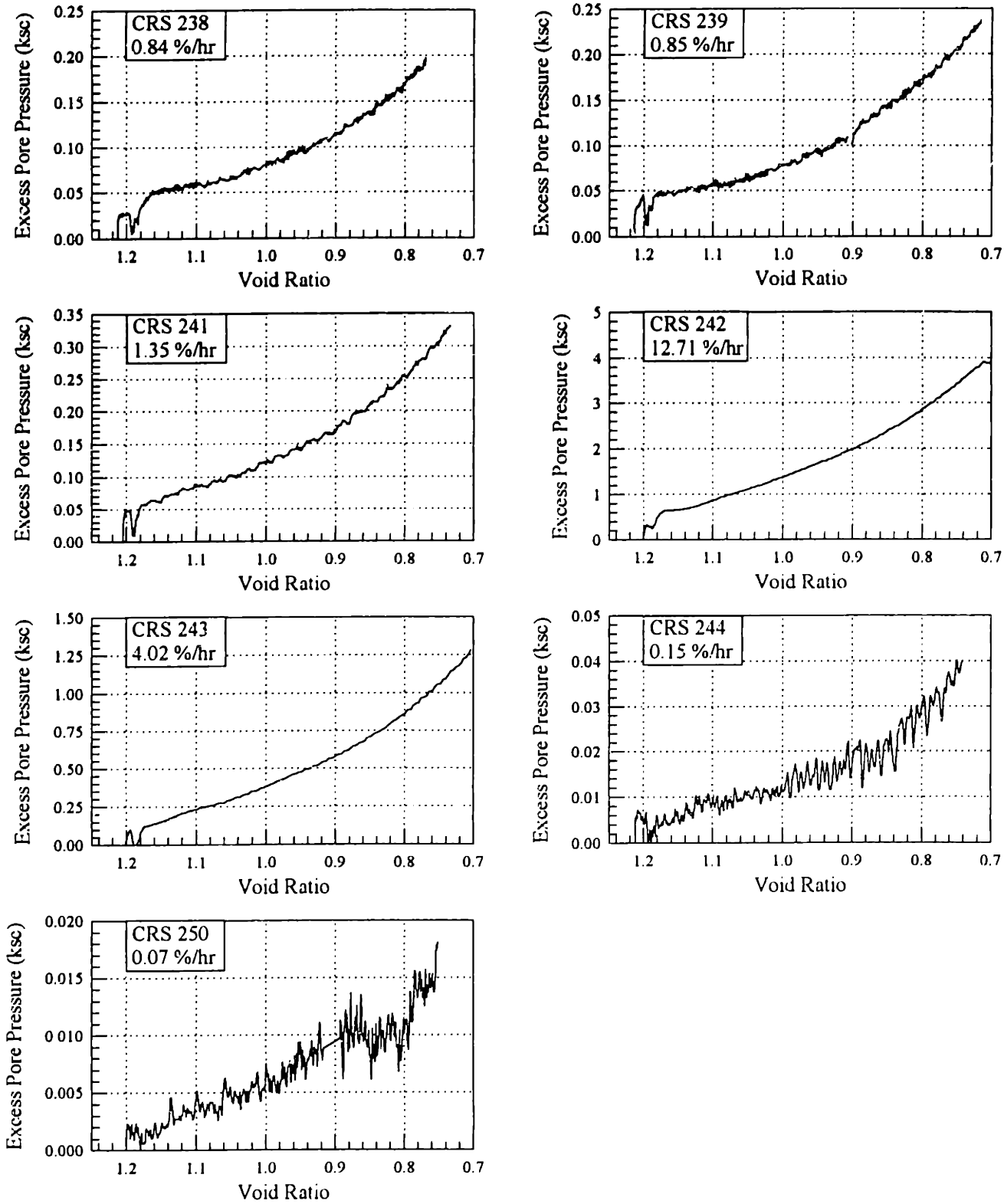

Figure 4.11 Excess Pore Pressure Curves during Constant Rate of Strain Consolidation in the Wissa Apparatus

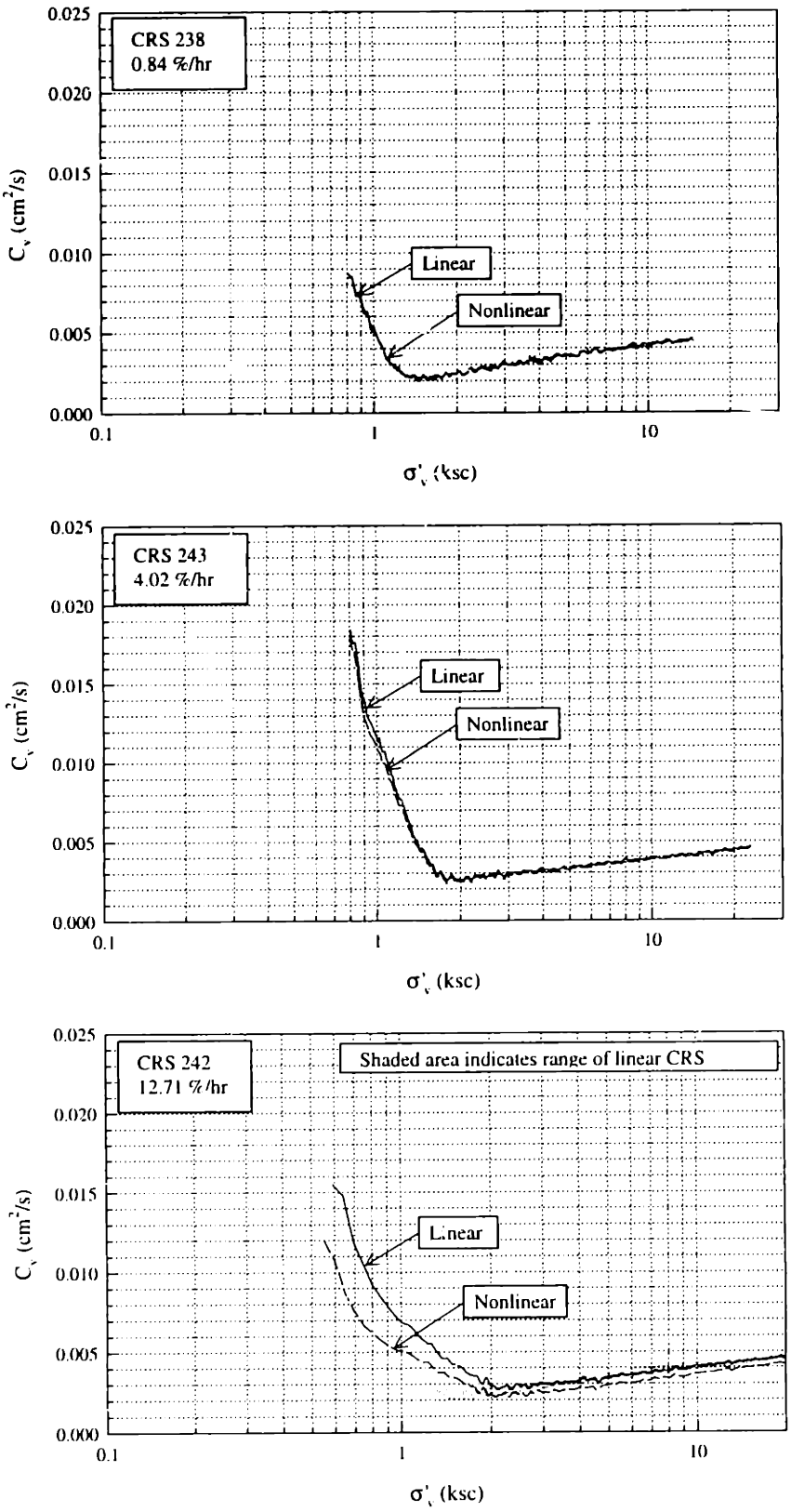

Figure 4.12 Linear vs Nonlinear Theory in Coefficient of Consolidation Results

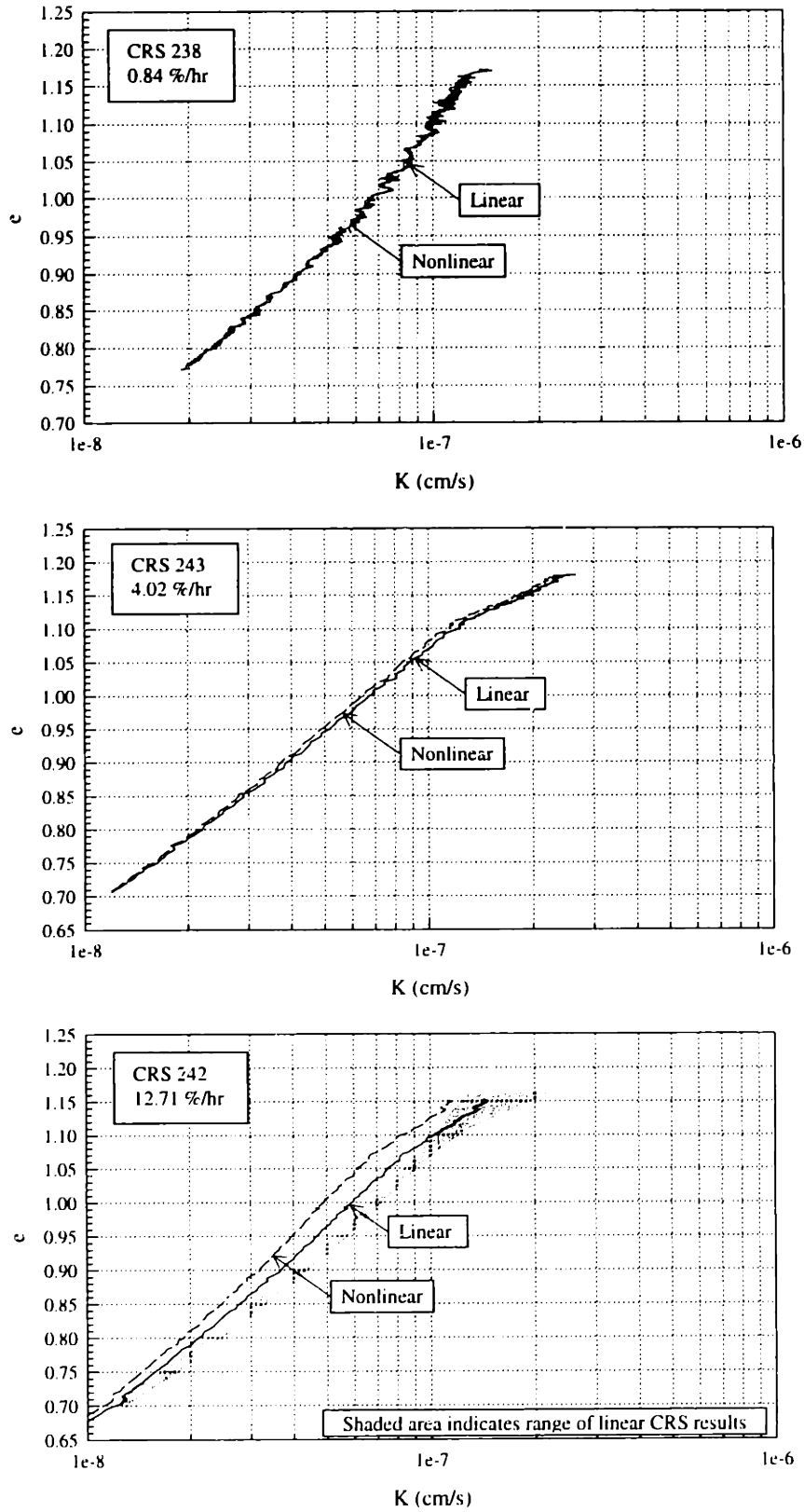

Figure 4.13 Linear vs Nonlinear Theory in Hydraulic Conductivity Results

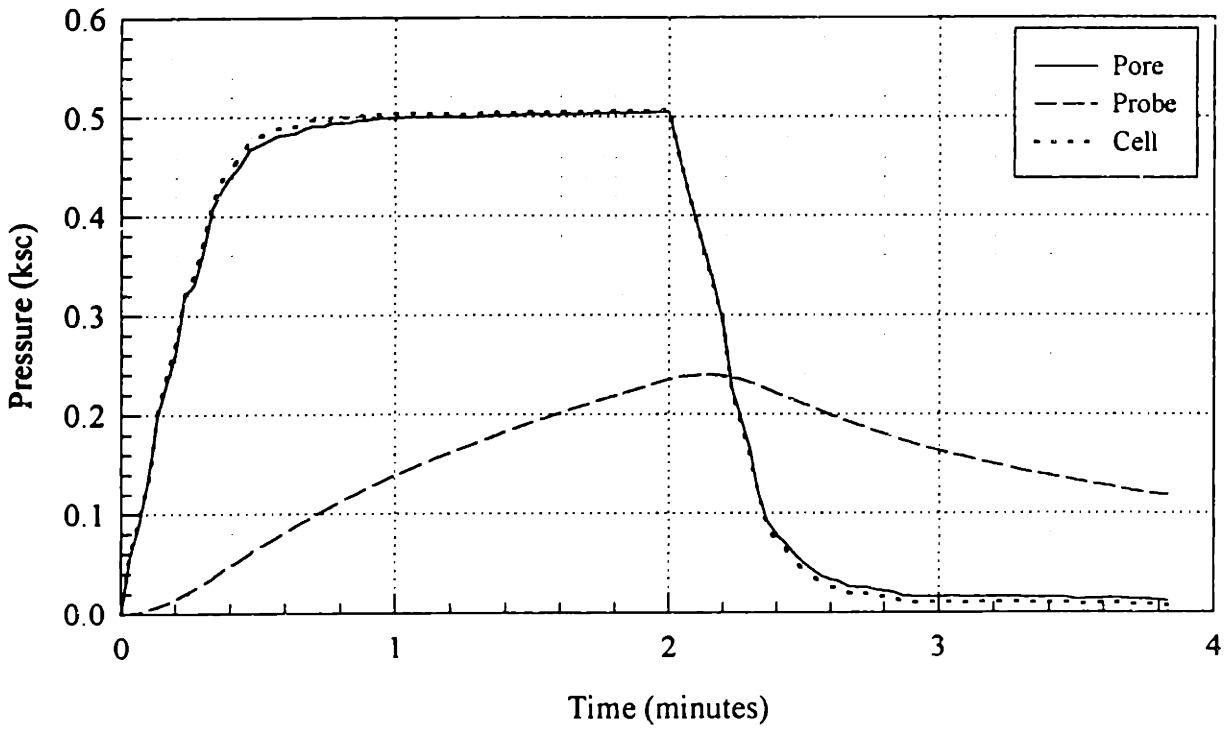

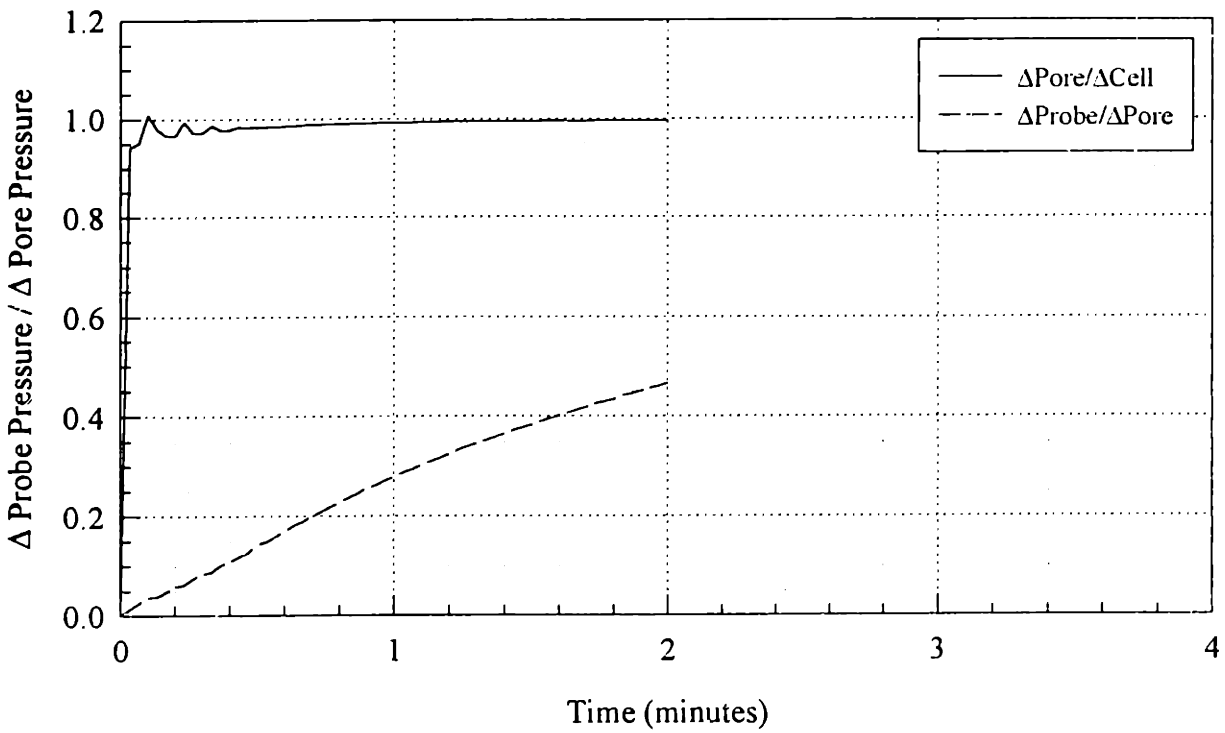

Figure 4.14 Response of Data Instruments Probe during B Value Check in Triaxial Apparatus

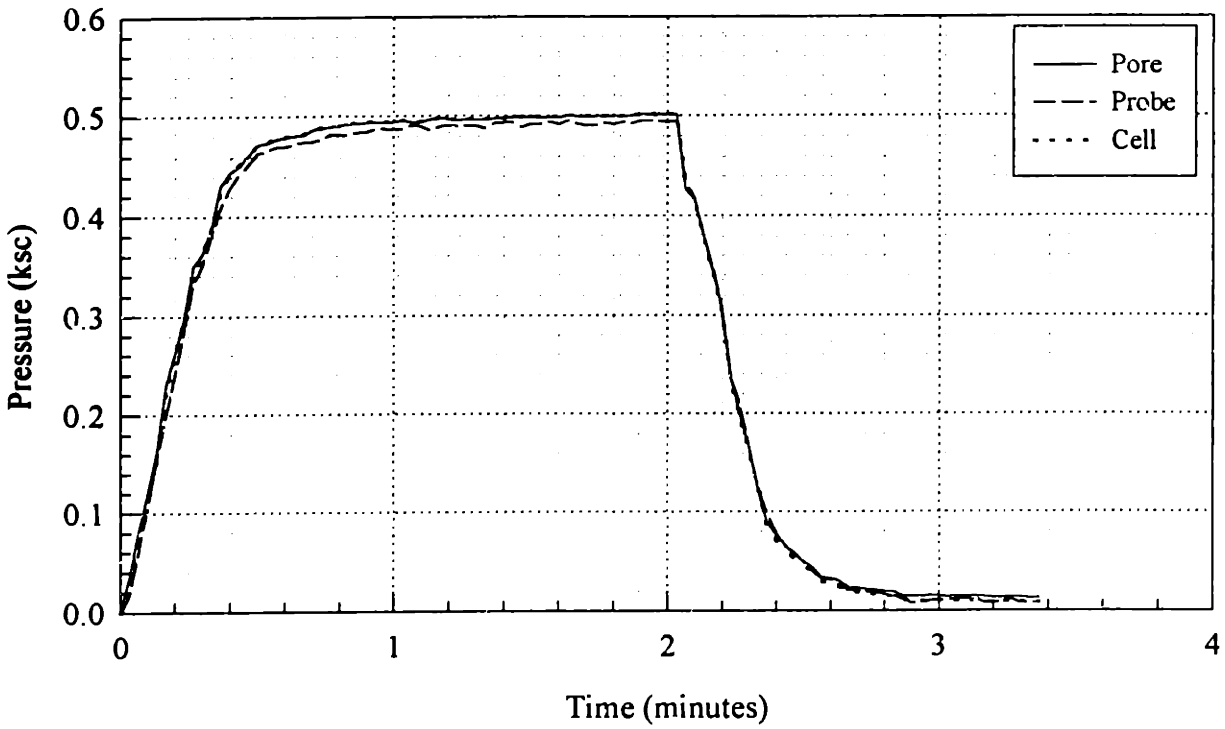

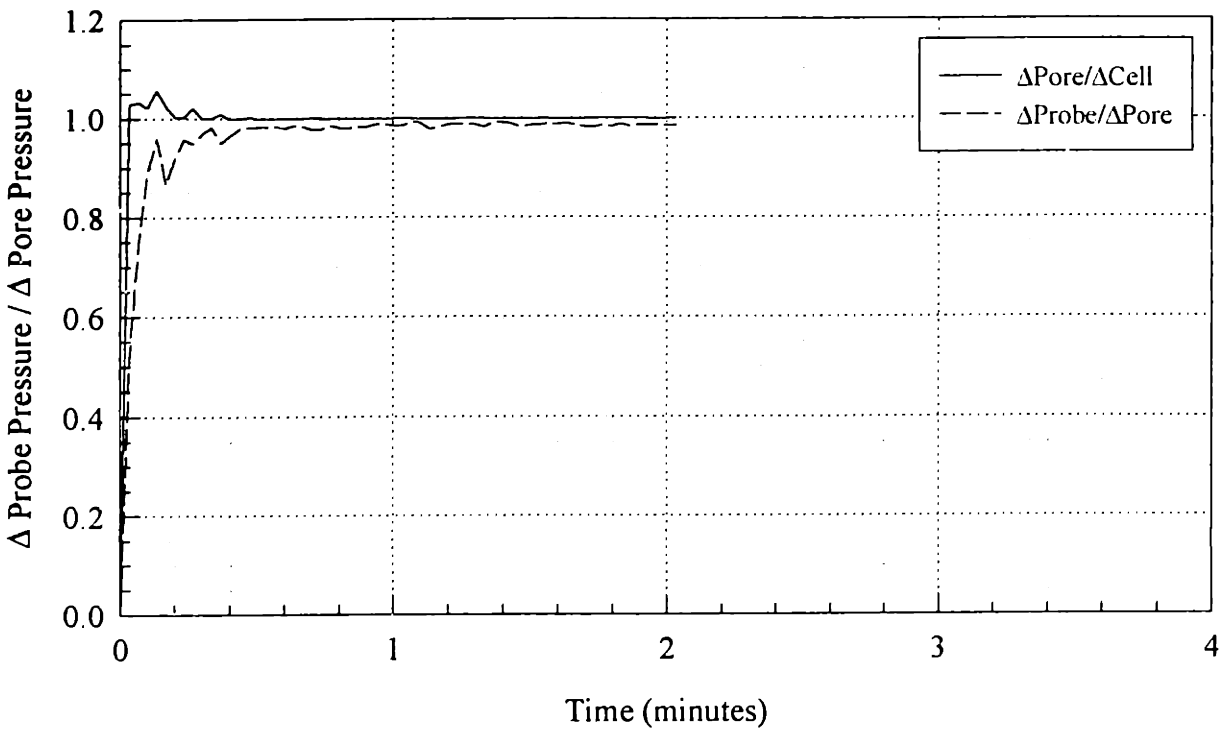

Figure 4.15 Typical Response of Kulite Probe during B Value Check in Triaxial Apparatus

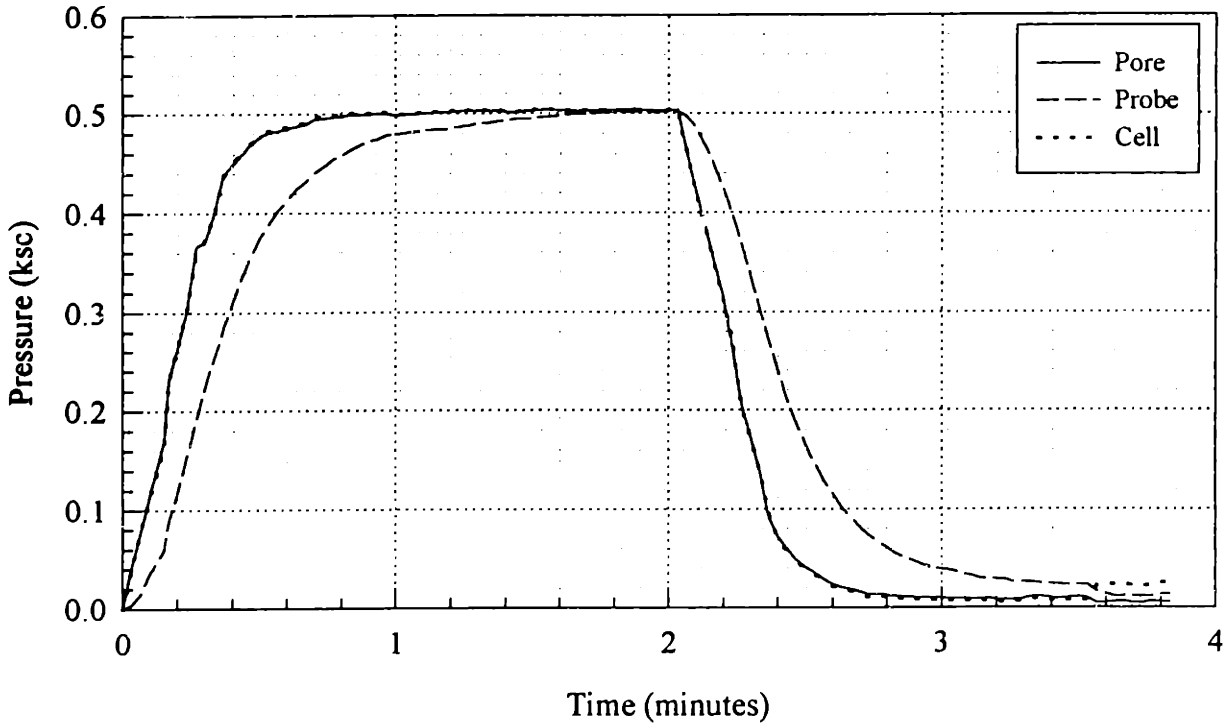

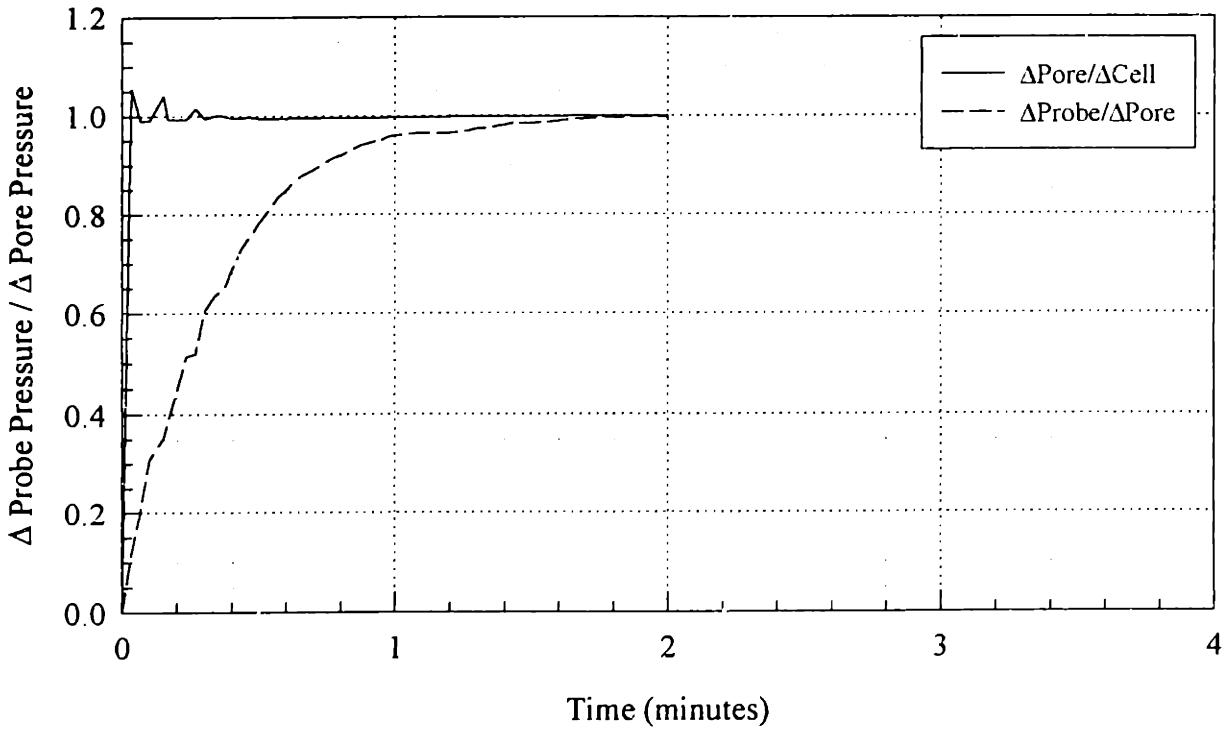

Figure 4.16 Poor Response of Kulite Probe during B Value Check in Triaxial Apparatus with No Ultrasound Prior to Setup

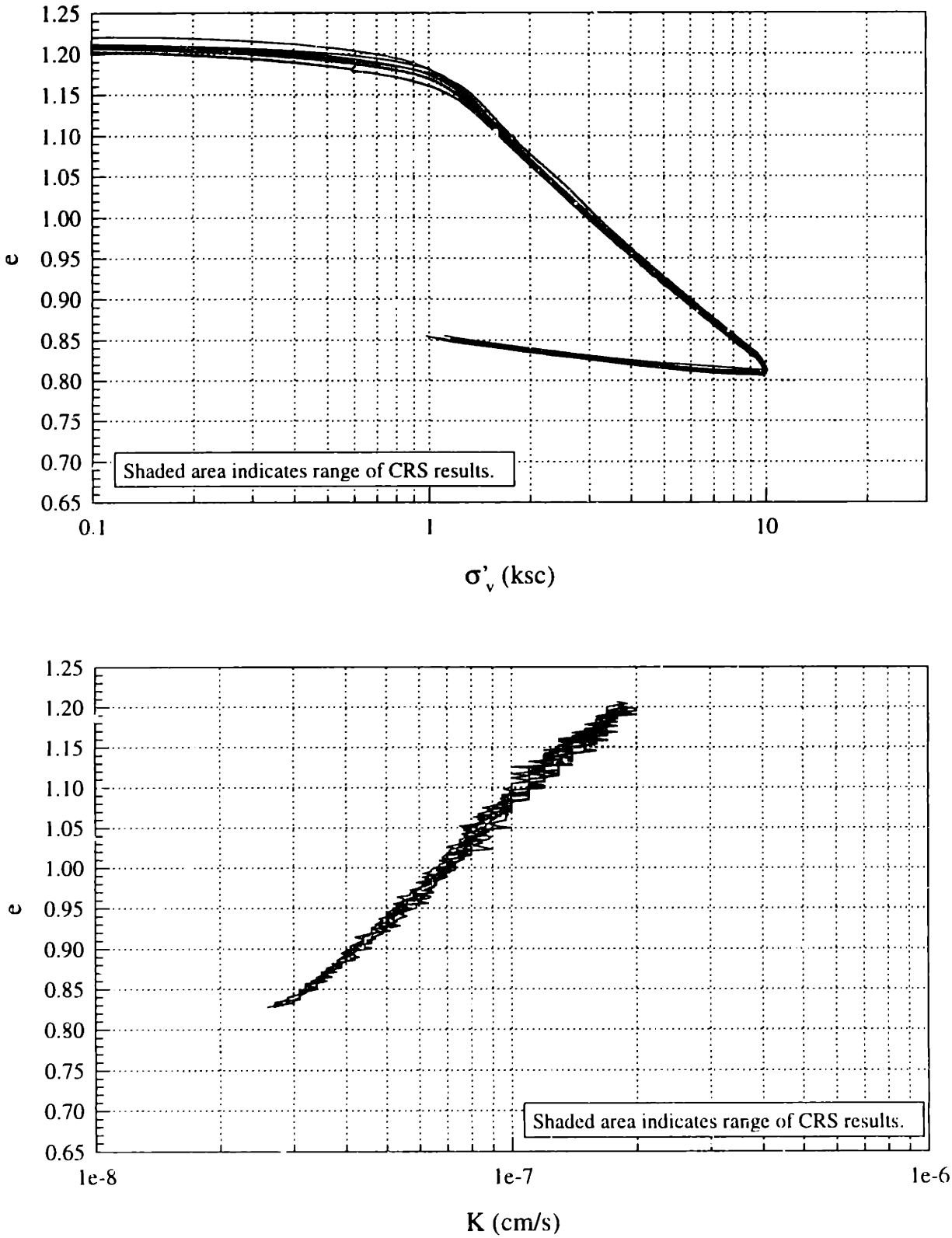

Figure 4.17 K_o Consolidation Results in the Triaxial Apparatus with Nc Radial Drainage and Height Varying from 2.28 cm to 4.46 cm: (a) Compression Curves; (b) Hydraulic Conductivity

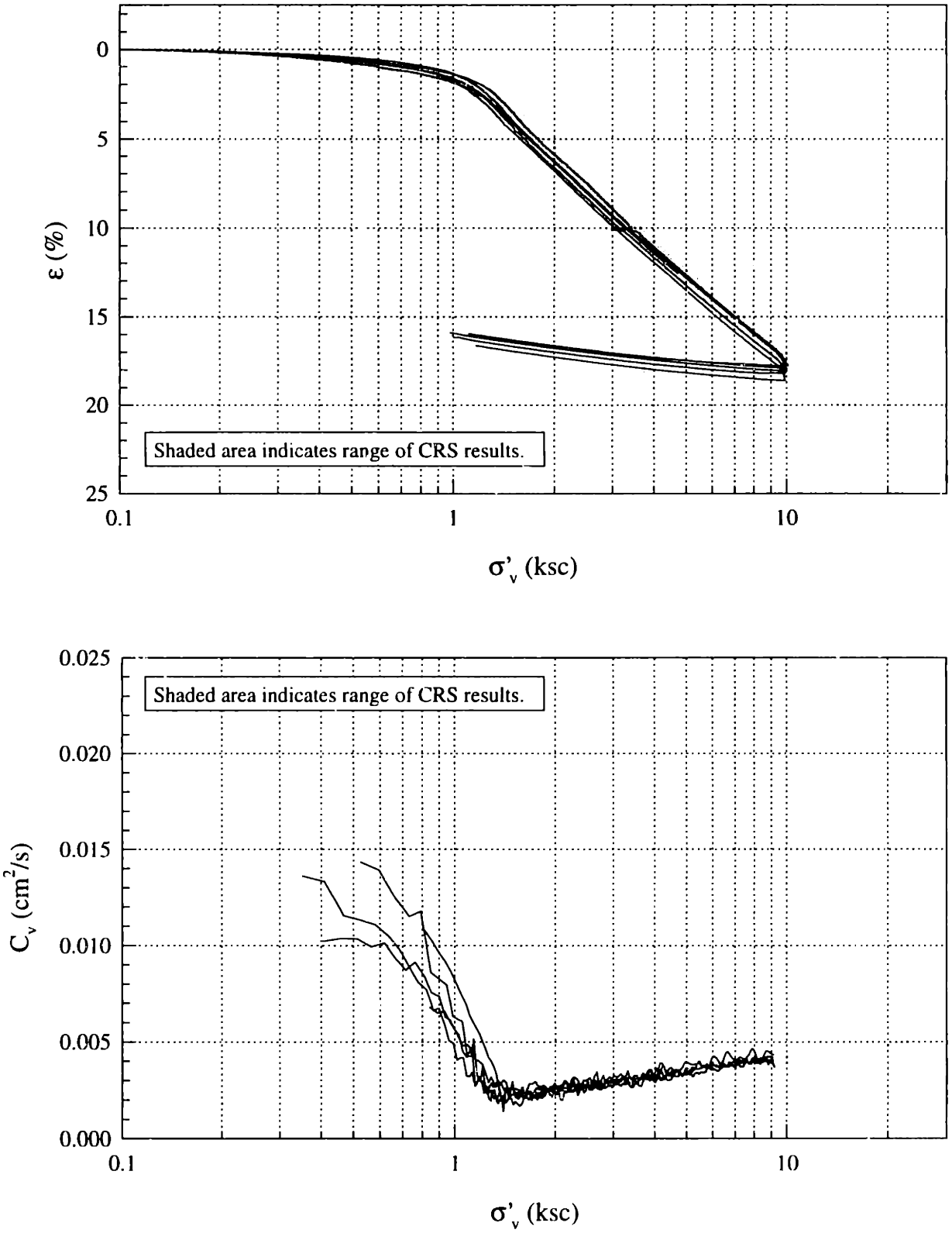

Figure 4.18 K_o Consolidation Results in the Triaxial Apparatus with No Radial Drainage and Height Varying from 2.28 cm to 4.46 cm: (a) Compression Curves; (b) Coefficient of Consolidation

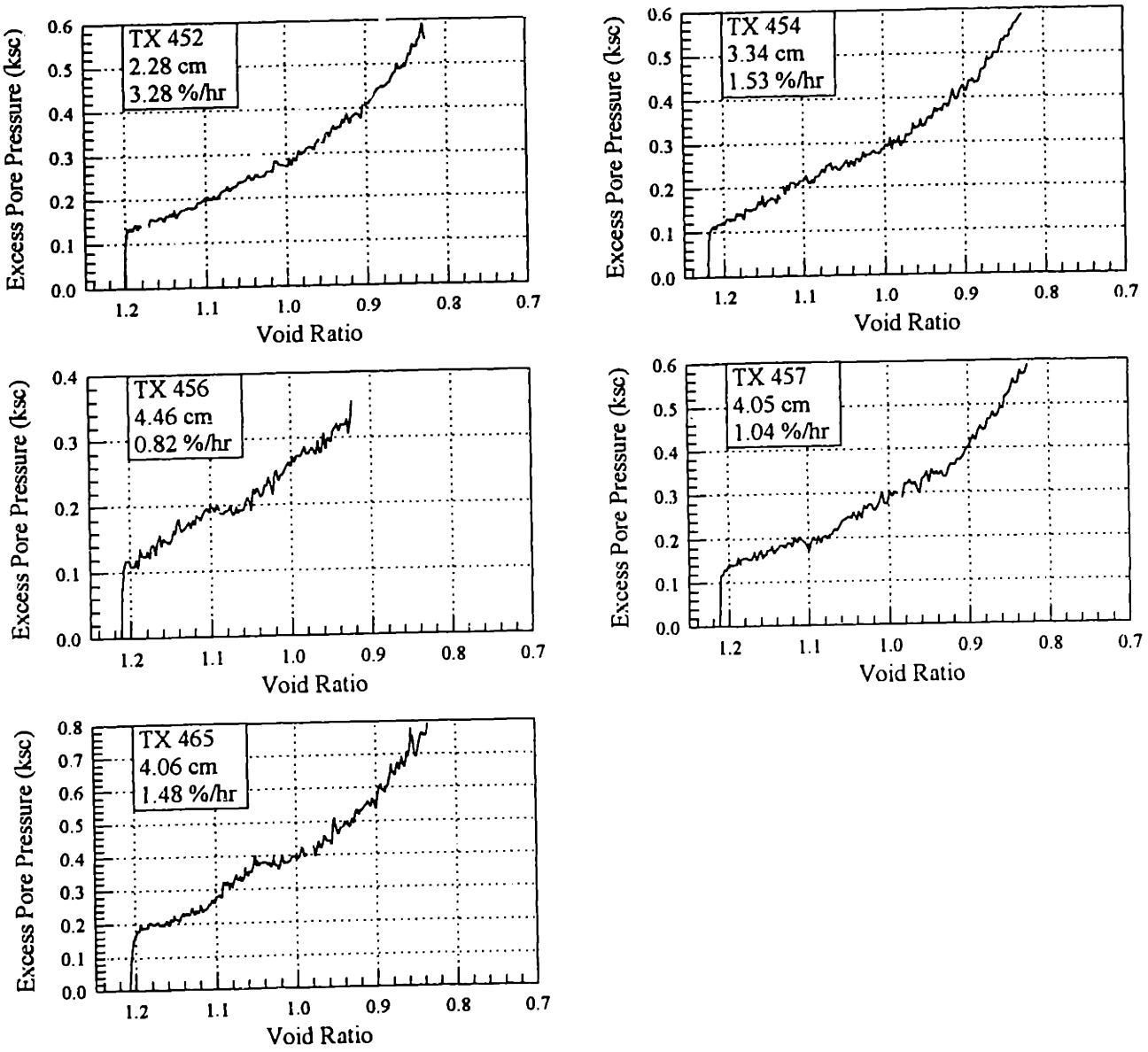

Figure 4.19 Excess Pore Pressure Curves during K_o Consolidation in the Triaxial Apparatus with No Radial Drainage and Height Varying from 2.28 cm to 4.46 cm

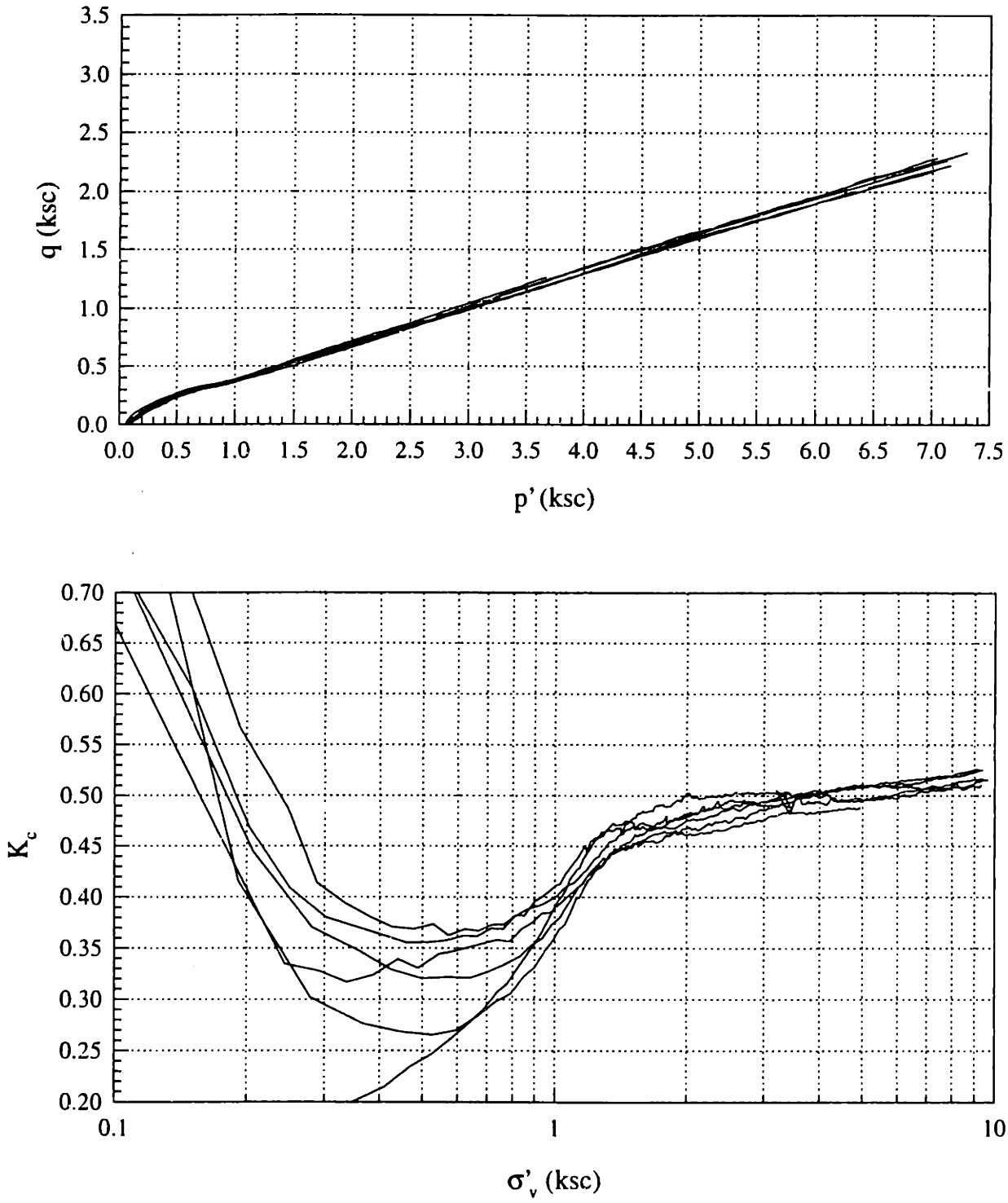

Figure 4.20 K_o Consolidation Results in the Triaxial Apparatus with No Radial Drainage and Height Varying from 2.28 cm to 4.46 cm: (a) Stress Paths; (b) Lateral Stress Coefficient

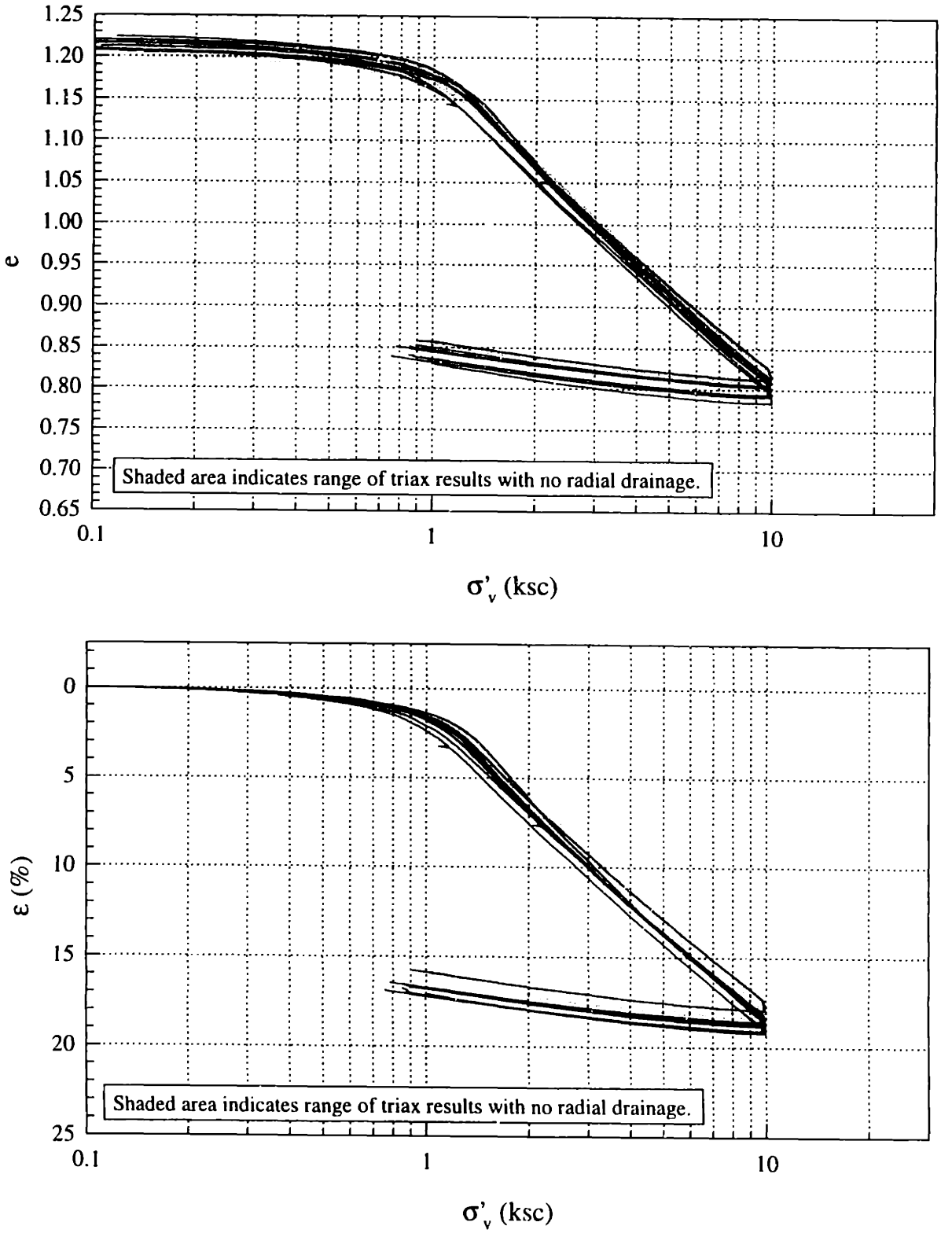

Figure 4.21 K_o Consolidation Results in the Triaxial Apparatus with Varying Radial Drainage Conditions: (a) Compression Curves with Void Ratio; (b) Compression Curves with Strain

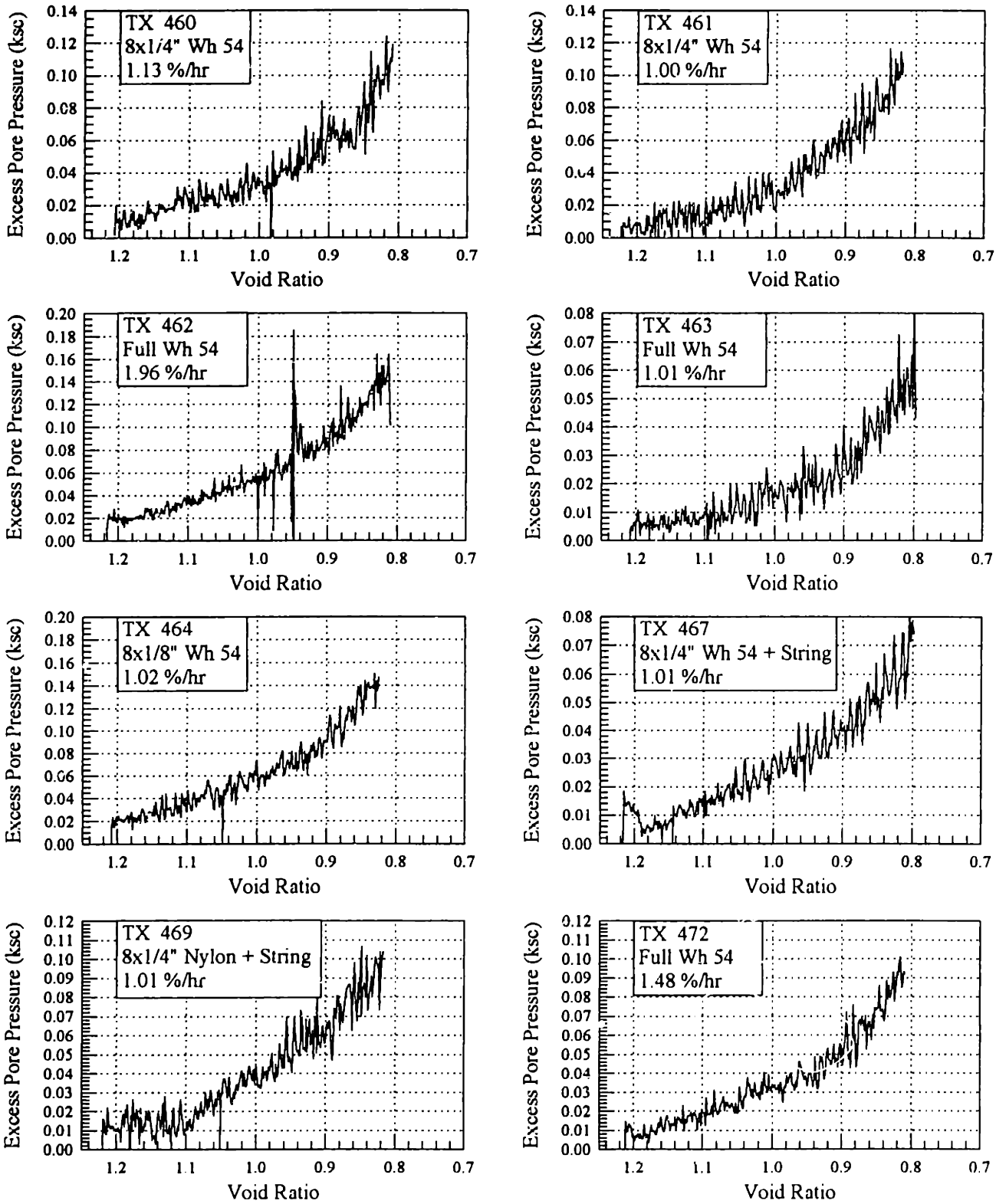

Figure 4.22 Excess Pore Pressure Curves during K_o Consolidation in the Triaxial Apparatus with Varying Radial Drainage Conditions

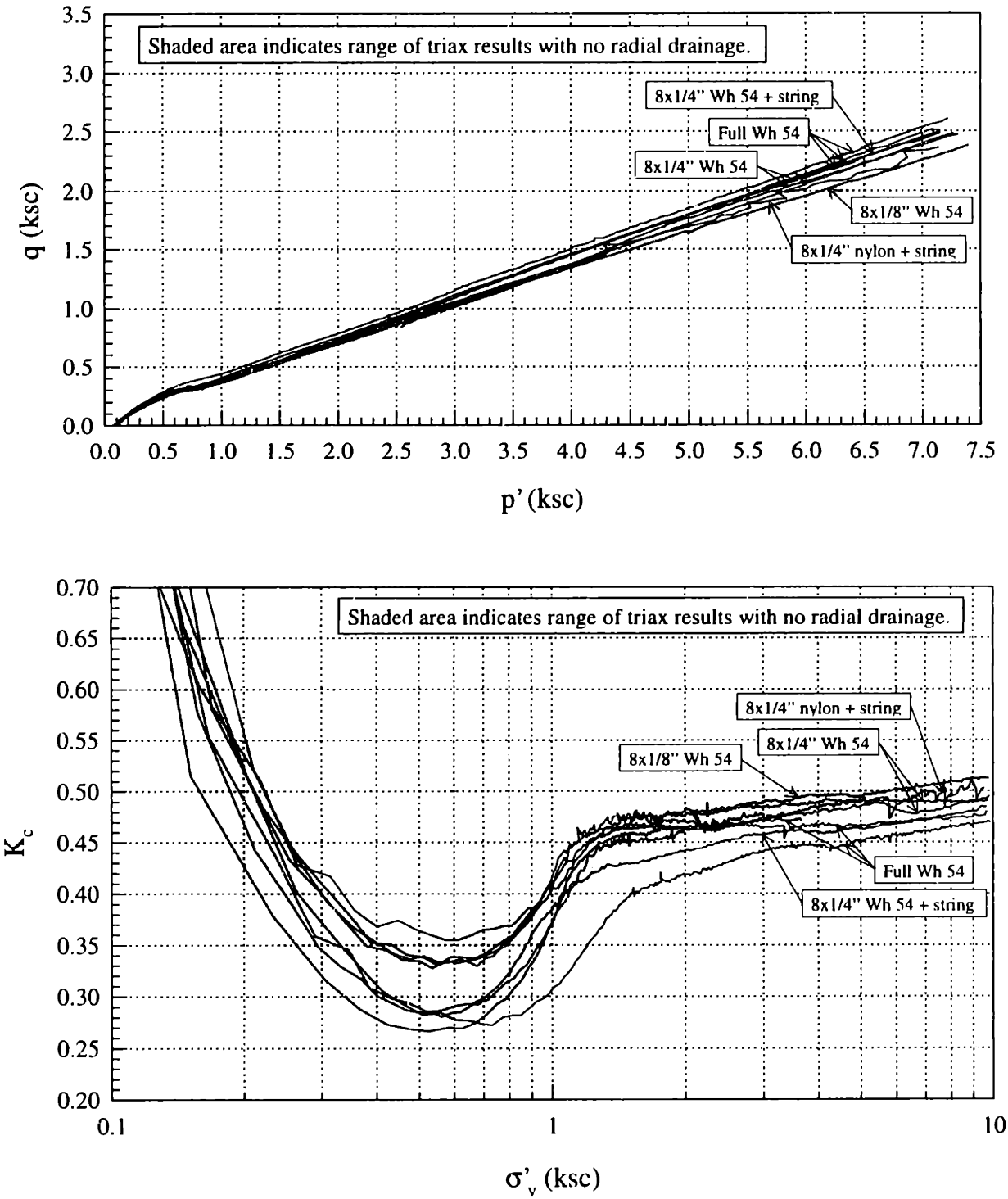

Figure 4.23 K_o Consolidation Results in the Triaxial Apparatus with Varying Radial Drainage Conditions: (a) Stress Paths; (b) Lateral Stress Coefficient

Chapter 5 Interpretation

5.1 Hydraulic Conductivity of the Filter Drains

In order to characterize the effectiveness of a filter drain system, the hydraulic conductivity of the drains must be well defined. Results of the measured hydraulic conductivity are presented in Section 4.1.3. They were performed on both Whatman 1 and Whatman 54 filter paper, however all of the triaxial tests in this research used Whatman 54, so only those results will be discussed here. The following section will summarize the equations of hydraulic conductivity of the drains and the limitations of the equations.

The hydraulic conductivity is a function of the total volume flushed through the drains, the confining stress, and the load history. It is assumed that the drains are under first time loading conditions throughout K_o consolidation, so load history is not a consideration. The only case where this is important is if the test is going to unload to create an overconsolidated specimen.

This research has characterized the effect of confining pressure on the hydraulic conductivity after flow has been forced through the drains to a steady state. Because the flow is much greater than that during testing on soil, the results are biased to lower hydraulic conductivity. The actual hydraulic conductivity may be up to 30 to 40 % higher. There may be an offset at all confining stresses or only at low stresses with the values at higher stresses approaching the correct values. The following equation was fit through first time loading data, with confining pressures from 0.5 ksc to 3 ksc, on Whatman 54:

$$K_{fp} = \exp\left(\frac{\sigma'+7.97}{-1.33}\right) \qquad \text{Equation 5.1}$$

K_{fp} is the hydraulic conductivity of the filter paper in cm/s and σ' is the confining stress, or the effective horizontal stress in the triaxial apparatus, in ksc. This is a close fit with an r^2 value of 0.998.

The data and best fit curve for these tests were show previously in Figure 4.8. Values of hydraulic conductivity quoted by Bishop and Gibson (1963) are also included in this curve. No

standard curve adequately fits the data. In order to define a relationship with confining pressure, one curve was fit through the three points at low confining pressures and a second fit between the third and fourth points.

$0<\sigma'<2.1$ ksc: $K_{fp} = 0.000625\sigma'^{-0.882}$ Equation 5.2

$\sigma'>2.1$ ksc: $K_{fp} = \exp\left(\frac{\sigma'+20.19}{-2.77}\right)$ Equation 5.3

The confining stress in the tests done for this research ranged from 0.5 ksc to 3 ksc. The confining stress in the tests with soil, however, reached as high as 5 ksc. The assumption is made here that the trend measured up to 3 ksc continues to higher stresses, however this does not agree with the trend in values quoted by Bishop and Gibson (1963). Because of the uncertainty in the hydraulic conductivity, calculations of the effectiveness of the drain system will be done twice using the values measured in this research and then again using the values quoted by Bishop and Gibson.

5.2 Factors Controlling the Magnitude of Excess Pore Pressure

Excess pore pressure curves for each test were presented in Chapter 4. The following sections provide an analysis of the pore pressure data with respect to the test parameters (rate, height, and drain coverage). This establishes basic relationships without considering the analytical solutions. The results are later interpreted with the theoretical solutions to evaluate the strength of the models.

5.2.1 Consolidation Strain Rate

The effect of consolidation strain rate on the generation of excess pore pressure is examined through the tests run in the Wissa consolidometer, ranging in rate from 0.07 %/hr to 12.71 %/hr, all at a height of approximately 2.35 cm. As expected. the excess pore pressure increases with increasing strain rate in an approximately linear relationship. Figure 5.1 shows curves of excess pore pressure as a function of strain rate at eight different void ratios. For each test, the excess pore pressure at different void ratios was read off of the plots in Figure 4.11. The CRS tests had large variability at stresses before the normally consolidated range of the soil. Therefore only results at a void ratio of 1.1 or lower are considered in this analysis. Results from earlier data

were examined but were not as consistent. Power functions provided a good fit through the data and Table 5.1 summarizes the values of these functions. The power for these equations ranges from approximately 1.04 to 1.05, with an average of 1.047 ± 0.005, indicating that there is almost exactly a linear relationship between excess pore pressure and strain rate.

5.2.2 Specimen Height

The relationship between specimen height and pore pressure generation is investigated through the tests run in the triaxial apparatus with no drainage and height ranging from 2.3 cm to 4.5 cm. Ideally, these tests would all be performed at the same strain rate, however a strain rate that generates reasonable pore pressures in the tall specimens results in almost negligible pore pressures in the shorter specimens. Since there is a linear relationship between pore pressure and strain rate, it is possible to normalize the data to examine the effect of height alone. The pore pressures (read off of Figure 4.19 at different void ratios) have been divided by the strain rate and plotted against height for a number of different void ratios. These data are presented in Figure 5.2. The triaxial tests were not strained to void ratios as low as in the CRS test, therefore the lowest void ratios plotted are 0.85 rather than 0.75. The initial data in the triaxial test is more consistent however, so a slightly higher void ratio of 1.15 is included in the analysis.

A square function is expected to characterize the relationship between pore pressure and height. Power functions are fit through the data and summarized in Table 5.2. The curves are also plotted in Figure 5.2 and provide very good fits, with r^2 values from 0.994 to 0.9996. The average power coefficient is 1.996 ± 0.07. This indicates that the excess pore pressure increases by the square of the increase in height (i.e. if the height doubles the excess pore pressure increases by a factor of 4).

5.2.3 Coverage of Radial Drains

The standard triaxial test uses eight ¼ inch drains to decrease excess pore pressures during consolidation. Most of the existing equations for effectiveness assume that drainage occurs over the entire curved surface of the specimen. The effect of decreasing coverage then has a large impact on the use of these equations.

The drain coverage effect is examined through four tests in the triaxial apparatus, all approximately the same height, K_o consolidated at 1 %/hr (test number 460, 461, 463, and 464). Three different arrangements of Whatman 54 filter paper were considered: 8 1/8 inch drains, 8 ¼ inch drains, and full coverage of the specimen by the drains. Figure 5.3 presents the excess pore pressure data for these tests (also shown in Figure 4.22 in separate plots). There is considerable scatter in the pore pressure data due to the instability of the transducer at such low pressures. To provide a smoother curve, a five point moving average has been plotted rather than the incremental data.

As expected, the pore pressure at a given void ratio increases with decrease in drain coverage. Table 5.3 calculates the ratio of pore pressure in tests with partial coverage to pore pressure in tests with total coverage. The pore pressures reported for ¼ inch drains are an average of two tests (number 460 and 461). The ratios for tests with ¼ inch drains are consistent, ranging from 1.98 to 2.16 with an average of 2.1. Dividing the filter drain perimeter in the test with full coverage by that with partial coverage provides an estimated ratio of 2.2. This is very consistent with the observed difference, implying that the increase in pore pressure with decrease in drain coverage is exactly equal to the ratio of drain coverage.

The ratios of pore pressure in tests with 1/8 inch drains to those with full coverage are less consistent. They gradually decrease during the test, ranging from 3.25 to 4.15 with an average of 3.7 in comparison to an estimated 4.4 based on drain perimeter. The estimated value is idealized, suggesting that the pore pressure in the center of the specimen is linearly effected by the coverage. The observed values being lower than this imply that the two dimensional nature of flow into the drains becomes important in the case of 1/8 drains. So although the pore pressure is higher than in a test with more coverage, the configuration is actually more efficient based on the observed ratio (3.7) being lower than the ideal ratio based on drain perimeter (4.4).

Considering the ratio of measured pore pressure in tests with radial drainage to the measured pore pressure in tests with no radial drainage indicates the effectiveness of the drains in reducing pore pressure generation. Table 5.4 summarizes these ratios at various void ratios throughout the

test. The pore pressure ratio for tests with radial drainage is expressed as a percent of the pressure measured in the test with no drains, making the most effective conditions those with the lowest values.

The pore pressure ratio increases with decrease in void ratio. Up to a void ratio of 0.95, the rate of increase is essentially constant. After this point the ratio increases at a slightly faster rate. The general increase over the test shows that drains become less effective as the test is performed. This indicates that the hydraulic conductivity of the drains must decrease more rapidly than the hydraulic conductivity of the soil.

5.2.4 Consolidation Strain Rate with Radial Drainage

The linear relationship between consolidation rate and excess pore pressure established in Section 5.2.1 was for tests with no radial drainage. Three tests were run on specimens of the same height with full coverage of Whatman 54 filter paper at 1 %/hr, 1.5 %/hr, and 2 %/hr (test numbers 462, 463, and 472) to determine the influence of strain rate on the excess pore pressure with drains present.

The pore pressure curves are plotted in Figure 5.4 (individual plots in Figure 4.22). All three curves have similar shapes but are shifted up with increase in strain rate. First the curves should be normalized by the strain rate as was established in Section 5.2.1. The remaining difference between the curves is the effect caused by the presence of filter drains. Dividing this normalized pore pressure by the rate again brings all three tests together. Figure 5.5 presents the pore pressure divided by the strain rate squared (the first normalizes, the second is the effect of the presence of drains). The three curves are almost identical, with the 1 %/hr test deviating slightly at low void ratios.

The cause of this behavior is not well understood. One possibility is that the pore pressure distribution within the specimen changes with the faster tests and is no longer parabolic. A second possibility is that having filter drains around the specimen speeds up consolidation on the outside of the specimen, allowing less water from the inside of the specimen to flow to the

drains. This behavior may be accelerated in the faster tests, adding to the increase in excess pore pressure.

5.3 Evaluation of Models

There were several models discussed in Chapter 2 that could provide a generalized framework for the prediction of the generation of excess pore pressure during consolidation. The first was the one dimensional model for the CRS test based on continuous deformation. The second was the coupled consolidation model for drained shear with continuous rate of stress application. The final concept was a modification to the drained shear model to account for the effectiveness of the drains. The following sections will evaluate the validity of each.

5.3.1 Constant Rate of Strain Consolidation Equations

The CRS test analysis, derived by Wissa et al (1971), provides simple equations widely used to predict the maximum pore pressure with no radial drainage for the oedometer sized specimens tested in the Wissa consolidometer. This theory has solutions for both a linear and nonlinear soil model, but because the linear model provided more consistent results, this is the only model being considered here.

This section considers whether the model provides reasonable results and if it can be more broadly applied to taller specimens in the triaxial apparatus. The main equation considered is:

$$u = \frac{1}{2}\frac{rH^2\gamma_w}{k} \qquad \text{Equation 5.4}$$

The analysis of the pore pressure data from CRS tests presented in Section 5.2.1 establishes a linear relationship between excess pore pressure and consolidation strain rate. Further, the analysis of data from various height specimens in the triaxial apparatus in Section 5.2.2 establishes a quadratic relationship between excess pore pressure and height. These two relationships both support the application of this equation.

The second support for the equation is the repeatability of the results of hydraulic conductivity under widely different rate and height conditions. Figure 4.17 summarizes the results in the

triaxial apparatus and also includes a shaded area for the CRS results. These results are remarkably similar, especially considering the typical variability for hydraulic conductivity measurements. The drawback of this model is that it does not consider any radial drainage conditions, so it cannot be easily applied to examine effects of the filter drains in the triaxial test.

The hydraulic conductivity for the fastest test, performed at 12.71 %/hr, deviates from the others, indicating that tests should not be performed at rates that produce this amount of excess pore pressure. The hydraulic conductivity for the test performed at 4.02 %/hr also begins to deviate slightly after a void ratio of 0.95.

This brings out an important issue in defining the maximum allowable rates and pore pressures in the CRS test. ASTM (D4186-89) recommends that a rate should be chosen such that the ratio of the excess pore pressure to the total stress lies between 3 and 30 % while Wissa et al (1971) recommend a ratio between 2 and 5 %. The pore pressure ratios of the test at 12.71 %/hr range from 35 to 15 %, and the test at 4.02 %/hr ranges from 11 to 5 %. This suggests that there may be an inconsistency with the recommendation. First, according to the ASTM guidelines, the two tests should provide acceptable results, however they clearly do not agree with the slower tests. And second, the test at 4.02 %/hr deviates at higher stresses, while the pore pressure ratio decreases at higher stresses. According to the guidelines, as the ratio gets smaller the results should improve, however the opposite trend is seen here.

Instead of considering the pore pressure ratio, perhaps the hydraulic gradient should be examined. For the test performed at 4.02 %/hr, the excess pore pressure at a void ratio of 0.95 is approximately 0.5 ksc (Figure 4.11), which is equivalent to an average hydraulic gradient of approximately 215. Values in the test at 12.71 %/hr are even larger. This is remarkably high, making laminar flow unlikely. For the hydraulic conductivity measurement in the flexible wall permeameter, ASTM (D5084-90) recommends a maximum hydraulic gradient of only 30 for soil with a hydraulic conductivity less than $1x10^{-7}$ cm/s. Although this may be lower than is necessary for the CRS test, it clearly shows that more consideration is necessary in setting the upper bound on the excess pore pressure.

The lower bound should also be examined to find the lowest values accurately read by the measuring system. Based on the data from this research program, the lower bound is not as clear. The excess pore pressures in the two slower tests (at 0.15 %/hr and 0.07 %/hr) were below 0.04 ksc and were definitely not stable enough for acceptable calculation of hydraulic conductivity and coefficient of consolidation. The early range of the test at 0.84 %/hr (after the transient effect) is at an excess pore pressure of approximately 0.05 ksc or a gradient of 20. The properties calculated at this point were reasonable, indicating that the minimum bound should be in this range.

5.3.2 Drained Shear Equations

The expressions derived by Gibson and Henkel (1954) and Bishop and Gibson (1963) for drained shear are examined here to determine if they provide reasonable results for K_o consolidation. Neglecting the exponential terms (which contribute only to the initial transient portion) from the more complete consolidation expression, the basic equation for the average degree of consolidation at any time is presented as:

$$\overline{U}_t = 1 - \frac{h^2}{\eta C_v t_t} \qquad \text{Equation 5.5}$$

To examine the validity of the theory for K_o consolidation, the equation may be applied to each increment of the test to calculate values of C_v. Because the equation is in terms of the average degree of consolidation, an average value of the excess pore pressure needs to be used rather than the maximum value that is measured by the probe. The data reduction program calculates the average effective stress based on a parabolic distribution of pore pressures as specified by Wissa et al (1971). The difference between the average effective stress and the total stress measured was taken as the average excess pore pressure. The degree of consolidation is then calculated as one minus the ratio of average excess pore pressure to change in total vertical stress. The change in total vertical stress is used because it is equivalent to the change in pore pressure in an undrained test. A η factor of 3 is used for the case of two ended drainage and no radial drains.

The calculation was performed on CRS tests consolidated at 0.84 %/hr, 4.02 %/hr, and 12.71 %/hr (test numbers 238, 242, 243). One point to note is that Equation 5.5 is developed for the conditions in which the rate of change in total stress is constant and the increase in pore pressure without drainage is proportional to the total stress change. Since the CRS tests are performed at a constant rate of strain, it is necessary to look at the rate of stress change. Figure 5.6 plots the change in total stress with time for the CRS test run at 0.84 %/hr (number 238). A straight line would indicate a constant rate of stress change. These data are linear only up to a stress of approximately 2.5 ksc, while the data of interest are those in the normally consolidated range up to 10 ksc where the stress rate smoothly increases.

Figure 5.7 presents the values of C_v calculated by both the CRS model and the drained shear model. The two have very different trends, the CRS results have a steady increase with decrease in void ratio while the drained shear results show a gradual decrease. The decrease may be due to the increased load rate after 2.5 ksc. Both results are very consistent with changes in strain rate.

Another method to evaluate the applicability of the equation is to perform tests in segments. Consider a test consolidated to a given stress level, then stopped to allow excess pore pressure to dissipate. If loading is resumed, the two sets of equations can be used to compute the material parameters. One CRS test (number 239) was consolidated to approximately 6 ksc, then stopped to allow pore pressure dissipation. Loading was then resumed at the previous rate. The coefficient of consolidation calculated by both methods is presented in Figure 5.8. The data up to the stop in loading is consistent with the results in Figure 5.7. Once loading is resumed there is an initial transient portion in the results calculated by both methods. The results by the CRS method then return to the same values as measured in the previous tests. The results by the drained shear method, however, reach a value of 0.003 cm^2/s at the end of the test compared to 0.0015 cm^2/s computed for the previous tests. This large difference is one more indication that Equation 5.5 cannot be applied to the K_o consolidation test, however it is difficult to draw definite conclusions because the loading condition does not exactly match the theory.

There is no direct way to confirm which of these models is correct since no other types of tests have been run (incremental oedometer for instance) to provide an accepted value of C_v. It has been established however that the hydraulic conductivity calculated from the Wissa equation is consistent with hydraulic conductivity measured by other types of tests (Sheehan and Watters, 1997). Therefore, the hydraulic conductivity based on the coefficient of consolidation and the coefficient of volume change, m_v is compared to the accepted Wissa values. Figure 5.9 presents both sets of results for the test run at 0.84 %/hr. As expected, the low values of C_v lead to K values that are also too low, indicating that the values of C_v are not correct.

5.3.3 Effectiveness Equations

Bishop and Gibson (1963) have defined an expression for the effectiveness of a drainage system:

$$\nu = \frac{\pi^2}{4}\frac{k_p}{k_r}\frac{R\delta}{h^2} \qquad \text{Equation 5.6}$$

where k_p = hydraulic conductivity of the filter paper (cm/s)
k_r = hydraulic conductivity of the soil in the radial direction (cm/s)
R = radius of specimen (cm)
δ = thickness of filter paper drain (0.15 mm)
h = drainage height of specimen (cm)

The hydraulic conductivity of the filter paper is calculated by the two methods described in Section 5.1 as a function of the measured effective horizontal stress. The hydraulic conductivity of the soil is calculated as a function of the measured void ratio. The equation used in this relationship is a log fit through the hydraulic conductivity data measured in the triaxial tests with no radial drainage. Figure 5.10 presents the data and curve fit. This provides the vertical hydraulic conductivity, however the equation above requires radial hydraulic conductivity. This is fairly uncertain but was assumed to be 1.5 times the vertical hydraulic conductivity based on research by Ting (1991).

Figure 5.11 presents the observed decrease in excess pore pressure due to radial drainage as a function of void ratio. The excess pore pressure in a test with radial drainage is expressed as a percentage of the excess pore pressure in a test with no radial drains. The calculated values of effectiveness for a typical test are presented in Figure 5.12. In order to define the effectiveness,

the horizontal stress is required (to define the hydraulic conductivity of the drains) along with the void ratio (to define the hydraulic conductivity of the soil). The relationship between these is essentially the same between tests, so results from one test (number 464) are plotted in Figure 5.12. The largest uncertainty is in the interpretation of the pressure in the drains. Here it was assumed that the pressure in the drains was equal to the pore pressure measured at the top of the specimen although the pressure at the bottom may be slightly more depending on the distribution of the excess pore pressure. The plot has two curves, one calculated using the filter paper hydraulic conductivity values quoted by Bishop and Gibson and the other using values measured in this research program.

The effectiveness curve based on this research has a peak value at a void ratio of 1 to 1.05 with a steady decrease at lower void ratios. The key factor in the shape of the curve is the ratio of the hydraulic conductivity of the filter paper to that of the soil. The peak is caused by a peak in this ratio. The effectiveness based on filter paper hydraulic conductivity defined by Bishop and Gibson is constant until a void ratio of approximately 0.95 where it begins to decrease.

The increase in effectiveness before the peak in the curve based on the measured hydraulic conductivity does not agree with the observed behavior. The observed pore pressure has a steady increase with decrease in void ratio (note that an increase in effectiveness should lead to a decrease in pore pressure). This difference may be the result of the early volume flow effects caused by flushing during the hydraulic conductivity measurements. The curve based on values quoted by Bishop and Gibson is more consistent with the behavior seen in Figure 5.11. The observed pore pressure seems to increase more quickly after a void ratio of 0.95, the same location that the calculated effectiveness starts to decrease. Most importantly, these curves illustrate the importance of adequately defining the filter paper hydraulic conductivity and the need for further investigation.

The expression actually relating v to excess pore pressure is an involved equation, shown in Bishop and Gibson (1963). The equation has not been solved here, so the theoretical effect of the calculated values of effectiveness is not established. However, it is important to note that the effectiveness should be considered on a log scale, indicating that the difference in v seen in

Figure 5.12 from 20 to 40 actually should have very little effect on the pore pressure. Table 2.3 summarized the effect of v on calculated times to failure, and it shows that the ratio of the calculated time of failure based on infinitely permeable drains to the actual time to failure based on the correct effectiveness changes from about 1.13 to 1.16 for the values calculated here.

5.4 Filter Drain Resistance

The load carried by the filter drains is still not accurately characterized. A preliminary analysis of data collected for the previous phase of this research is considered here. These tests were not run specifically to examine the drain correction, so there are some inconsistencies that limit the applicability of the data to this issue. Several consecutive tests (numbers 454, 457, 461, 462, and 463) show fairly consistent trends in the data with varying amounts of filter paper, however other tests deviate from this trend and are not included in the analysis. The stress paths of these tests play an important role in explaining the inconsistencies.

Figure 5.13 presents the stress strain curves of these five tests up to 6% strain, with no load correction applied. Beyond this point, the tests cross back and forth with no trend in the data. At various increments in strain, the effective stress is read off of the plot for each test. The values for tests with the same drainage conditions are averaged (number 454 and 457, 462 and 463). The stress is then converted to load by dividing by the area of the specimen. Finally the difference in load between the different drain arrangements is divided by the difference in drain perimeter to provide a correction factor in kg/cm. These data are shown in Table 5.5 and the average is plotted in Figure 5.14.

The average value increases to strain of approximately 3% then levels off at 0.16 kg/cm. This is fairly consistent with the recommended linearly increasing correction to a maximum of 0.19 kg/cm at 2 to 3 % strain. These tests however have been selectively chosen, leaving out some that do not follow the trend at all. It is important to examine the stress paths followed by the tests. It is possible that the disparity between tests is the result of following slightly different stress paths, rather than actual differences in load carried by the filter drains. There is too much

uncertainty in this analysis to state that it is the actual behavior of the drains, it is simply one step towards better characterization.

One last point regarding the behavior of the drains during loading is that the standard correction assumes that the drains buckle at 2 to 3 % strain. Observations during the tests did not reveal any visible buckling at this strain level. It was not until strains between 6 and 8 % that very small buckles were visible. This is one more indication that the current method of correction needs consideration.

Void Ratio	Coefficient	Power	r^2
1.1	0.060	1.054	0.997
1.05	0.073	1.049	0.999
1	0.090	1.048	0.9992
0.95	0.112	1.047	0.9995
0.9	0.138	1.041	0.9994
0.85	0.166	1.051	0.9996
0.8	0.201	1.044	0.9995
0.75	0.240	1.042	0.9996
Average:		1.047	
Standard Deviation:		0.005	

Excess Pore Pressure = Coefficient * Strain Rate ^{Power}
Excess Pore Pressure (ksc)
Strain Rate (%/hr)

Table 5.1 Effect of Strain Rate on Excess Pore Pressure

Void Ratio	Coefficient	Power	r^2
1.15	0.010	1.978	0.994
1.1	0.010	2.106	0.997
1.05	0.013	2.046	0.997
1	0.017	1.973	0.998
0.95	0.022	1.910	0.998
0.9	0.027	1.919	0.999
0.85	0.029	2.040	0.9996
Average:		1.996	
Standard Deviation:		0.071	

Excess Pore Pressure/Strain Rate = Coefficient * Height ^{Power}
Excess Pore Pressure (ksc)
Strain Rate (%/hr)
Height (cm)

Table 5.2 Effect of Height on Excess Pore Pressure

	u_e (ksc)			u_e / $u_{e\ full}$	
e	full (11.08 cm)	8x1/4" (5.08 cm)	8x1/8" (2.54 cm)	8x1/4"	8x1/8"
1.15	0.007	0.013	0.028	1.98	4.15
1.1	0.009	0.018	0.035	2.09	4.01
1.05	0.011	0.024	0.044	2.11	3.86
1	0.015	0.032	0.056	2.11	3.71
0.95	0.020	0.043	0.073	2.10	3.56
0.9	0.028	0.060	0.093	2.16	3.32
0.85	0.039	0.082	0.127	2.09	3.25
Drain Perimeter Ratio (Full / Partial):				2.2	4.4
Average:				2.1	3.7
Standard Deviation:				0.06	0.34

Figure 5.3 Effect of Drain Coverage on Excess Pore Pressure

	u_e (ksc)				u_e / $u_{e\ none}$ (%)		
e	none (0 cm)	full (11.08 cm)	8x1/4" (5.08 cm)	8x1/8" (2.54 cm)	full	8x1/4"	8x1/8"
1.15	0.167	0.007	0.013	0.028	3.99	7.88	16.57
1.1	0.197	0.009	0.018	0.035	4.39	9.16	17.57
1.05	0.234	0.011	0.024	0.044	4.84	10.24	18.68
1	0.281	0.015	0.032	0.056	5.37	11.33	19.92
0.95	0.340	0.020	0.043	0.073	5.99	12.61	21.31
0.9	0.417	0.028	0.060	0.093	6.72	14.51	22.32
0.85	0.516	0.039	0.082	0.127	7.59	15.87	24.68

Figure 5.4 Effect of Radial Drainage on Excess Pore Pressure

Strain (%)	Stress with No Drains (ksc)			5.08 cm (ksc)	Stress with 11.09 cm (ksc)			Correction (kg/cm)			
	454	457	Ave	461	462	463	Ave	none - 5.08	none - 11.09	5.08 - 11.09	ave
0	0.09	0.10	0.09	0.10	0.12	0.10	0.11	0.026	0.016	0.008	0.017
0.25	0.28	0.24	0.26	0.31	0.34	0.32	0.33	0.100	0.064	0.034	0.066
0.5	0.45	0.39	0.42	0.49	0.53	0.51	0.52	0.135	0.092	0.056	0.095
0.75	0.59	0.54	0.57	0.64	0.70	0.68	0.69	0.147	0.108	0.074	0.110
1	0.71	0.68	0.70	0.77	0.84	0.82	0.83	0.147	0.115	0.089	0.117
1.25	0.81	0.81	0.81	0.88	0.96	0.94	0.95	0.141	0.120	0.102	0.121
1.5	0.90	0.92	0.91	0.98	1.06	1.04	1.05	0.136	0.123	0.112	0.124
1.75	0.98	1.01	0.99	1.06	1.15	1.13	1.14	0.132	0.126	0.120	0.126
2	1.04	1.09	1.06	1.13	1.22	1.20	1.21	0.132	0.130	0.128	0.130
2.25	1.10	1.15	1.12	1.19	1.28	1.27	1.28	0.134	0.134	0.134	0.134
2.5	1.15	1.20	1.18	1.25	1.34	1.33	1.33	0.138	0.139	0.140	0.139
2.75	1.19	1.25	1.22	1.29	1.39	1.38	1.38	0.142	0.144	0.145	0.144
3	1.24	1.29	1.26	1.34	1.44	1.42	1.43	0.146	0.148	0.150	0.148
3.25	1.28	1.33	1.30	1.38	1.48	1.47	1.47	0.148	0.152	0.156	0.152
3.5	1.32	1.36	1.34	1.42	1.52	1.51	1.52	0.147	0.155	0.161	0.154
3.75	1.36	1.40	1.38	1.45	1.56	1.55	1.56	0.145	0.156	0.166	0.156
4	1.40	1.44	1.42	1.49	1.61	1.59	1.60	0.140	0.157	0.171	0.156
4.25	1.44	1.49	1.46	1.53	1.65	1.63	1.64	0.135	0.158	0.177	0.156
4.5	1.48	1.53	1.51	1.57	1.69	1.68	1.69	0.129	0.158	0.182	0.156
4.75	1.53	1.58	1.55	1.62	1.74	1.72	1.73	0.124	0.159	0.188	0.157
5	1.58	1.62	1.60	1.66	1.79	1.77	1.78	0.121	0.160	0.193	0.158
5.25	1.63	1.66	1.65	1.71	1.84	1.82	1.83	0.120	0.162	0.197	0.160
5.5	1.68	1.71	1.70	1.76	1.90	1.87	1.88	0.119	0.164	0.201	0.161
5.75	1.74	1.76	1.75	1.81	1.95	1.92	1.94	0.116	0.163	0.203	0.161
6	1.79	1.82	1.81	1.86	2.00	1.97	1.99	0.106	0.159	0.204	0.156

Table 5.5 Calculation of Filter Drain Correction

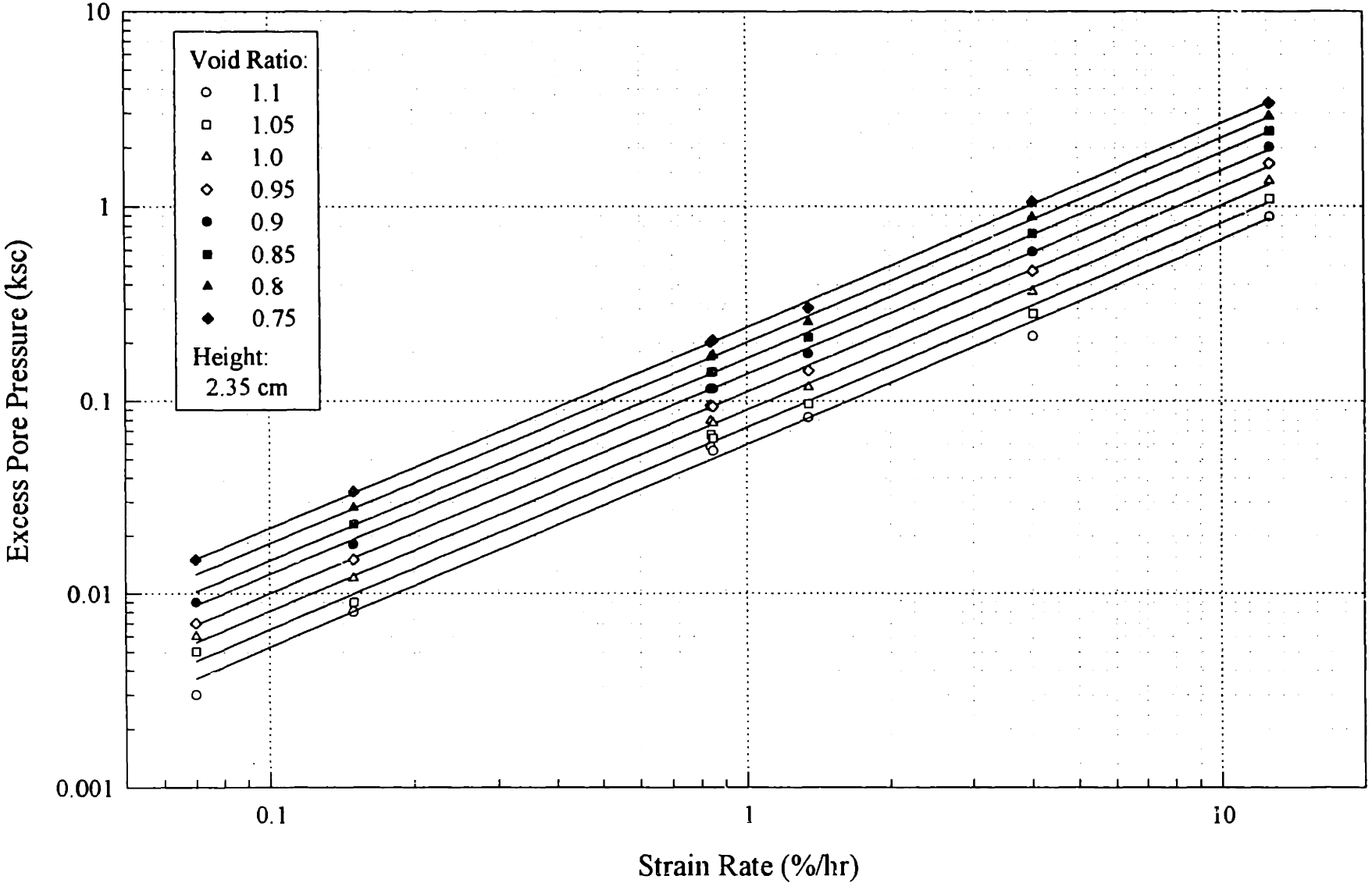

Figure 5.1 Effect of Consolidation Strain Rate on Excess Pore Pressure

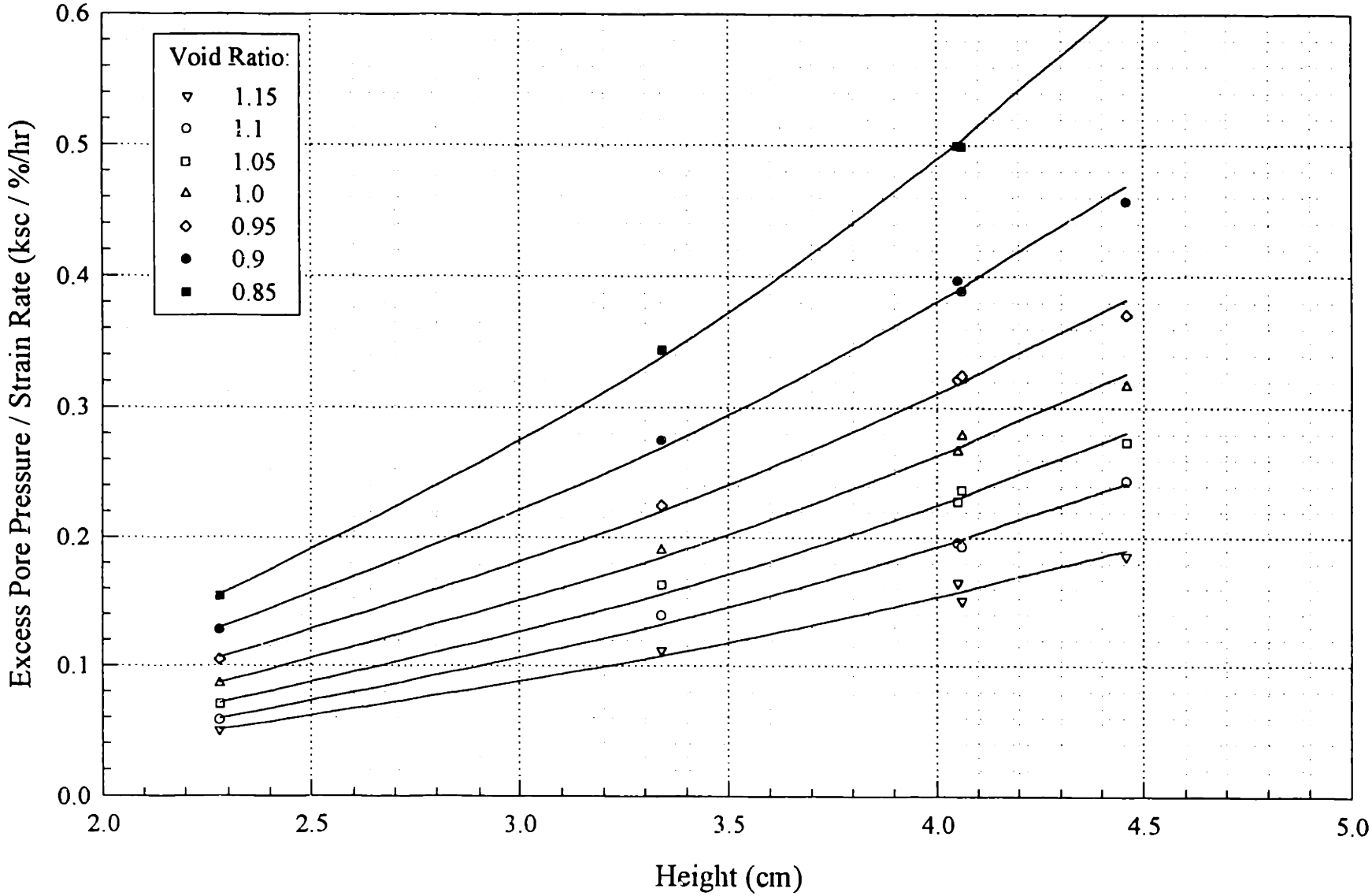

Figure 5.2 Effect of Height on Excess Pore Pressure

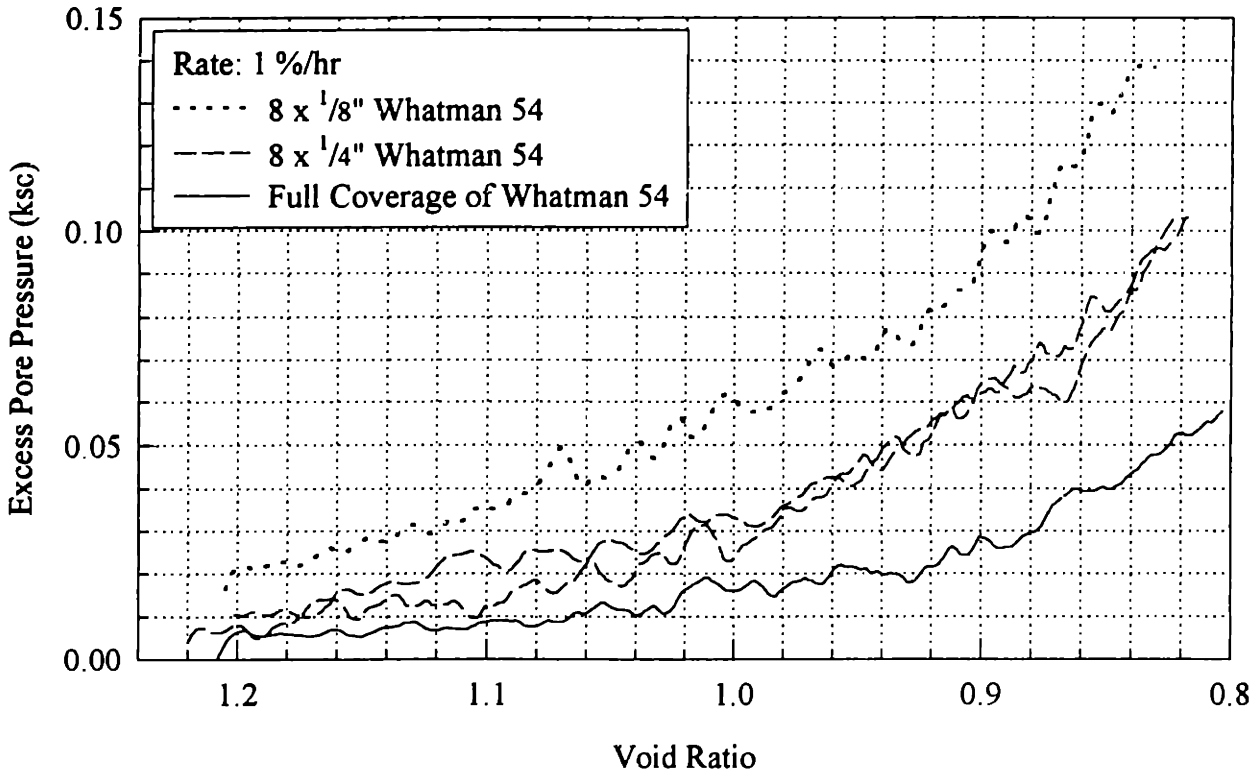

Figure 5.3 Effect of Amount of Drain Coverage on Excess Pore Pressure

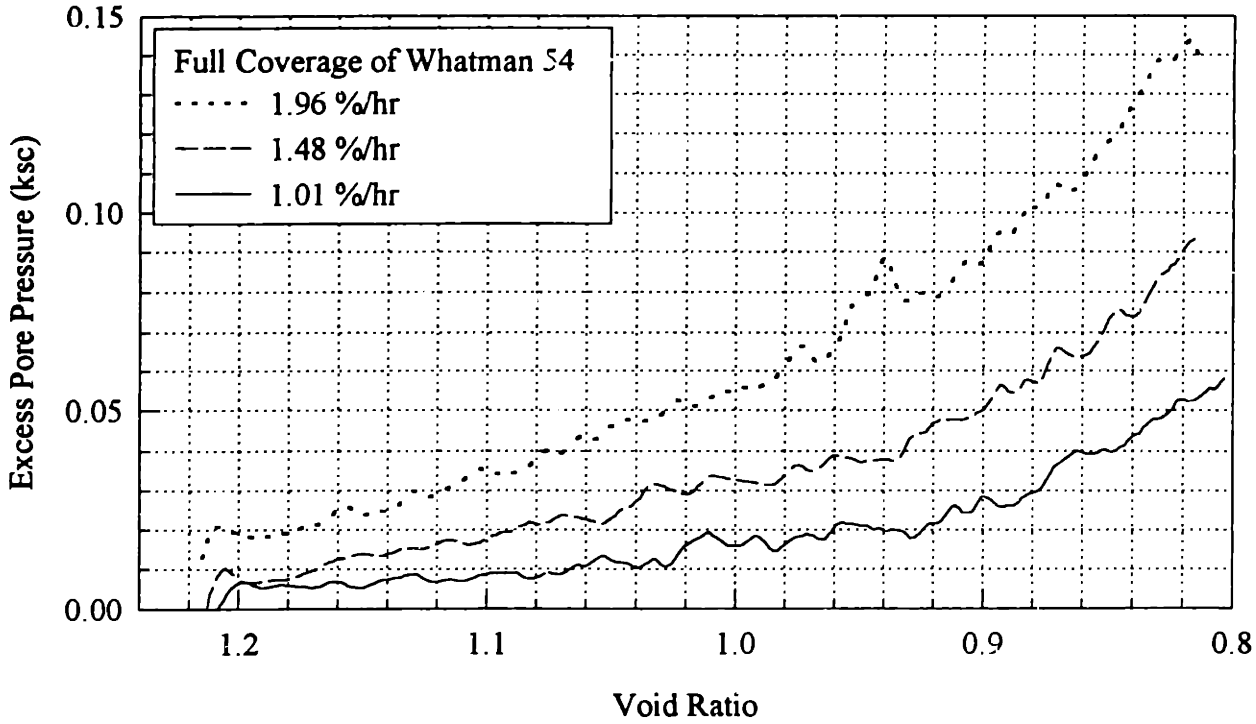

Figure 5.4 Effect of Strain Rate on Excess Pore Pressure in Tests with Full Coverage by Whatman 54 Filter Paper

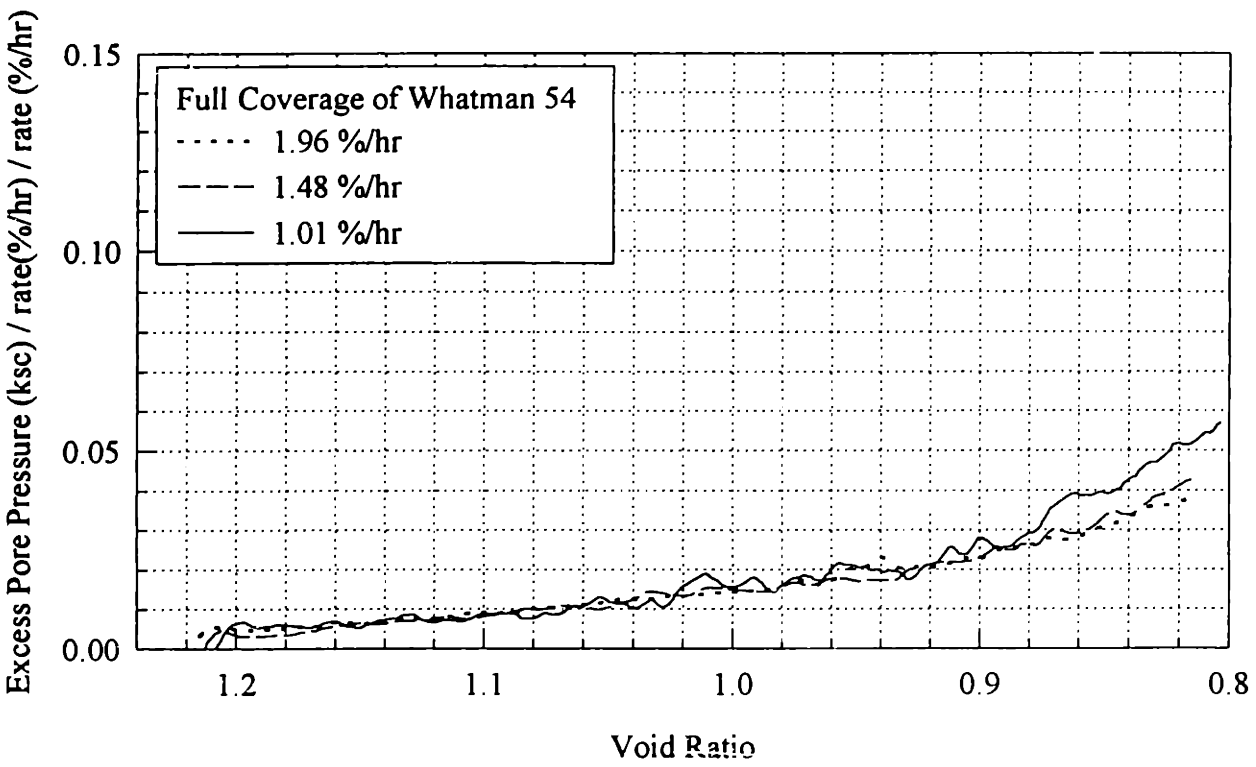

Figure 5.5 Normalized Excess Pore Pressure in Tests with Full Coverage by Whatman 54 Filter Paper

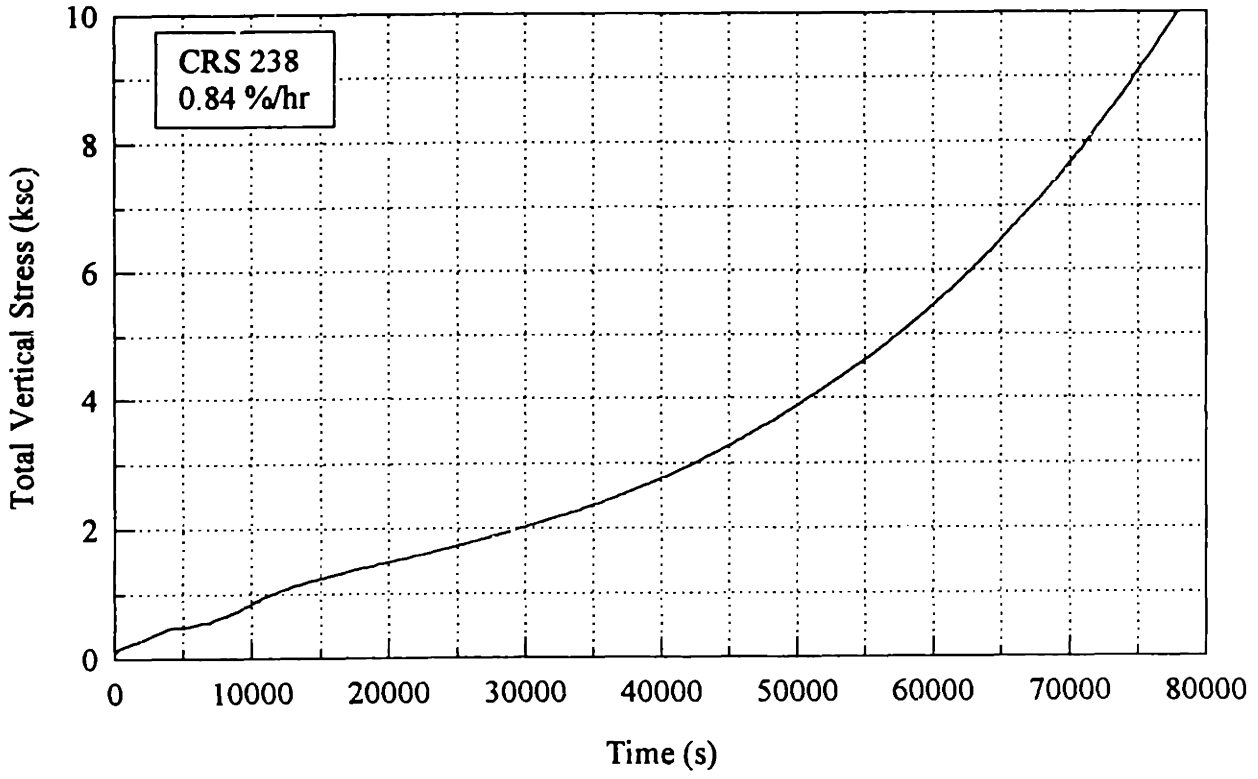

Figure 5.6 Loading Rate in the Constant Rate of Strain Consolidation Test

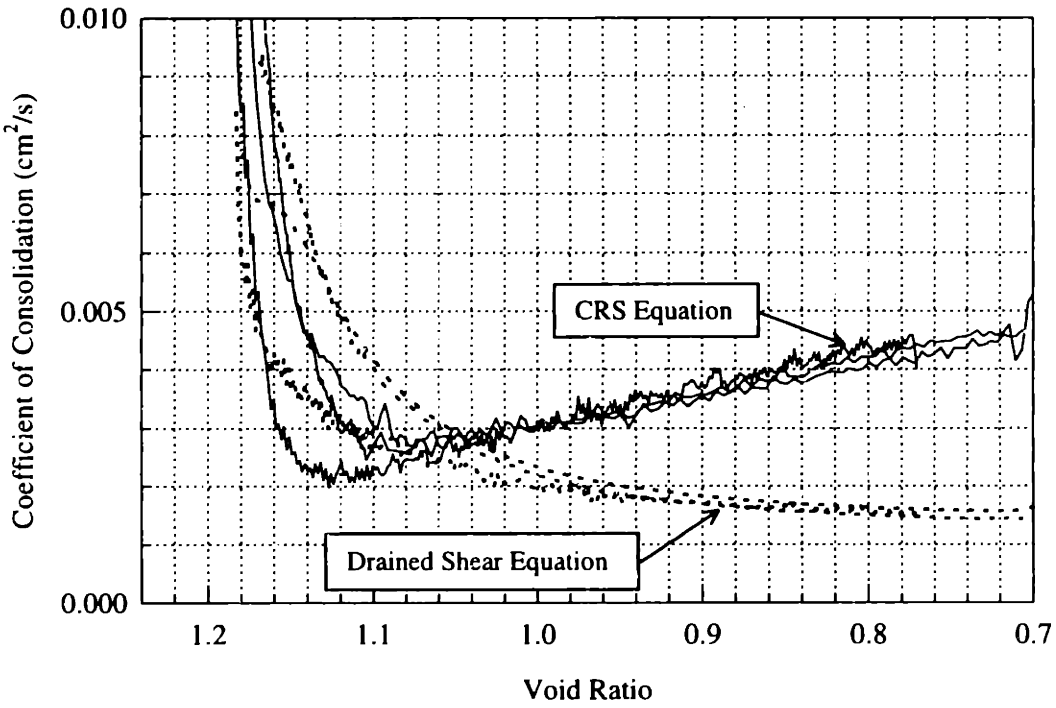

Figure 5.7 Coefficient of Consolidation Calculated by Both CRS and Drained Shear Equations

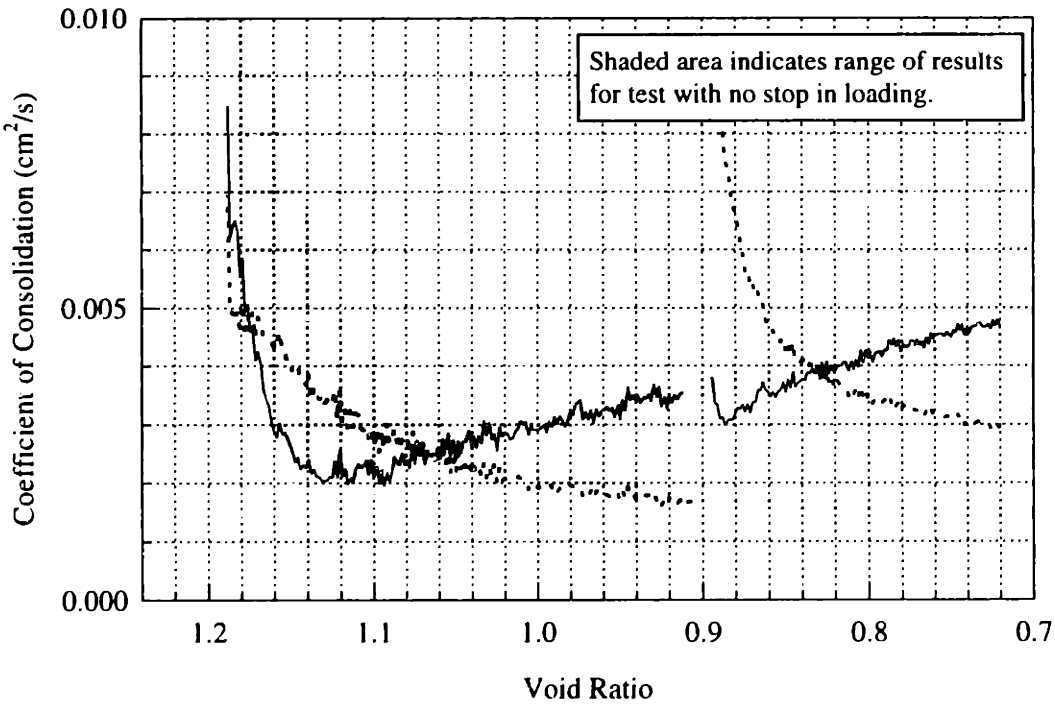

Figure 5.8 Coefficient of Consolidation Calculated by Both CRS and Drained Shear Equations with Stop in Loading to Allow Excess Pore Pressure Dissipation

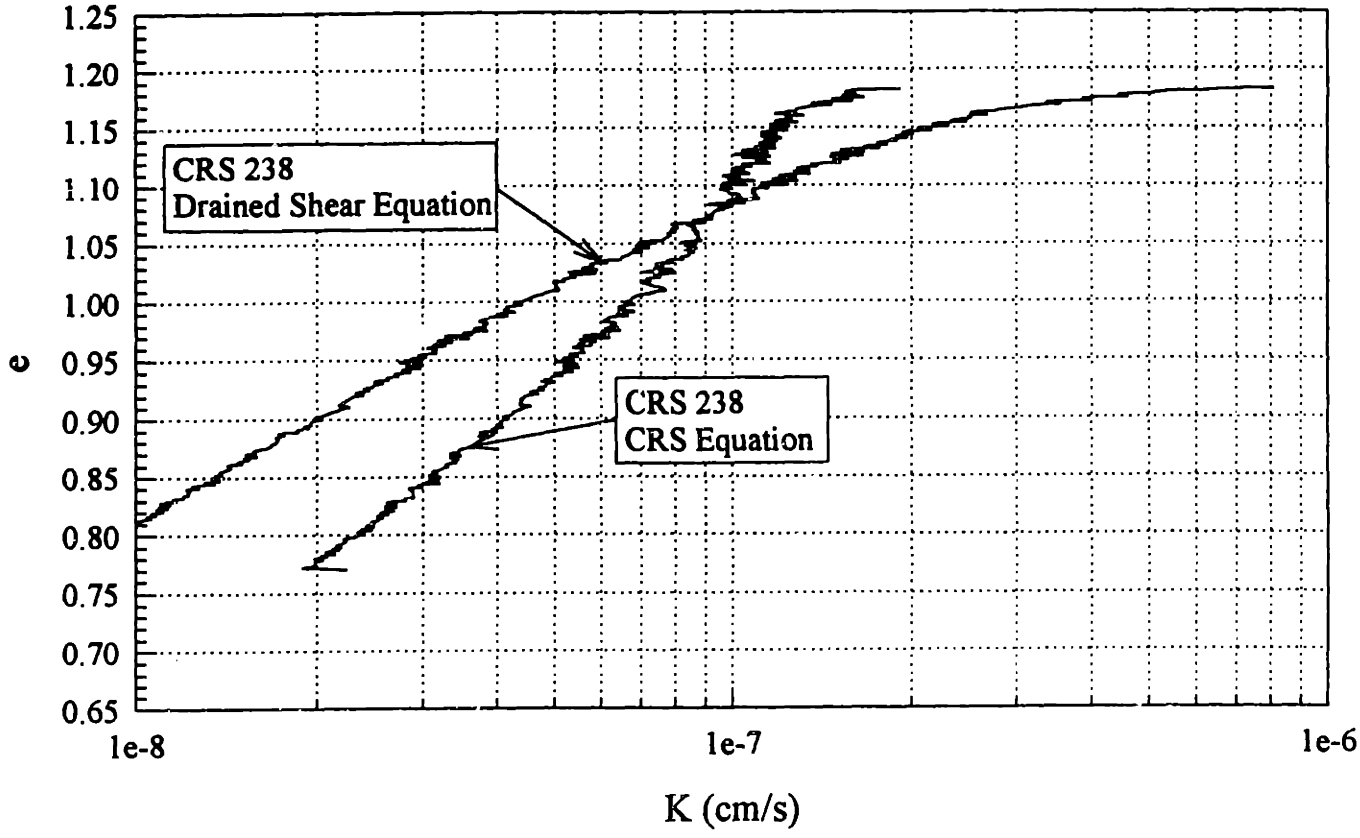

Figure 5.9 Hydraulic Conductivity Calculated by Both CRS and Drained Shear Equations

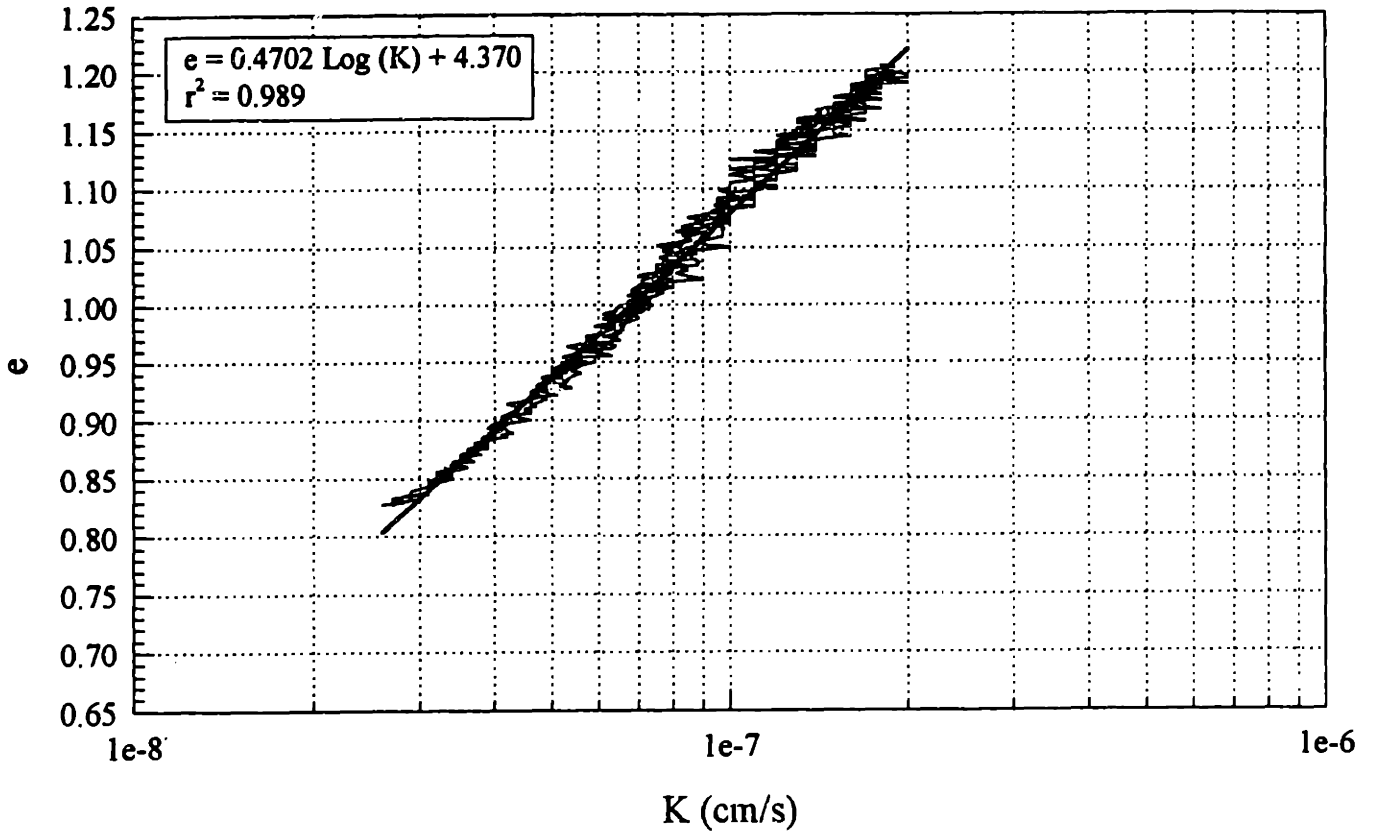

Figure 5.10 Curve Fit through Hydraulic Conductivity Data from Triaxial Tests with No Radial Drainage

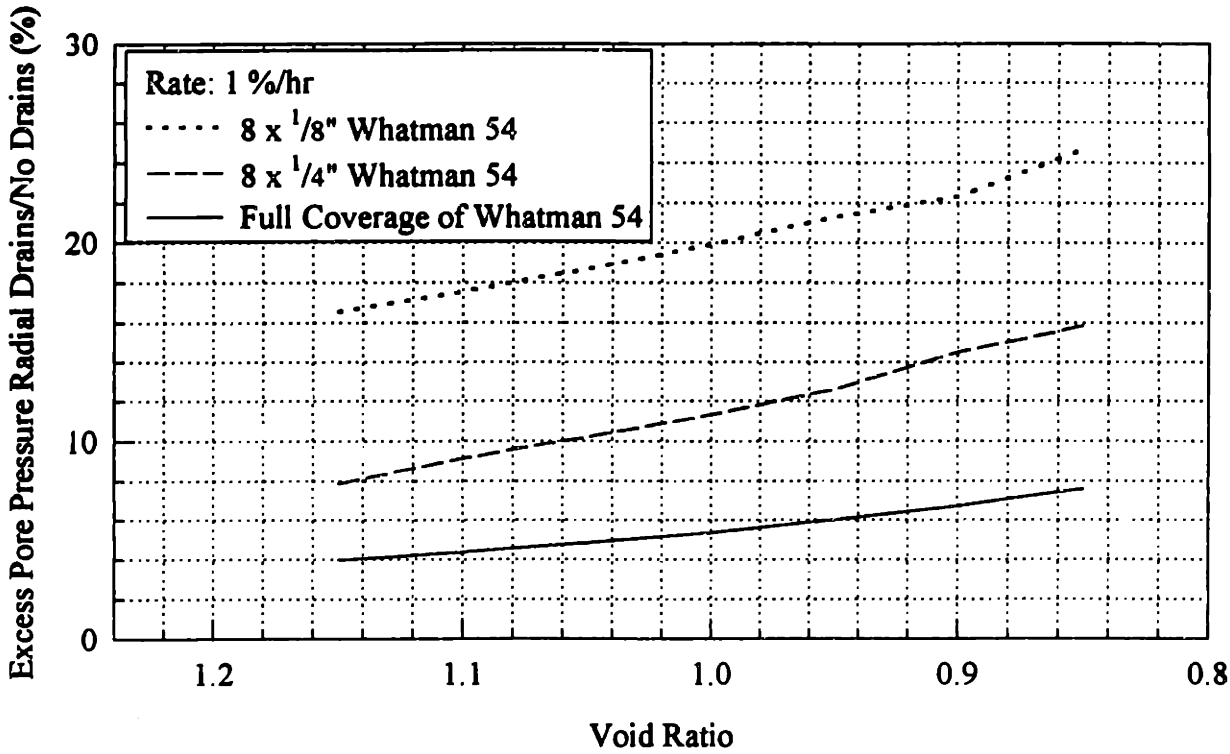

Figure 5.11 Effect of Radial Drainage on Excess Pore Pressure

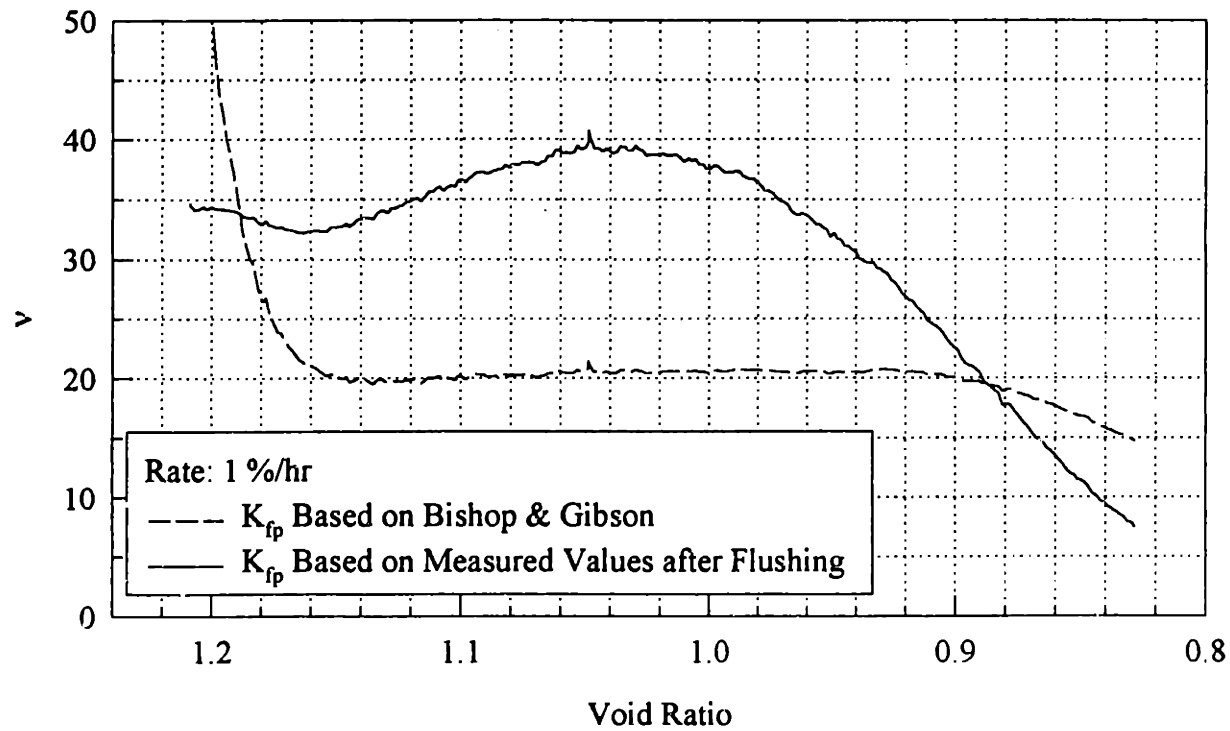

Figure 5.12 Effectiveness of Drainage Systems

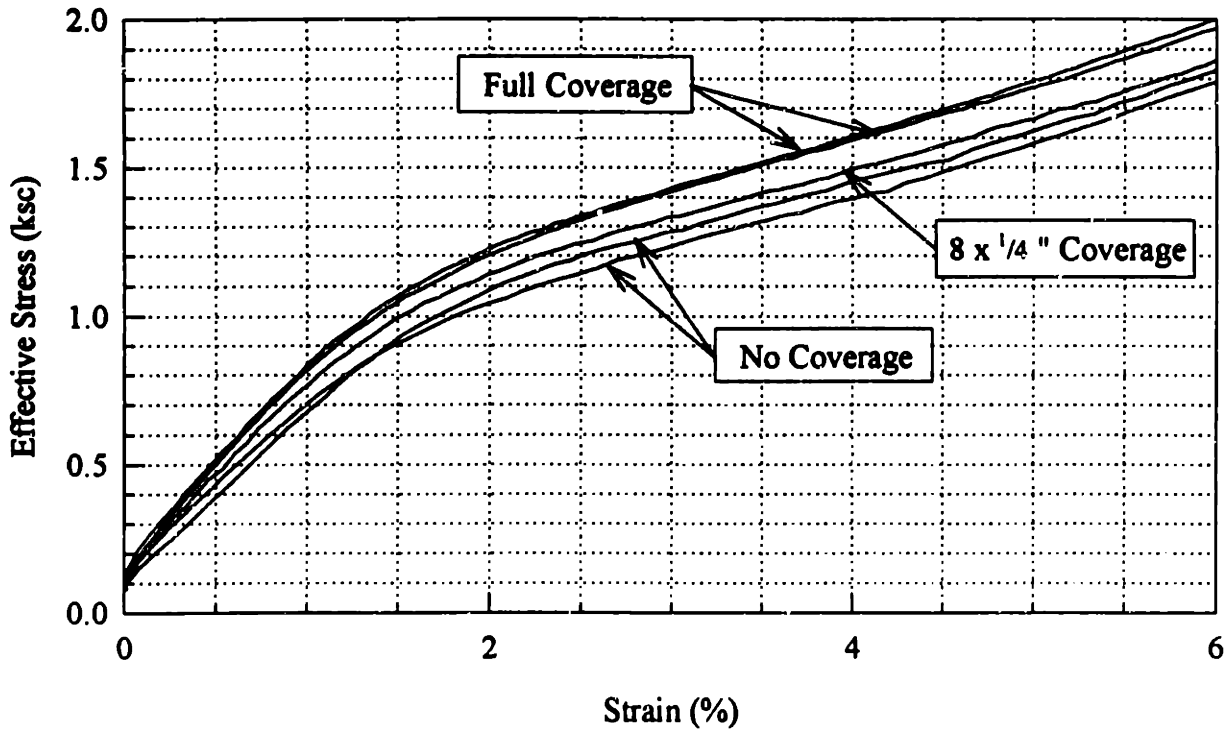

Figure 5.13 Stress Strain Curves for Determination of Filter Drain Correction

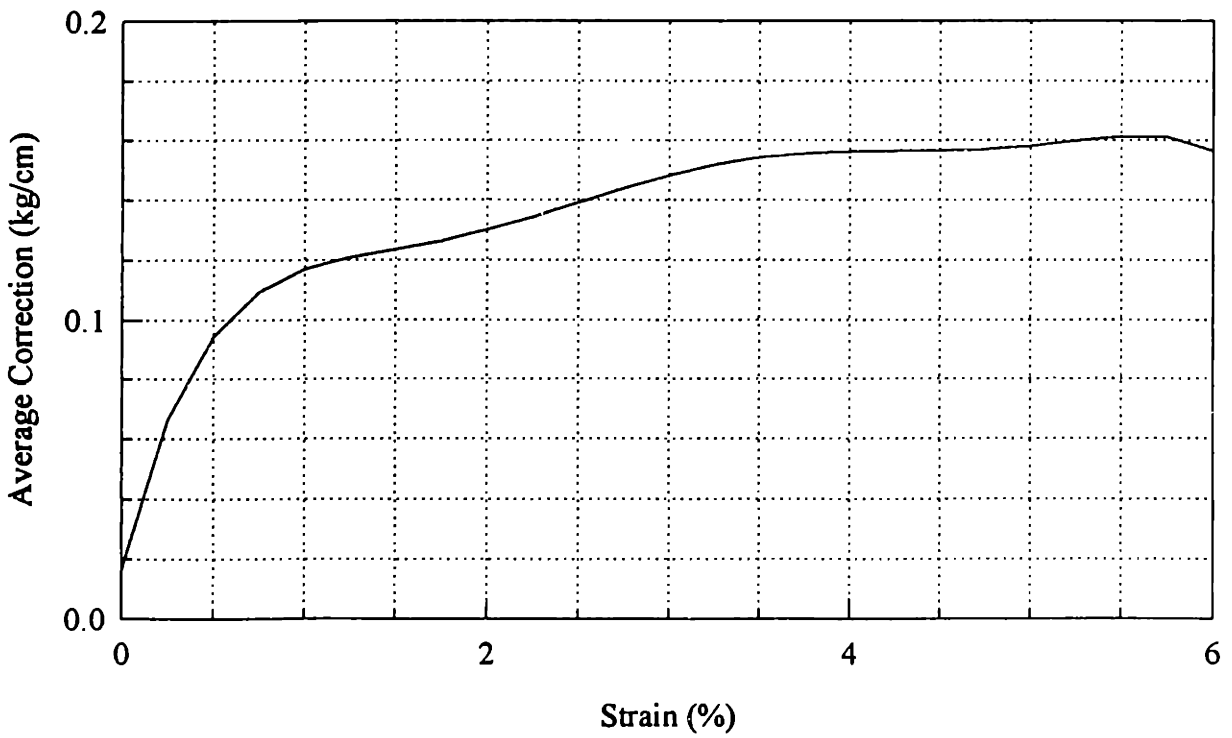

Figure 5.14 Estimate of Filter Drain Correction Factor

Chapter 6 Summary, Conclusions, and Recommendations

6.1 Summary and Conclusions

6.1.1 Test Material

Resedimented Boston Blue Clay (RBBC) was chosen as the test material for this research. It is a saturated and uniform material with constant properties between specimens, allowing the test variables to be compared more precisely. The procedures for the resedimentation process are well established, with modifications by recent researchers to improve the technique.

Because of the extensive past research with RBBC, the engineering properties are well established. Therefore general soil behavior is already determined and used in analytical research to model RBBC properties. Based on index tests, the current batch is typical of past batches, allowing easy integration into the existing data.

The material is a lean illitic glacio-marine clay with engineering behavior typical of natural uncemented clay deposits with similar index properties (plastic limit = 22.6%, liquid limit = 45.2%, clay fraction = 58%). Therefore, measured trends and testing recommendations may be generalized to other materials by adjusting to specific site conditions.

6.1.2 Equipment Development and Evaluation

The standard MIT automated stress path triaxial apparatus was modified for two phases of this research. The first modification provided a constant pressure source at the top of the specimen by manually controlling the air pressure applied to an air water interface. This allowed constant flow tests to define the hydraulic conductivity of the filter drains.

The second, more extensive, modification was made in order to take an additional pore pressure measurement inside the soil specimen. The triaxial base was replaced by a base with a removable pedestal. Both the base and the pedestal have an opening through the center that allow a probe to be inserted into the soil. The pressure measuring device is a stainless steel

needle probe with an inside diameter of 0.023 cm, developed by Cauble (1996). The probe has a small porous stone in the tip and a transducer connected to the base to measure the pressure.

The response time of the pore pressure measuring device caused some difficulties with the use of the probe. A delay is caused because a small but finite amount of water must flow into the probe for the transducer face to deflect and measure a change in pressure. The time for this to occur depends on the hydraulic conductivity of the surrounding soil and stiffness of the transducer. Different transducers have different face diameters and deflections and therefore different response times.

The pressure transducer typically used in the geotechnical laboratory at MIT is made by Data Instruments. This transducer is fairly stable and readily available in a range of capacities. Because of the convenience, a number of tests were initially performed with this transducer. Checking the response time by applying an undrained hydrostatic pressure increase (shown in Figure 4.14) made it clear that the probe was too slow. The alternative was the Kulite transducer with a much smaller face diameter and deflection. The stability of the transducer is not as good and it is very sensitive to temperature changes. Therefore the temperature control in the triaxial apparatus enclosure was controlled more closely (25±0.2°C). The response time with the Kulite transducer showed a large improvement (shown in Figure 4.15) so the transducer was used for the remainder of the tests.

A number of constant rate of strain (CRS) consolidation tests were performed in the Wissa consolidometer. The results from this type of test are widely accepted. A number of tests were then run in the modified triaxial apparatus under similar height, rate, and drainage conditions. These results were compared to the CRS results to confirm that the new device provided acceptable results. Figure 4.17 and Figure 4.18 show that the tests fall within a very narrow range and provide excellent agreement with the CRS results, supporting the use of the new equipment. The narrow band of results also supports the assumption that the test material is uniform and has constant properties between tests.

6.1.3 Experimental Results

Using the triaxial apparatus with the constant flow modification allowed characterization of the hydraulic conductivity of the filter paper drains with changes in total volume through the paper, confining stress, and load history (Figures 4.6 through 4.8). Because there is an initial decrease in hydraulic conductivity as water flows through the drains, the values were measured after flushing to a steady state. The consequence is that the hydraulic conductivity values measured are approximately 30 to 40 % lower than the values in true testing conditions. It is unknown if this is an offset at all stresses or only at low levels.

Using both the Wissa consolidometer and the modified triaxial equipment, a number of tests were run to examine the influence of strain rate, height, and drainage conditions on the magnitude of excess pore pressure at the base of the specimen. The first set of CRS tests were performed on specimens of standard height with rates ranging from 0.07 %/hr to 12.71 %/hr. Examining the excess pore pressure at a given void ratio for each test (Figure 5.1) firmly establishes a linear increase in pore pressure with increase in rate.

Switching to the triaxial apparatus allowed a number of tests to be performed at heights ranging from 2.3 cm (approximately the height of the CRS specimen) to 4.5 cm (slightly greater than the drainage height in the standard triaxial specimen). In these tests, there was no bottom drainage, so the excess pore pressure was measured in the center of the base where it is at a maximum. In this case the pore pressures were normalized by the strain rate. The normalized pore pressure at various void ratios for each test (Figure 5.2) determined that the pore pressure increases by the square of the increase in height.

The previous tests were all run with no radial drainage. To examine the effect of drain coverage, a set of tests were run at the same rate but with the following configurations of Whatman 54 filter paper: 8 1/8 inch drains, 8 ¼ inch drains, and full coverage by the drains. These tests showed that the drains caused a dramatic decrease in pore pressure. During the tests, the hydraulic conductivity of the soil decreases by slightly less than one order of magnitude while the drains decrease by almost two orders of magnitude, causing a decrease in effectiveness over the test.

The ratio of excess pore pressure in tests with partial drainage to excess pore pressure in tests with full coverage is compared to the idealized value based on the ratio of the drain perimeter for full coverage to drain perimeter for partial coverage (Table 5.3). The idealized ratio for the ¼ inch drains of 2.2 very closely approximates the average observed ratio of 2.1. The idealized ratio for the 1/8 drains (4.4) actually overestimates the excess pore pressure with partial drainage (3.7 observed). This indicates that the two dimensional nature of the radial flow to the drains becomes important, making the 1/8 inch drains a more efficient arrangement (although actual pore pressures are higher).

The strain rate effect was also evaluated in tests with radial drainage. Three tests of the same height and full coverage by Whatman 54 were performed at different rates (Figure 5.4). Even after normalizing the pore pressure by the strain rate, the three curves were still significantly different. However, dividing the normalized data by the strain rate again did make all three pore pressure curves nearly identical (Figure 5.5). This was an unexpected result: the excess pore pressure is a function of the strain rate squared when radial drains are present. This may be due to a different pore pressure distribution within the specimen or an increased rate of consolidation near the outside surface of the specimen.

The load carried by the filter drains was examined by analyzing the stress strain curves of tests with different filter paper configurations. These tests, however, had slight variations in stress paths that caused greater changes in the load than the presence of filter drains. Visual observations during these tests show that the paper buckled at strains between 6 and 8 % compared to the 2 to 3 % typically assumed when applying load corrections.

6.1.4 Inferences for Standard Testing

6.1.4.1 Constant Rate of Strain Consolidation Test

For CRS testing, ASTM recommends that the ratio of excess pore pressure to total stress should lie between 3 and 30 % to provide acceptable results. However, data from this testing program that is inside this range shows error in the hydraulic conductivity results. It appears that the

pressure recommendation should therefore be defined in terms of hydraulic gradient, with an upper limit of approximately 215. The lower limit is a function of the pore pressure transducer and in this case was roughly 0.05 ksc, a hydraulic gradient of 20.

The consistency of results using Wissa's linear theory indicates that the theory works well even for log-linear soil. Three of the tests at different strain rates were evaluated using Wissa's nonlinear theory as well (Figure 4.12 and 4.13). Results were similar to the linear theory at low strain rates, with a slight decrease in hydraulic conductivity and coefficient of consolidation. The test performed at 12.71 %/hr however was significantly different, shifting even farther away from the band of data calculated for the other tests. The increased deviation with strain rate supports the use of the linear theory.

The data was also analyzed using a theory derived to model pore pressure generation in drained shear tests. Results of the coefficient of consolidation show different trends than found by the CRS theory and inconsistencies with changes in load history. The loading conditions for the theory are slightly different than achieved in the constant rate of strain tests and may be the cause of the differences between the thoeries.

6.1.4.2 Triaxial K_o Consolidation

The K_o consolidation phase of triaxial testing is typically performed at a rate of 0.1 %/hr. Most of the triaxial tests in this research were performed at approximately 1 %/hr and higher, an entire order of magnitude larger. The excess pore pressures with 8 ¼ inch drains (which are also used during standard triaxial tests) were very low (maximum 0.1 ksc) while the geometry remained cylindrical. This indicates that the consolidation rates used for standard triaxial tests can be increased to reduce time.

The effectiveness of the drainage system is defined by Bishop and Gibson (1963) in terms of the ratio of the hydraulic conductivity of the filter paper to that of the soil. The general trends in the calculated values do agree with those observed, however the data illustrates the importance of accurately defining the hydraulic conductivity of the filter drains.

The unresolved problem in these tests however was that the stress paths with filter paper tended to be slightly higher than those for tests with no filter paper, with lower values of the lateral stress coefficient. There was also a small radial strain measured at the end of the tests, an increasing problem with increase in filter paper coverage. This may be the result of the additional cross sectional area with the thickness of the drains.

6.2 Recommendations for Future Research

6.2.1 Equipment Development

Although the current Kulite transducer has been adequate for this research, it has a very large capacity (500 psi) which leads to poor resolution at the low pressures measured with filter drains present. Purchasing a new 200 psi transducer would greatly improve the readings at lower pressure levels, allowing measurements to be made in slower tests that more closely represent the current consolidation methods. A better but more extreme modification would be to redesign the probe with a differential transducer (15 psi) referenced to the backpressure.

A second triaxial base and a removable pedestal have been machined to allow both bottom drainage and a mid-height probe measurement. This is necessary for the full height tests and evaluation of shear data. The base has additional space to the side of the probe opening to allow copper tubing to connect to the bottom drainage. The pedestal has one small opening in the center for the needle probe with threading to attach the brass connector that holds the probe in place. The second opening on the top of the pedestal is larger and is connected to the copper drainage lines on the bottom. The bottom porous stone will need an opening the size of the probe cored out of the center to allow the probe to be inserted into the specimen. The correct connections need to be made to connect the top and bottom drainage lines. The plexiglass chamber and support posts for the full height specimen will need to be used rather than the shorter ones used for this research. The top plate, pressure/volume controllers, and computer control may be used in their current state. The computer gain rates will need to be adjusted to account for the full size specimen.

6.2.2 Further Experimental Investigation

Several more constant rate of strain consolidation tests should be performed in the Wissa consolidometer to determine the range of pressures acceptable for CRS testing. The following are suggested:

- Tests at rates slightly higher than 4 %/hr. This appears to produce pore pressures close to the upper limit on the hydraulic gradient. Systematic tests should separate excess pore pressure from hydraulic conductivity using strain rate to establish the gradient effect.
- Tests at rates slightly higher than 0.15 %/hr. The lower bound based on ability of the pore pressure measuring system is produced by rates between the 0.15 %/hr and 0.84 %/hr that were used in this research.
- Change the transducer for more sensitivity and investigate slower rates to study the transition between primary and secondary compression.
- More consideration over why the nonlinear theory results are not as consistent as the linear theory although some sources (Sheahan and Watters, 1997) strongly support the use of nonlinear theory.
- Constant head hydraulic conductivity tests to confirm the relationship between hydraulic conductivity and void ratio.
- Tests on two different soil types to examine relationships with higher and lower hydraulic conductivity.

Better characterization of the filter paper hydraulic conductivity is required to determine:

- The behavior of the system losses.
- The dependence of the properties of the paper on filter paper direction. A large variability was observed within one sheet of paper in tests on Whatman 1 filter paper.
- The behavior of initial decrease in hydraulic conductivity with water flushing. The flushing for the tests in this research was always performed at a confining pressure of 0.5 ksc. Flushing at higher stresses should be evaluated.
- The behavior of the drains at higher stress levels. The tests performed only reached confining stresses of 3 ksc while stresses in triaxial tests reached over 5 ksc.
- The effect of soil on the hydraulic conductivity. It is possible that for fine grained soils, the filter drains become clogged and effectively decrease the hydraulic conductivity. A method

of measuring the hydraulic conductivity of the drains as a function of stress with the soil in place needs to be developed.

- The buckling load of the drains. Previous tests had different stress paths so it was difficult to evaluate the differences in load due to filter paper only.
- The strain at buckling. The observed strain is much higher than that currently assumed in the correction.
- The equations developed for the drained shear tests (Gibson and Henkel, 1954) assume a constant rate of stress change. Modifying the test to perform constant rate of stress tests at various stress rates would allow comparison of the results of the two models under correct boundary conditions.

The triaxial testing program has established an initial characterization of the filter drain effect on excess pore pressures and the choice of strain rates for K_o consolidation. Future testing should attempt to explain some of the observed trends:

- The excess pore pressure changes linearly with change in rate with no radial drainage present. With drains present, however, the pore pressure changes by the rate squared. Tests could be run with the probe at different heights in the soil to determine the pore pressure distribution within the specimen and consider the cause of this difference.
- The specimens with filter drains have slightly higher stress paths and lower lateral stress coefficients. This is most likely the result of the small radial strain observed at the end of testing. Possibly, the cross sectional area entered into the computer control program should be modified to take into account the area of the drains. Some experimentation with the area may explain the behavior.
- Spiral drains are used during extension tests. Tests should determine the effect of spiral drains on excess pore pressure.
- As suggested for CRS tests, several different soil types would provide higher and lower hydraulic conductivity. This would also determine how different values of effectiveness effect the excess pore pressure.

Research has been on the consolidation phase of triaxial testing only. The following shear behavior should be examined:

- If consolidation prior to shear is performed at higher rates and there are small excess pore pressures generated, the effect on the undrained shear behavior needs to be considered. With the new base and pedestal, tests with both top and bottom drainage may be performed while measuring the pressure in the center. Tests consolidated at different rates can then be sheared at the standard 0.5 %/hr to determine the effect on drained strength.
- Tests should be performed to examine how pore pressures generated during drained shear differ from those generated during consolidation.
- Drains are used in undrained shear to aid in redistribution of pore pressures. Tests performed with excess pore pressure measurements in the center can determine their effectiveness.

References

American Society for Testing and Materials (1997) *Annual Book of ASTM Standards*, Vol. 04.08, Philadelphia, PA.

Berre, T. (1982) "Triaxial Testing at the Norwegian Geotechnical Institute," *Geotechnical Testing Journal*, 5, pp. 3-17.

Bishop, A.W., Blight, G.E. and Donald, I.B. (1960) "Discussion on testing equipment techniques and errors," *Proc. Research Conf. On Shear Strength of Cohesive Soils*, ASCE, pp. 1027-1042.

Bishop, A.W. and Gibson, R.E. (1963) "The influence of the provisions for boundary drainage on strength and consolidation characteristics of soils measured in the triaxial apparatus," *Special Technical Publication No. 361*, ASTM, Philadelphia, PA, pp. 435-451.

Bishop, A.W. and Henkel, D.J. (1962) *The Measurement of Soil Properties in the Triaxial Test*, 2nd ed., Edward Arnold, London.

Cauble, D.F. (1996) "An experimental investigation of the behavior of a model suction caisson in a cohesive soil," Ph.D. Thesis, Department of Civil Engineering, MIT, Cambridge, MA.

DeJosselin De Jong, G. (1953) "Consolidation around pore pressure meters," *Journal of Applied Physics*, 24(7), pp. 922-928.

Duncan, J.M. and Seed, H.B. (1967) "Corrections for strength test data," *Journal of the Soil Mechanics and Foundations Division*, ASCE, 93(SM5), pp. 121-137.

Germaine, J.T. (1982) "Development of the directional shear cell for measuring cross anisotropic clay properties," Ph.D. Thesis, Department of Civil Engineering, MIT, Cambridge, MA.

Germaine, J.T. and Ladd, C.C. (1988) "Triaxial testing of saturated cohesive soils," *Advanced Triaxial Testing of Soil and Rock*, ASTM STP 977, Philadelphia, pp. 421-459.

Gibson, R.E. (1963) "An analysis of system flexibility and its effect on time-lag in pore-water pressure measurements," *Géotechnique*, 13, pp. 1-11.

Gibson, R.E. and Henkel, D.J. (1954) "Influence of duration of tests at constant rate of strain on measured "drained" strength," *Géotechnique*, 4, pp. 6-15.

Henderson, E. (1994) "Evaluation of time response of pore pressure measurements," M.S. Thesis, Department of Civil and Environmental Engineering, MIT, Cambridge, MA.

Jurgenson, L. (1934) "The shearing resistance of soils," *Journ. Boston Society of Civil Engineers*, 21, pp. 242-275.

Kutter, B.L., Sathialingam, N. and Herrmann, L.R. (1990) "Effects if arching on response time of miniature pore pressure transducer in clay," *Geotechnical Testing Journal*, 13(3), pp. 164-178.

Ladd, C.C. (1991) "22nd Terzaghi Lecture: Stability analysis during staged construction," *Journal of Geotechnical Engineering*, ASCE, 117(4), pp. 540-615

Ladd, R.S. (1998) Personal Communication.

Lerouil, S., Kabbaj, M., Tavenas, F. and Bouchard, R. (1985) "Stress-strain-strain rate relation for the compressibility of sensitive natural clays," *Géotechnique*, 35(2), pp. 159-180.

Olson, R.E. and Kiefer, M.L. (1963) "Effect of lateral filter paper drains on the triaxial shear characteristics of soils," *Special Technical Publication No. 361*, ASTM, Philadelphia, PA, pp. 482-491.

Santagata, M.C. (1994) "Simulation of Sampling Disturbance in Soft Clays Using Triaxial Element Tests," M.S. Thesis, Department of Civil and Environmental Engineering, MIT, Cambridge, MA.

Santagata, M.C. (1998) "Factors affecting the pre-failure non-linearity of cohesive soils," Department of Civil and Environmental Engineering, MIT, Cambridge, MA.

Seah, T.H. (1990) "Anisotropy of Resedimented Boston Blue Clay," Ph.D. Thesis, Department of Civil Engineering, MIT, Cambridge, MA.

Sheahan, T.C. and Watters, P.J. (1997) "Experimental Verificaton of CRS Consolidation Theory," *Journal of Geotechnical and Geoenvironmental Engineering*, 123(5), pp. 430-437.

Sjoblom, K.J. (1998) Personal Communication.

Smith, R.E. and Wahls, H.E. (1969) "Consolidation under constant rate of strain," *Journal of the Soil Mechanics and Foundations Division*, ASCE, 95(SM2), pp. 519-539.

Taylor, D.W. and Clough, R.H. (1951) "Report on research on shearing characteristics of clay," MIT.

Ting, Nai-Hsin. (1991) "Effects of disturbance on consolidation with vertical drains," M.S. Thesis, Department of Civil and Environmental Engineering, MIT, Cambridge, MA.

Wissa, A.E.Z., Christian, J.T., Davis, E.H. and Heiberg, S. (1971) "Consolidation at constant rate of strain," *Journal of the Soil Mechanics and Foundations Division*, ASCE, 97(SM10), pp. 1393-1413.

Appendix

MIT Geotechnical Laboratory

Atterberg Limits

Soil Sample: RBBC420

Test Number: 1

Date Tested: 7/17/98

Specific Gravity, G_s: 2.78

Tested By: EAF

Plastic Limit

Trial Number	1	2	3	4	5	6	7	8
Sample Identification	CR6	J38	42					
Mass of Wet Sample and Tare [g]	16.27	16.25	16.76					
Mass of Dry Sample and Tare [g]	15.36	15.26	15.56					
Mass of Water [g], Ww	0.91	0.99	1.2					
Tare [g]	11.37	10.89	10.19					
Mass of Dry Sample [g], Ws	3.99	4.37	5.37					
Water Content [%], W	22.8%	22.7%	22.3%					

Liquid Limit

Trial Number	1	2	3	4	5	6	7	8
Sample Identification	J40	L19	J50	D19	J37			
Number of Blows	11	16	20	27	40			
Mass of Wet Sample and Tare [g]	33.24	23	28.71	32.21	32.35			
Mass of Dry Sample and Tare [g]	25.83	18.58	23.11	25.59	26			
Mass of Water [g], Ww	7.41	4.42	5.6	6.62	6.35			
Tare [g]	11.06	9.29	10.96	10.79	11.18			
Mass of Dry Sample [g], Ws	14.77	9.29	12.15	14.8	14.82			
Water Content [%], W	50.2%	47.6%	46.1%	44.7%	42.8%			

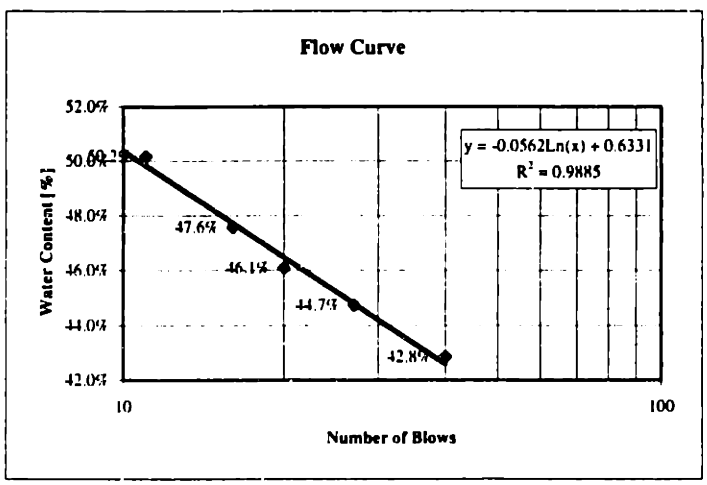

Results Summary

Plastic Limit	Liquid Limit
22.6%	45.2%

Constant Rate of Strain Consolidation Procedure

Apparatus Preparation

1. Choose appropriate strain rate and set gears.
2. Ultrasound top porous stone and nylon filter paper.
3. Remove water reservoir and leave a small pool of water on the ceramic stone in the base.
4. Grease o-rings and place the larger two in the grooves on the base plate.
5. With the cell chamber resting horizontally, apply a vacuum to the top of the piston (using hose from wet/dry vacuum cleaner is convenient) and gently push piston up. After a small nudge, the vacuum should pull it up. This is to retract the piston without damaging the diaphragm.
6. Secure the piston with the piston clamp. The LVDT holder is also attached to the clamp with a spacer (washer) in between so that the LVDT rests on the top of the chamber.
7. With a small puddle of water on the ceramic stone in the base, read the pore pressure zero from the voltmeter.
8. Tightly screw the threaded rod into the load cell and read the load cell zero.
9. Apply a small amount of pressure to the manifold from the mercury pots. Open the valve to one of the loose pieces of tubing until water drips from the tubing. Close the valve from the mercury pots to the manifold and hold the phreatic surface in the open end of the tubing even with the level of the ceramic stone. Read the chamber pressure zero.
10. Fill a large glass beaker with distilled water and place on the shelf above the apparatus.
11. Make sure that the level of mercury in the mercury pots is close to the silver tape line. If not, water must be drawn into the screw pump, then forced into the mercury pots (during which time the valve to the chamber transducer must be closed because pressure builds up in the manifold).

Specimen Preparation

1. Measure the height of the specimen ring and the depth of the recess tool at least three times each with the depth micrometer.
2. Measure the diameter of the specimen ring at least three times with the calipers. The thickness of the nylon filter paper is also measured with the calipers.

3. Lightly grease the inside of both the specimen ring and the cutting shoe.
4. Mass the greased specimen ring and the filter paper (slightly damp).
5. Mass four tares for water contents (rough cuts, trimmings, top cut, and bottom cut).
6. Connect the correct lucite top cap (which fits over the specimen ring) to the piston of the trimming device, with the piston held up with a rubber band. There is a different top cap that fits the specimen ring for the new Trautwein CRS.
7. Extrude approximately 1.5 inches of soil from the tube following normal procedures and keeping track of specimen orientation. Or if using RBBC, rough cut the diameter with a wire saw to within 1/8" of the final diameter. Take a water content of rough cuts.
8 Cut the ends of the soil perpendicular to the sides using the miter box and wire saw and place specimen on wax paper and a plexiglass plate.
9. Cut a piece of wax paper to fit the bottom lucite platen of the trimming device. If slightly wet, this will stick to the lucite and makes soil placement easier. Set the platen on the soil, centered as well as possible. If there are imperfections (hard oxidized areas from the tube for instance), the soil may be positioned to one side to avoid these. Pick up the soil and platen using the plexiglass plate under them, turn them right side up, and place into the trimming device.
10. Fit the cutting shoe and specimen ring together (with groove for o-ring facing down, therefore the soil should have the top facing up) and connect them to the lucite top cap. These will separate under their own weight, so the piston must then be set down on the soil to keep everything held together.
11. Push the trimming shoe slightly into the soil and trim excess soil with a small spatula. Repeat with small pushes into the soil and take the water content of the trimmings.
12. Before reaching the bottom, trim the soil at an angle from the bottom lucite platen. Otherwise as the cutting edge reaches the bottom, soil tends break off and pull soil from under the trimming edge.
13. Once the trimming edge reaches the bottom, push the piston down until soil is visible just above the specimen ring (this can be seen through the lucite top cap).
14. Separate the lucite top cap from the specimen ring by holding the ring in place and lifting the piston up. Separate the cutting shoe from the specimen ring by holding the specimen ring in place and pushing the shoe down.

15. With the specimen ring held sideways, cut excess soil from the bottom edge (the side with the o-ring groove) using a wire saw. This side is then placed down on wax paper and plexiglass plate.
16. Make the final cut for the top surface with a wire saw followed by a straight edge to finish. Take water contents of both the top and bottom cut.
17. Blot the nylon filter paper with a paper towel to remove excess water then place it on the top surface of the soil.
18. Turn the specimen ring upside down, placing the surface with the filter paper onto the recess tool. Make sure the ring is firmly down against the recess tool, and make the final cut for the bottom surface.
19. Mass the specimen and specimen ring to provide the initial total mass.

Specimen Setup

1. Wipe off the water on the ceramic stone in the base with a paper towel and immediately set down the specimen ring, centered as well as possible.
2. The height of the specimen can be calculated based on the depth of the recess tool and the height of the specimen ring, however discrepancies were found between this and the height measured directly. Therefore, once set on the base, the distance from the ring to the specimen should be measured with the depth micrometer.
3. Place the smaller o-ring over the specimen ring and push it towards the o-ring groove (it doesn't need to be pushed into the groove, it will be pushed in place by the outer retaining ring).
4. Set the outer brass retaining ring over the specimen ring and secure with three allen screws. These should be tightened until they bottom out, otherwise alignment problems may occur.
5. One more depth measurement is taken, using the depth micrometer to measure the distance between the brass ring and the specimen. This measurement is taken again at the end of the test and provides a check on the change in height during the test.
6. Set the porous stone on a paper towel to remove excess water, then place it on the specimen.
7. Set the chamber on the bottom plate and secure with four large bolts.
8. Holding the piston up, loosen the piston clamp and set the piston set down on the specimen. It is clear when it is in place by the feel of the top cap hitting the stone.

9. Adjust the DCDT so that it is in range and will continue to be throughout loading.
10. Set the loading bullet on the piston and manually move the load frame platen up until the load cell is in contact with the bullet and small seating load (~1 kg) is applied to the specimen. Record this load cell reading as the seating load. At this point, also record the DCDT zero.
11. Siphon water from the glass beaker through the plastic tubing into the bottom of the chamber. Close the air vent at the top of the chamber once water flows out.
12. Remove the tubing from the beaker to the chamber and attach the tubing from the manifold to the chamber (as when taking the cell zero, force some water to flow from the tube to make sure there aren't air bubbles caught in the system).
13. Make sure the valves are open from the chamber to the manifold and from the manifold to the mercury pots.

Backpressure Saturation with Height Corrections

1. Raise mercury pots to increase the chamber pressure to 0.25 ksc. Each pressure increment must be left on until the pressure throughout the specimen is in equilibrium. For Boston Blue Clay this takes approximately 20 minutes but varies depending on the type of soil. The pore pressure read through the base of the specimen will stop changing when equilibrium is reached.
2. Make a table including the following:

σ_c (ksc)	Load (mv)	Load (kg)	δ_{load} (cm)	δ_{cell} (cm)	δ (cm)	δ (v)	Target dcdt
0	seating load		base defl.				Zero
0.25							
0.5							
0.75							
1.0							
1.5							
2.0							
2.5							
3.0							
4.0							

3. The load for the first line of data is the seating load recorded during setup. The load applied to the specimen in kg is calculated as:

   load = load measured by load cell $-\sigma_c * A_p + W_p$

   where A_p is the area of the piston (3.37 cm^2) and W_p is the weight of the piston (2.02 kg).
4. The deflection due to change in load, δ_{load}, for the seating load is calculated as a base value and will be subtracted from later corrections. The equation for this is:

   $\delta_{load} = 0.0031 * load^{0.2351}$
5. The deflection due to change in cell pressure, δ_{cell}, for the first line is zero, but will be later calculated as:

   $\delta_{cell} = 0.001 * \sigma_c$
6. Just before applying the increment to 0.5 ksc, read the load (this could be done before applying 0.25 ksc, but it is easier to apply the first increment immediately and start corrections with 0.5 ksc). Calculate the load on the specimen, δ_{load}, and δ_{cell}. The total deflection, δ(cm), is calculated as δ_{load} – base deflection + δ_{cell}. This is converted into a voltage, δ(v), based on the DCDT calibration factor. The target DCDT is calculated as the DCDT zero + δ(v).
7. Raise the mercury pots to apply the 0.5 ksc chamber pressure. Immediately after applying the pressure, manually adjust the piston until the DCDT reaches the target value. In order to manually adjust the load frame the clutch should be engaged (chain pulled out).
8. Repeat this process: wait until equilibrium, read the load, calculate the target DCDT value, and apply the next pressure.
9. Finally, the backpressure of 4 ksc should be left on overnight.

Consolidation

1. Before starting each stage of the test, record the voltages on the data sheet.
2. Start a data acquisition file. The first line of data should be before loading occurs when the system is in equilibrium and there is no excess pore pressure.
3. Release the clutch (let the chain go in) and move the motor switch to the forward position. Check to see that the load is picking up, sometimes the gears between the drive train and gear box are not engaged.

4. Load to the desired strain or load, with a maximum change in load cell voltage of 150 mV. The zero on the load cell in the CRS is approximately 50 mV, so stay under 200 mV.

Secondary Compression

1. When the desired load is reached, turn off the motor and engage the clutch.
2. Close the air vent at the top of the air jack.
3. Make sure the air pressure is turned down and open the valve to connect the air pressure to the air jack.
4. Increase the pressure in the air jack slowly until load picks up.
5. Continue to increase the pressure while lowering the loading platform manually. The fine knob is difficult to turn by hand, so use a socket wrench. Ideally the load should stay the same on the specimen through this process.
6. The platform should be lowered until there is a visible gap between the load cell block and the load frame cross arm. The load on the specimen is now maintained at a constant value by the air jack. There is some stick slip behavior of the diaphragm in the air jack, so the load may decrease slightly, then jump back the original value. This is typically left on for 24 hours.

Unloading

1. Before unloading, the load needs to be shifted back so it is carried by the load frame rather than the air jack. The steps above are reversed, decreasing the air pressure gradually and moving the platform up manually.
2. Close the valve from the air pressure to the air jack and open the air vent on the air jack.
3. Release the clutch and move the motor switch to the reverse position.

Equipment Disassembly

1. Stop the motor and end the data acquisition file.
2. As when pressuring up, the chamber pressure is decreased slowly in increments. This is to ensure that the ceramic stone in the base does not cavitate.
3. Once the mercury pots are down to 0.25 ksc, close the valve from the pots to the manifold and from the manifold to the chamber. Open the air vent on the top of the chamber.

4. Once the pore pressure is steady, close the air vent and detach the tube from the manifold to the chamber.
5. Connect plastic tubing, open the air vent, and drain the cell.
6. Lock the piston in place.
7. Move the loading platform down and remove the loading bullet and threaded rod.
8. Remove the bolts and the outer chamber.
9. Remove the porous stone and ultrasound to clean.
10. Measure the distance from the outer brass ring to the specimen.
11. Remove the brass ring.
12. Remove the specimen and specimen ring by sliding horizontally until they are loose. Sometimes the specimen is difficult to remove and a piece of wire may be slid between the base and the specimen ring to break the suction.
13. As soon as the specimen is removed, put water on the bottom ceramic stone.
14. Mass the specimen and specimen ring.
15. Extrude the specimen and place it in a tare in the oven to obtain the mass of solids.
16. Clean the base (Scotchbright pads may be used to scrub soil off the stone) and o-rings. Also clean the threaded holes for the allen screws with a q-tip.
17. Leave a covered reservoir of water on the ceramic stone to keep it saturated.

MIT GEOTECHNICAL LABORATORY
REFERENCE DATA
CRS TEST

Project: _____ Boring # _____ Date Start _____
Test = _____ Sample # _____ Date Complete _____
_____ Depth _____ Tested By _____

	CH#	Make / SN	CF	Zero @ start	Zero (V/Vin)	Zero @ finish
Cell Pressure						
Pore Pressure						
Vertical Disp.						
Vertical Load						
Vin						

Ht. Sample Ring _____ Ht. Recess Tool _____ Filter Paper Thickness _____
_____ _____ _____
_____ _____ _____
ave. H_{sr} (cm) _____ ave. H_{RT} (cm) _____ ave. t_{FP} (cm) _____

Dia Sample Ring _____ Wt. sample & tare (g) _____
$H_{trim} = (H_{SR} - H_{RT} - t_{FP})$ (cm) _____ Wt. sample ring, filter paper, grease (tare) (g) _____
_____ A_S (cm^2) _____
_____ Wt. sample (g) (M_s) _____
ave. Dia (cm) _____ V_{tot} (cm^3) _____ Wt. top cap, stone, filter paper (g) _____

Location					Final
Container #					
wt. cont & wet soil (g)					
wt. cont & dry soil (g)					
wt. water (g)					
wt. container (g)					
wt. dry soil (g)					(M_s)
water content (%)					

ave. initial WC (%) _____

Location of specimen (X-ray markers) _____
Torvanes: above: _____ below: _____
small shoe (x 2.5) _____ _____
standard (x 1.0) _____ _____
large shoe (x 0.2) ave. torvane _____ ave. torvane _____
Material Description (color, moisture, texture, layering, disturbance, sensitivity):

Z_{ti} _____ Z_{fi} _____

	CH #	end pressure up	end of loading	end of sec. comp.	end unload
Cell Pressure					
Pore Pressure					
Vertical Disp					
Vertical Load					
Vin					
date / time					
initials					

G_s _____ $V_v = V_{tot} - V_{solids}$ _____
$V_{solids} = M_s / G_s$ _____ $V_w = M_t - M_s$ _____
$H_{solids} = V_{solids} / A_s$ _____ S_i (%) $= V_w / V_v$ _____

Filter Paper Hydraulic Conductivity Measurement Procedure

Apparatus Preparation

1. Ensure that pore pressure lines are saturated: check the response of the pressure transducer by pressing on the bore hole (should get increment of several mv).
2. With pore pressure transducer open to the specimen only, measure the zero.
3. Flush water through the top drainage line.
4. Set the piston on the pressure/volume controller so that the volumetric LVDT is in range.
5. Measure the volumetric LVDT zero.
6. Close the top valve to the pore pressure/volume controller.
7. Close the top valve to the cell pressure/volume controller.
8. Grease the three large o-rings. Place two in the top plate and one in the base.
9. Grease the small o-rings in the bolts which secure the top plate.
10. Clean and grease the top cap and bottom pedestal.
11. Set the rubber sleeves around the top cap and pedestal such that the stone thickness is covered. Flip the top sleeve up so that it does not hang below the top cap.
12. Locate the first thin membrane around the pedestal with roll close to top edge.
13. Fix with 2 o-rings.
14. Place the second membrane over the o-rings with roll between the top o-ring and the first membrane roll.
15. Fix with one o-ring between the first 2 o-rings.
16. Flip the bottom rubber sleeve down over the top roll so that it does not extend over the top of the pedestal.
17. Leave a puddle of water on the base.
18. Place 4 o-rings on stretcher and set this over the pedestal.
19. Ultrasound the stones.

Setup

1. Cut a piece of filter paper to exactly wrap around the lucite dummy and extend approximately 5 mm beyond each end of the dummy.

2. Using tape with a small amount of adhesive (the colored labeling tape is convenient), lightly tape the dry filter paper around the dummy. Too much adhesive will tear the filter paper during removal.
3. Place the stones on a paper towel to remove excess water.
4. Place the bottom stone on the pedestal.
5. Carefully place the dummy with the filter paper extending below it on the stone. The filter paper should cover or extend slightly beyond the stone.
6. Place the second stone on top of the dummy. Again the filter paper should cover the stone.
7. Lower the piston and lock in place with the split collar clamp.
8. Flip both top and bottom rubber sleeves over the stones.
9. Roll the membrane partway up the dummy, removing the tape before the membrane covers it.
10. With the filter paper secure, water may be sprayed on to the accessible paper to help in saturation.
11. Finish rolling the membrane up.
12. Fix with 2 o-rings on the top cap.
13. Roll the second membrane over the dummy.
14. Fix with third o-ring between the first two. The last o-ring is available if the third one misses.
15. If the last o-ring is not necessary, release it on the pedestal.
16. Attach o-ring stretcher above top cap with a piece of wire through the two holes in the stretcher.
17. Make sure there is no water near the pins in the base for the load cell. Plug in load cell. The load will not be read during the test, but plugging it in keeps the wire secure during the test.
18. Place the plexiglass cylinder in the o-ring groove in the base.
19. Set the top plate in place and tighten the six bolts.
20. Place a steel ball on top of the piston and raise the triaxial cell until the ball is in contact with the load frame cross arm.
21. Fill the cell with silicon oil. When the oil is level with the center of the dummy, close the valve to the oil supply and read the cell pressure zero.

22. Open the valve and finish filling the cell. When oil flows out the top air vent, decrease the pressure applied to the oil supply, close the valve to the oil supply, and then close the air vent.
23. Run the triaxial setup program (at the dos prompt, type 'gwbasic setup.bas') and fill in all the data. The load and the axial displacement are not important during these tests, so enter zero as the calibration factor for these two devices.
24. When complete, continue to the computer control option.
25. Check that all computed values are reasonable.

Backpressure Saturation

1. Open top and bottom drainage lines and choose the hydrostatic pressure option.
2. Start data acquisition. The overnight data is helpful to ensure that there are no leaks.
3. Because there is no soil present backpressure saturation can occur quickly. Enter several large increments, ending with a cell pressure of 4.5 ksc and a pore pressure of 4 ksc.
4. Turn on motors to the pore pressure and cell pressure computer control but leave the axial motor off.
5. Allow overnight equilibration.

Continuous Flow to Equilibrium

1. Attach the air pressure to the top of the pressure chamber with the air water interface.
2. Slowly increase the pressure until it is roughly equal to the pore pressure according to the air pressure dial gauge.
3. Turn off the pore motor.
4. Turn the valve to connect the top drainage line to the pressure chamber rather than the pressure/volume controller.
5. Watching the pore pressure value on the voltmeter, adjust the air pressure until the pore pressure is back to its initial value (approximately 4 ksc).
6. Start data acquisition.
7. After a few readings have passed, turn the pore motor to manual control and adjust the potentiometer so there is a low flow through the specimen. Look at the pore pressure. It should be slightly higher than its original value (by approximately 0.05 ksc).

8. Continue to force water through the system until the LVDT is almost out of range.
9. Stop flow and reset the LVDT.
10. Continue flow again until a steady state is reached. This is clear when the pore pressure is steady.

Flow Tests

1. Start data acquisition.
2. After a few readings have passed, force flow by turning the pore pressure to manual control. Let this run for approximately 5 minutes (test length can vary greatly).
3. Stop flow and wait for equilibrium (less than 1 minute).
4. Repeat this process for three different flow rates.
5. Change the cell pressure by the following schedule and run three flow tests at each confining pressure: 4.5, 5, 6, 5, 4.5, 5, 6, 7 ksc. Any schedule can be followed realizing that the hydraulic conductivity is load history dependent.

MIT GEOTECHNICAL LABORATORY
REFERENCE DATA
HYDRAULIC CONDUCTIVITY CHECK

Project _____ Sample _____ Tested By _____ Date Start _____
Test Number _____ Filter Paper _____ Geometry _____ Date Finish _____

Filter Paper: Thickness _____ Perimeter _____ Length _____
_____ _____ _____
_____ _____ _____
ave _____ ave _____ ave _____

Membranes: Type _____

Sample: Length _____ Diameter _____
_____ _____
_____ _____
ave _____ ave _____

Zeros

	Channel #	Make/SN	CF	Zero @ Start	Zero @ Finish
Axial Displ				/	/
Cell Pressure				/	/
Load Cell				/	/
Pore Pressure				/	/
Volume				/	/

Process Documentation

Process	Date/Time	File Name	Axial	Cell	Load	Pore	Vol	Vin

Saturation Check

Date/Time	Back Pressure	Pressure Increment	B Value	Vol. Strain

Conductivity Tests

Trial No	File Name	Date	Time	Cell	Top	Bottom	Comments

K_o Consolidation in Triaxial Apparatus with Excess Pore Pressure Procedure
(primarily taken directly from 1.37 class notes and modified for needle probe)

Apparatus Preparation

1. Set piston on a dummy and the stones and filter paper that will be used during the test. Measure z_3 from the piston to the housing for the bearings with the depth micrometer.
2. Ensure pore lines are saturated: check the response of the pressure transducer by pressing on the bore hole (should get increment of several mv).
3. With the pore pressure transducer open to the top drainage line but closed to the pressure volume controller, measure the pore pressure zero.
4. Flush water through top drainage line.
5. Set the piston so the volumetric LVDT is in range.
6. Close top valve to the pore pressure/volume controller.
7. Close top valve to the cell pressure/volume controller.
8. Measure load cell zero.
9. Grease the three large o-rings. Place two in the top plate and one in the base.
10. Grease the small o-rings in the bolts which secure the top plate.
11. Clean and grease top cap and bottom pedestal.
12. Set rubber sleeve around top cap such that the stone thickness is covered. No rubber sleeve in necessary on the pedestal since there is no bottom stone.
13. Locate the first thin membrane around the pedestal with roll close to top edge.
14. Fix with 2 o-rings.
15. Place the second membrane over the o-rings with roll between the top o-ring and first membrane roll.
16. Fix with one o-ring between the first 2 o-rings.
17. Place 4 o-rings on stretcher and set this over the pedestal.
18. If testing with filter paper, tuck strips between membrane and pedestal. If full coverage of drains is desired cut one piece of filter paper to cover the specimen. Then cut strips partway down, leaving them connected at the bottom. Tuck the connected part between membrane and pedestal and let strips fall away from pedestal.
19. Ultrasound the stones and the probe.

20. Make sure there are no air bubbles caught in the threads of the probe. A toothbrush or small piece of wire may be used to remove air.
21. Connect the Kulite transducer to the probe underwater.
22. Put the probe in place through the pedestal and slightly tighten the brass connector. Mark a line (or use tape) on the outside of the probe to indicate the correct position of the probe during testing.
23. Pull the probe back down so that the tip is just below with the pedestal. Later when the specimen is in place, the probe will be moved up into place.
24. Check the probe response by pushing on the tip (should get 0.5 to 1 mv).
25. Leave a small puddle of water on the tip of the probe.
26. Retract piston (gently) and lock in place with split collar.

Specimen Preparation

1. Rough cut the specimen with a wire saw and obtain several water contents.
2. Place specimen in miter box. For very short specimens, use the miter box that has been modified.
3. Rough cut cylinder with miter box.
4. Final cut specimen with miter box.
5. Wrap specimen in one layer of wax paper that is 3 mm shorter than the final specimen height.
6. Place specimen in split mold and gently tighten.
7. For short specimens, use a recess tool to push the specimen to one end of split mold. Trim the end with wire saw and finish with straight edge.
8. Blot filter paper with paper towel to remove excess water.
9. Place filter paper on trimmed edge.
10. Use recess tool to push specimen to the other end of the split mold. Trim with wire saw and finish with straight edge.
11. Take several water contents of trimmings and end cuts.
12. Measure height and diameter directly with calipers.
13. Mass the specimen.

Setup

1. Remove excess water from around the pedestal.
2. Place specimen directly on pedestal with filter paper on top.
3. Remove excess water from top porous stone with a paper towel and slide onto specimen.
4. Lower the piston and lock in place.
5. Take z_3 measurement with depth micrometer. When locking the piston, the split collar usually pulls the piston up slightly. For this reason the z_3 measurement is often not consistent with the height measured directly on the specimen.
6. Locate the filter drains along the sides of the specimen and tuck ends under top rubber sleeve.
7. Roll the membrane over the specimen.
8. Fix with 2 o-rings on the top cap.
9. Roll second membrane over specimen.
10. Fix with third o-ring between the first two. The last o-ring is available if the third one misses.
11. If the last o-ring is not necessary, release it on the pedestal.
12. Move the probe up into place and lock in place by completely tightening brass connector.
13. Make sure there is no water near the pins in the base for the load cell. Plug in load cell.
14. Place the pexiglass cylinder in the o-ring groove in the base.
15. Set the top plate in place and tighten the six bolts.
16. Attach the LVDT gauge bar and the piston clamp.
17. Connect the LVDT and move it into range. The zero may be read at this point, however because the split collar pulls up the piston it is not usually correct.
18. Place a steel ball on top of the piston clamp and raise the triaxial cell until the ball is in contact with the load frame cross arm.
19. Engage the axial motor drive system (put lever to fine control and pull out clutch).
20. Lock the piston clamp and the cross arm together with screw clamps. Don't make the system completely tight. This allows room for the piston to move down and come in complete contact with the specimen when the split collar clamp is released.
21. Release the split collar clamp and measure the axial LVDT zero. If the screw clamps are still loose, tighten.

22. Fill the cell with silicon oil. When the oil is level with the center of the specimen, close the valve to the oil supply and read the cell pressure zero.
23. Open the valve and finish filling the cell. When oil flows out the top air vent, decrease the pressure applied to the oil supply, close the valve to the oil supply, and then close the air vent. Do not close the vent before closing off the oil supply.
24. Run the triaxial setup program (at the dos prompt, type 'gwbasic setup.bas') and fill in all the data.
25. When complete, continue to the computer control option.
26. Check that all computed values are reasonable.
27. Make sure the valve to the pore pressure/volume control device is closed.
28. Select the initial undrained pressure up option and apply enough pressure to cause positive pore pressures. For RBBC, 0.25 ksc cell pressure and 0.1 kg deviator stress is typical.
29. For specimens from the field that may not be saturated, this is typically left on overnight. For RBBC, a few hours is usually adequate.

Backpressure Saturation

1. Record values from the end of pressure up.
2. Set the pressure in the lines to the pressure/volume control device equal to the pore pressure.
3. Open the drainage lines.
4. Measure the volumetric LVDT zero.
5. Start data acquisition readings.
6. Using the hydrostatic option, increase the pore pressure and cell pressure in small increments keeping the same effective stress as measured at the end of pressure up. For this research it was convenient to follow the same schedule as used in CRS backpressure saturation in 30 minute increments: 0.25, 0.5, 0.75, 1, 1.5, 2, 2.5, 3, 4 ksc. These are the values for the pore pressure, while the cell pressure values are approximately 0.1 ksc higher depending on the difference measured at the end of pressure up.
7. Allow overnight equilibration.

Response Time Check / B Value

1. Because of the issues with the response time of the probe, it is important to check the response time before consolidation. Setup data acquisition to take frequent readings (as quickly as 2 seconds).
2. Choose the B value option.
3. Close the drainage lines.
4. Apply 0.5 ksc increment in cell pressure.
5. Once the B value is measured and the pressure back down to the original values, stop data acquisition and open the drainage lines.
6. Return to hold stress to allow the system to come to equilibrium again (approximately 1 hour). This is important so that the pore pressure and probe pressure are exactly equal at the beginning of consolidation.

K_o Consolidation

1. Record the values from the end of backpressure saturation.
2. Exit the program and change the value of the pore pressure gain to a higher value (from 0.2 to 0.4 in MIT03 is adequate). This is because at higher consolidation stresses, a given change in pore pressure does not require as much volume change.
3. Enter the setup program again (in gwbasic, type '"load setup' then 'run'). Assuming that any axial strain is due to seating errors, reset the zeros in the setup program so that both the axial strain and volumetric strain are zero.
4. Enter the computer control program again.
5. At this point the computer program does not have a target pore pressure value. It is necessary to go into hold stress briefly (do not actually switch the motors on though) so the computer will store this value as the target.
6. Start data acquisition
7. Now choose the K_o consolidation option. The values given for the area and height should be very close to those measured initially, so enter to continue.
8. The rate entered in the computer is not the same rate actually applied. Convert the strain rate goal to what is entered in the computer (a calibration should be done before tests are run).

9. Enter the effective stress limit. For the research on RBBC, 10 ksc is a good choice. This leads to a maximum cell pressure of approximately 9 ksc. The plexiglass chamber can withstand higher pressures, but for standard tests there is no need to overstress the chamber.
10. Once the volumetric LVDT approaches the end of its range, stop loading and turn off the motors.
11. Force a reading on data acquisition so the final reading is recorded.
12. Reset the LVDT so that it is at the other end of its range.
13. Exit the program and return to the setup program. Recalculate the volumetric zero so that the volumetric strain after resetting the LVDT is the same as before resetting it.
14. Again force a reading so the new value is recorded. These two values will need to be used when reducing the data.
15. Return to the control program. Again it is necessary to go into hold stress briefly so the computer stores the correct target pore pressure.
16. Return to loading.
17. The final stress is typically left on for 24 hours for secondary compression.
18. To unload, again choose the K_o option. This time enter a negative strain rate and a final effective stress around 1 ksc.

MIT
GEOTECHNICAL LABORATORY
TRIAXIAL TESTING REFERENCE DATA SHEET

Project_____ Boring_____ Depth_____ Test by/date_____
Test No._____ Sample_____ Specimen Loc_____ Test Type _____

1. INSTRUMENTS	Make/No.	Calib Factor	Zero at Start	Zero at Finish
PP Transducer			v_{in}=	v_{in}=
CP Transducer			v_{in}=	v_{in}=
Load Cell			v_{in}=	v_{in}=
Axial DCDT			v_{in}=	v_{in}=
Vol DCDT			v_{in}=	v_{in}=

Cell No. _____ Weight of Accessories - DCDT Arm _____
Piston Area(A_p)_____ Extension_____
Piston Weight(w_p)_____ Moment break_____
$W_o = W_p + W_a$ = _____ Total (W_a) _____

System Compliance(to 2 ksc) Compliance=$\frac{\Delta DCDT \times DCDTCF}{\Delta PP \times PPCF}$=_____cc/ksc

	START	FINISH
Vol. DCDT	_____	_____
PP Trans	_____	_____

PP response to push = _____mv

Filter Paper _____ T_{FP} _____ Cell Fluid _____
Membranes _____ T_m _____ Pore Fluid _____

2. SPECIMEN DATA

Weights and Measures				
Location				
Tare No.				
Tare & Wet Soil				
Tare & Dry Soil				
Tare				
W_c (%)				
Torvane (ksc)				

z_3 w/Dummy,Stones,FP
1 _____
2 _____
3 _____
Ave(Z_d)_____

z_3 w/specimen
1 _____
2 _____
3 _____
Ave(Z_s)_____

Specimen Diameter
Top___-___=_____
Mid___-___=_____
Bot___-___=_____
Ave(d_i)_____

Tare+Specimen_____
Tare _____
Specimen(W_{Ti})_____

Dummy Ht(H_d)_____

after membranes Yes or No

If Yes $T_{cor}=T_m+T_{FP}$
if No $T_{cor}=0$

3. CALCULATIONS

$H_i = H_d - z_d + z_s$ =_____cm
$D_i = d_i - T_{cor}$ =_____cm

$A_i = \pi D_i^2/4$=_____cm^2
$V_i = H_i \times A_i$=_____cm^3

$\gamma_{wet} = W_{Ti}/V_i$=_____%
σ'_{vo} est=_____ksc

4. SPECIMEN DESCRIPTION & NOTES

MIT
GEOTECHNICAL LABORATORY
TRIAXIAL TESTING REFERENCE DATA SHEET

5. PROCESS DOCUMENTATION

Test _____

	Values at the End of ...											
	DAP Chn'l	Local Chn'l	(A) SETUP			(B) PRESSURE UP			(C) SATURATE		
			DVM	Computer Volts	Computer Eng	DVM	Computer Volts	Computer Eng	DVM	Computer Volts	Computer Eng
Axial DCDT											
Cell Pres											
Load Cell											
Pore Pres											
Vol DCDT											
V in.											
Date											
Time											

Saturation Check

Date/Time	Back Pressure	Pressure Increment	B value	Vol. Strain

	Values at the End of ...								
	(D) CONSOLIDATION			(E) SWELLING			(F) SHEARING		
	DVM	Computer Volts	Computer Eng	DVM	Computer Volts	Computer Eng	DVM	Computer Volts	Computer Eng
Axial DCDT									
Cell Pres									
Load Cell									
Pore Pres									
Vol DCDT									
V in.									
Date									
Time									

6. DATA ACQUISITION FILES

File Name	Time / Date	Process	Remarks

TX$\phi\phi\phi\psi\gamma\gamma$

TX - Triaxial
$\phi\phi\phi$ - Test number (sequential)
$\gamma\gamma$ - sequence number

ψ = I - Pressure up
B - Back Pressure
C - Consolidation
S - Shear
P - Preshear
L - Leak Check

MIT
GEOTECHNICAL LABORATORY
TRIAXIAL TESTING REFERENCE DATA SHEET

7. SPECIAL NOTES Test _____

@ B compute initial effective stress $\sigma'_1 = \sigma_c - u_i$ = _____

@ C change vol DCDT zero to have $\epsilon_a = \epsilon_{vol}$

New Zero = Zero+ $(\epsilon_a - \epsilon_{vol})$ x V_i/100/Vol CF = _____

@ D for SHANSEP test be sure

ϵ_a > 10%

σ'_{vmax} is on for 24 hrs prior to unload (for OC test) or shear

@ D or E prior to undrained shear

close drain line for 30 min and monitor P.P.

P.P. open _____ P.P. closed _____ P.P. 30 min ____

8. POST SHEAR MEASUREMENTS

	Weights & Measures				
Location					
Tare No.					
Tare & wet soil					
Tare & dry soil					
Tare					
W_c (%)					
z_3 w/specimen	Specimen Diameter			T_{ave}+Specimen _____	
1.	Top _____ - _____ = _____			T_{ave} _____	
2.	Mid _____ - _____ = _____			Specimen(W_{Tf}) _____	
3.	Bot _____ - _____ = _____				
Ave Z_s	Ave(d_f) = _____				
	with membranes Yes or No				

Radiograph Yes or No Picture Yes or No

Description:

Front Side

9. CALCULATIONS

$H_f = H_d - Z_d + Z_s$ = _____cm	$A_f = \pi D_f^2/4$ = _____cm^2	$\gamma_{wet} = W_{T_f}/V_f$ = _____g/cc
$D_f = d_f - T_{cor}$ = _____cm	$V_f = H_f$ x A_f = _____cm^3	W_s = _____ g